Technical Note

1975-11

T. P. McGarty

The Statistical Characteristics of Diffuse Multipath Radiation and Its Effect on Antenna Performance

25 March 1975

Prepared for the Federal Aviation Administration by

Lincoln Laboratory

MASSACHUSETTS INSTITUTE OF TECHNOLOGY

LEXINGTON, MASSACHUSETTS

Technical Report Documentation Page

1. Report No.	2. Government Accession No.	3. Recipient's Cotolog No.
ESD-TR-75-145		

4. Title and Subtitle	5. Report Date
The Statistical Characteristics of Diffuse Multipath Radiation and Its Effect on Antenna Performance	25 March 1975
	6. Performing Organization Code
7. Author(s)	8. Performing Organization Report No.
McGarty, Terrence P.	Technical Note 1975-11
9. Performing Organization Name and Address	10. Work Unit No. (TRAIS) 45364
Massachusetts Institute of Technology Lincoln Laboratory P.O. Box 73 Lexington, MA 02173	Project No. 034-241-012
	11. Contract or Grant No. IAG DOT-FA72WA1-261
	13. Type of Report and Period Covered
12. Sponsoring Agency Name and Address	Technical Note
Department of Transportation Federal Aviation Administration Systems Research and Development Service Washington, DC 20591	14. Sponsoring Agency Code

15. Supplementary Notes

The work reported in this document was performed at Lincoln Laboratory, a center for research operated by Massachusetts Institute of Technology under Air Force Contract F19628-73-C-0002.

16. Abstract

Diffuse multipath is a random phenomenon that arises out of the diffraction of waves from rough surfaces. This form of multipath can, in turn, affect the angle estimation performance of monopulse antenna systems. In order to evaluate its effect, it is necessary to obtain the channel spread function that results. This function is basically the wave number spectrum of the resulting random field generated by the scattering. To do this, use is made of the Kodis-Barrick scattering cross section and Wagner's shadowing function. The evaluation is performed for the specific geometry of a spherical earth. Evaluation of the system performance degradation is also made for various system configurations.

17. Key Words		18. Distribution Statement
diffuse multipath electromagnetic propagation random fields array performance	communications channels radar/sonar monopulse radar	Document is available to the public through the National Technical Information Service, Springfield, Virginia 22151.

19. Security Classif. (of this report)	20. Security Classif. (of this page)	21. No. of Pages	
Unclassified	Unclassified	166	

Form DOT F 1700.7 (8-72) Reproduction of completed page authorized

TABLE OF CONTENTS

TABLE OF CONTENTS (cont.)

LIST OF ILLUSTRATIONS

LIST OF ILLUSTRATIONS (cont).

TABLE

Section 1

SUMMARY AND RESULTS

When a signal propagates from a source to a receiver over the earth's surface, the field incident on the receiving aperture is composed of both the free space component and those components arising from reflections and diffractions from the interface between free space and the earth. The reflected and diffracted component is commonly broken into two separate parts: the specular multipath return, and the diffuse multipath return. The specular component is usually well defined in terms of its amplitude, phase, and incident direction. It is a plane wave and, as such, is uniquely specified by its direction. The diffuse component, however, arises out of the random nature of the scattering surface and as such is nondeterministic. It does not come from a given direction but from a continuum. It is this form of multipath that is studied in this report.

1.1 Problem Definition

The earth's surface has a height distribution that is random in nature so that when one tries to solve the propagation of electromagnetic waves over such surfaces, the solution must take this fact into consideration. The randomness arises out of the hills, structures, vegetation, or ocean waves that exist. When electromagnetic waves are incident on these surfaces they tend to diffract and the resulting field is spread over many scattered directions.

If we consider the specific case of an Air Traffic Control (ATC) sensor attempting to locate a beacon equipped aircraft, then as a result of the diffuse multipath, the return field viewed at the sensor resulting from a beacon reply, is a combination of a direct signal, a specular multipath, and a diffuse multipath. The multipath signals, since they are not coming from the direction of the aircraft, may tend to deteriorate the performance of the sensor in its ability to determine the location of the aircraft.

The basic problem then is for a fixed receiving aperture and, with some distribution of sensors over that aperture, how greatly does diffuse multipath degrade the angle estimation performance? For example, the aperture may be a planar array of dipoles with a given horizontal and vertical distribution. The angle estimation in such an array may be done by some form of beam forming algorithms. In contrast the array may be a beam formed sum difference monopulse antenna. For both of these cases performance evaluations are sought.

To determine performance, it is first necessary to characterize the diffuse multipath which in turn leads to the characterization of the scattering surface. The simplest characterization is that of a sphere whose surface is randomly perturbed with some statistical regularity. The nature of the statistical behavior of the surface is of some importance in determining the structure of the diffuse field. The characterizations of the diffuse multipath can be given in terms of a random electromagnetic field resulting from a scattering from the random surface.

The problem discussed in this report is an extension of the work reported elsewhere to the areas mentioned above and in so doing, it completes

the study of diffuse multipath begun earlier. To place our approach in perspective we will first review the previous literature and then briefly outline the remainder of the report.

One of the first analytical and experimental studies of scattering was performed by Kerr (1951) in an attempt to analyze the effect of sea surface scattering on radar performance. The approach used by Kerr was to obtain a scattering cross section for the sea surface. A more detailed approach was undertaken by Rice (1951) when he modeled the surface by means of a deterministic polynomial and then solved the stochastic problem. His approach was a combination of both deterministic and stochastic analysis and directed at sea surface scattering. A different approach using the Kirchoff approximation was presented by Eckart (1953) and was directed at acoustic scattering from rough surfaces. Equations for the excess pressure field were obtained and then averaged. The resulting equations were then solved for the required quantities. This was later followed by Ament (1953, 1956), using a similar approach.

Using the Kirchoff technique, Hoffman (1955) extended the analysis to the vector problem encountered in electromagnetic field problems. Other attempts were made by Clark and Hendry (1964) to evaluate backscattering effects. The prime reference using the Kirchoff method is Beckmann and Spizzichino (1963). Their results give the field decomposition in terms of different scattered directions. They are based on a Gaussian surface behavior with knowledge of surface standard deviations and correlation lengths. These approaches use the technique of averaging the propagation equations and then solving. However, all such techniques require some form of closure argument

on higher order moments. Experiments yielding values for the surface properties have been discussed by Fung and Moore, and Hayre and Moore.

Most of these previous results are not suitable for an analysis of estimator performance, however. It was shown by McGarty (1974), for the case of angle of arrival estimation with an array, that a function called the channel spread function was necessary to evaluate performance. This function gives the intensity of radiation incident at the receiver from all directions. This function cannot be obtained directly from the Beckmann and Spizzichino model. However, analyses by Kodis (1966) and Barrick (1968) provide exactly what is necessary for the performance determination. Their analyses obtain a scattering cross section that relates the scattered radiation to a specific direction for a specified incident direction. The method of analysis differs greatly from others in that it solves the scattering problem first, using a stationary phase technique (similar to Twersky (1957)), and then an averaging technique. The averaging technique yields a very physical formula for the scattering cross section. It is in terms of the average number of scatterers, the average surface curvature (following Longuet-Higgins), and reflection coefficients.

1.2 Purpose of Study

This study has four specific purposes.

1. MODEL DIFFUSE MULTIPATH FOR A SPHERICAL EARTH.
   To perform this task it was first necessary to characterize the scattering surface. Using both experimentally determined data and analytically evaluated models, the scattering surface can be modeled as a Gaussian random field. With this model, it is

then possible to apply the Kodis-Barrick theory to the surface and determine the scattering cross section. The channel spread function (wave number spectrum) can be obtained for either a spherical earth or a flat earth once the scattering cross section is evaluated. The channel spread function (CSF) provides the power density of the diffuse field from every azimuth elevation direction at a given point.

2. EVALUATE THE EFFECTS OF DIFFUSE MULTIPATH ON THE ARRIVAL ANGLE ESTIMATION PERFORMANCE FOR DISCRETE ELEMENT ARRAY ANTENNAS.

The characterization of the diffuse field provides the basis for evaluating the degradation or improvement of angle estimation accuracy. This report considers only discrete element array antennas (arrays of dipoles) and evaluates the effects of diffuse multipath on the performance of optimum processors. By optimum processors we mean the class of maximum likelihood estimators. Depending on the nature of characterization of the direct (free space) signal, an optimum processor can be obtained. These processors are, in general, beam formers that search over all possible incident directions for the one maximizing the processor output. The performance of such processors (via the Cramer-Rao [CR] bound) acts as upper bounds to the performance of suboptimum processors.

3. EVALUATE THE EFFECTS OF DIFFUSE MULTIPATH ON MONOPULSE AZIMUTH ESTIMATION.

The type of sensor chosen for the proposed DABS system is a monopulse off boresight angle estimator. Its realization may be in many forms; however one specific realization is with a planar array forming a sum and difference beam. A great deal of previous work has been done evaluating the effects of specular multipath on such a processor. However, only some fragmented analyses have been performed on the diffuse multipath effects. Thus in this report we have set forth to evaluate the performance of a monopulse processor using the CSF developed. This processor can then be compared to the optimum processors to see how much of a margin of improvement can be obtained.

4. DETERMINE METHODS TO REDUCE THE DELETERIOUS EFFECTS OF DIFFUSE MULTIPATH.

In those cases where diffuse multipath causes degradation in performance, it is important to know the measures that can be taken to eliminate these effects. In particular, with monopulse azimuth estimates, large vertical apertures have been suggested as a way to eliminate both specular and diffuse errors. It has been shown that for specular multipath, a large vertical aperture does eliminate the multipath induced bias errors. Similar effects can be studied with monopulse and diffuse multipath using the CSF and the performance evaluations obtained.

These are the main purposes of this study. Of particular interest is the geometry that one finds in an air to ground surveillance link with special emphasis on the DABS implementation. The results obtained are more general, however, and thus this study addresses many other issues not specifically outlined in this section.

1.3 Results of the Study

This report has provided many results that apply directly to DABS and the general ATC problem as well as to areas of a more general nature. The following are the specific results and conclusions reached.

1. DIFFUSE MULTIPATH CAN BE COMPLETELY CHARACTERIZED BY THE CHANNEL SPREAD FUNCTION FOR A WIDE CLASS OF SURFACE CHARACTERIZATIONS.

   As previously discussed, the diffuse field is dependent upon the surface characterization. In this report a rather robust set of surface characterizations has been chosen, and a statistical description of the scattered electromagnetic field has been obtained. The second order statistics of the field are obtained by considering the field as received at the aperture of a sensor resulting from an excitation by a source (a beacon equipped aircraft) at a location well defined with respect to the sensor. The result is the channel spread function, which provides the energy density at the receiving aperture in terms of azimuth and elevation. The CSF depends upon the sensor and source geometries, the surface statistics in terms of its r. m. s slope, the source antenna pattern,

as well as shadowing effects. The CSF provides a complete analytical characterization of the diffuse field.

2. DIFFUSE MULTIPATH CAN BE SIGNIFICANTLY REDUCED BY SHADOWING.

Shadowing results when surfaces are not directly irradiated by the incident electromagnetic field due to blockage. The characterization of this type of effect is quite difficult for random surfaces, but there exist several viable models, particularly the one by Wagner. Using this model, the total power of the diffuse multipath is decreased significantly at low elevation angles as a result of surface blockage. The difference between including shadowing effects and disregarding them at angles on the order of 1 to 2^{o} is on the order of 10 to 20 dB in power. Thus when shadowing is included in the model as it is in the actual propagation medium, the total diffuse power can be significantly reduced.

3. OPTIMUM PROCESSORS UTILIZE THE DIFFUSE COMPONENT TO IMPROVE ANGLE ESTIMATION PERFORMANCE.

The optimum processor is a maximum likelihood estimator of the arrival angle. To obtain an estimate with such a processor, it is necessary to form many beams and determine on which one the signal is arriving. This entails a great deal of processing and uses all the information presented the sensor over its entire aperture. Such processors require outputs from each dipole and as such are quite complicated. However when such processors are used in the presence of diffuse multipath, which is centered

at the azimuth direction of the incident plane wave, these processors can utilize this information to improve the estimate. In effect the optimum processor utilizes the information regarding source location in the diffuse field that generated it, and reduces source location uncertainty. The result is presented in terms of the Cramer-Rao bound on angle estimate variance. For the optimum processor, a decrease in the estimate variance can, in theory, be obtained by processing both the direct and diffuse fields.

4. MONOPULSE AZIMUTH PERFORMANCE IS ALWAYS DEGRADED BY THE PRESENCE OF DIFFUSE MULTIPATH.

In contrast to an optimum multibeam processor, the two beam sum-difference monopulse processors always have their performance degraded by diffuse multipath. This can best be understood by noting that for a monopulse processor, both beams point toward the target whose position is to be estimated. The result is that the diffuse component acts as noise and raises the effective noise level. The azimuth estimation performance is then degraded. The degradation can be a factor of 2 to 3 above the noise standard deviation and almost an order of magnitude above the performance obtained with an optimum processor. However, for the purposes of a DABS/ATC sensor, the performance is still acceptable even in the worst diffuse multipath conditions. Moreover, the diffuse errors are still an order of magnitude

smaller than those generated by specular multipath. An important point to note however is that in contrast to noise, the diffuse multipath azimuth error does not depend on the signal strength. This is because as this signal level is raised, the diffuse level is also raised proportionately.

5. VERTICAL APERTURE IS USEFUL IN REDUCING MONOPULSE DIFFUSE MULTIPATH AZIMUTH ERRORS.

   The CSF shows that the diffuse multipath is concentrated at the horizon corresponding to small negative elevation angles. This implies that for targets at angles above 1^{o} to 2^{o}, vertical aperture can be used to reduce the effect of diffuse multipath. At smaller elevation angles, the diffuse field is self limiting as a result of shadowing and spreading in azimuth. The net result is that for angles greater than 1.5^{o} vertical aperture helps, and for angles less than this diffuse multipath is itself small. Thus vertical aperture works best where the diffuse field is strongest. This fact is demonstrated with data from radial flights performed at DABS Experimental Facility (DABSEF).

These five results are the main conclusions of this study. They show that the diffuse field can be characterized and its effect on azimuth accuracy analytically evaluated.

1.4 Summary of the Report

The main text of this report presents a detailed summary of the analysis of the diffuse field and the array performance. The specifics of the analyses are contained in the Appendices.

In Section 2, the model for the received signal is developed. It is assumed that future analyses will be concerned with arrays so that the spatial model is for point detectors over a given aperture. The time behavior is also defined in terms of the bandpass nature of the received signal. The model of the diffuse signal is presented and its statistics discussed. The resulting voltage output is derived and related to the incident electric field. The main result of this modeling is the introduction of the channel spread function.

Section 3 will evaluate the channel spread function for a spherical earth. The surface irregularities are modeled as a homogeneous time invariant Gaussian random field. Using the Kodis-Barrick theory, the scattering cross section is evaluated. Shadowing effects are included in the model using the results of Wagner. Specific results on the evaluation of the CSF for various geometries and surface roughness are presented.

The performance and structure of various angle estimators are discussed in Section 4. The signal model developed in Section 2 is used as a basis for various estimator structures. The optimum maximum likelihood estimators for both spread and unspread channels are discussed in this section. A detailed comparison of structure and performance is made under the varying assumptions of signal structure. Particular emphasis is placed upon the monopulse processor, and its performance is compared to that of the optimum processor.

SECTION 2

THE SIGNAL MODEL

When a signal is transmitted from a source at a given location and received by a sensor at another point, the total signal can be broken down into four parts. They are the free space portion, the specular multipath portion, the diffuse multipath term, and noise. The specific description of the received signal depends upon the source characteristics, the propagation nature of the medium, and the type of sensor used to measure the fields incident upon it. To allow the extension of the results obtained in this report to as wide a variety of sensors as possible, the received signal is best described as received by a point detector (a single dipole) located at a specific point in the receiving aperture. With this type of description, an extension to arbitrary sensor beam patterns can be made by appropriate phasing and weighting of the individual point sensors.

The aperture of the receiving sensor can be defined with respect to an arbitrary coordinate system as shown in Fig. 1. In this aperture, $\mathcal{A}$, we can locate a specific point defined by a vector $\underline{r}$. If a sensor is placed at this point, then its output voltage as a function of time is given by r(t). This voltage depends upon the incident electromagnetic field that is propagating at a frequency, f_c, the carrier frequency. Thus r(t) is actually a signal modulated at this carrier frequency. In general the modulation on r(t) is narrowband

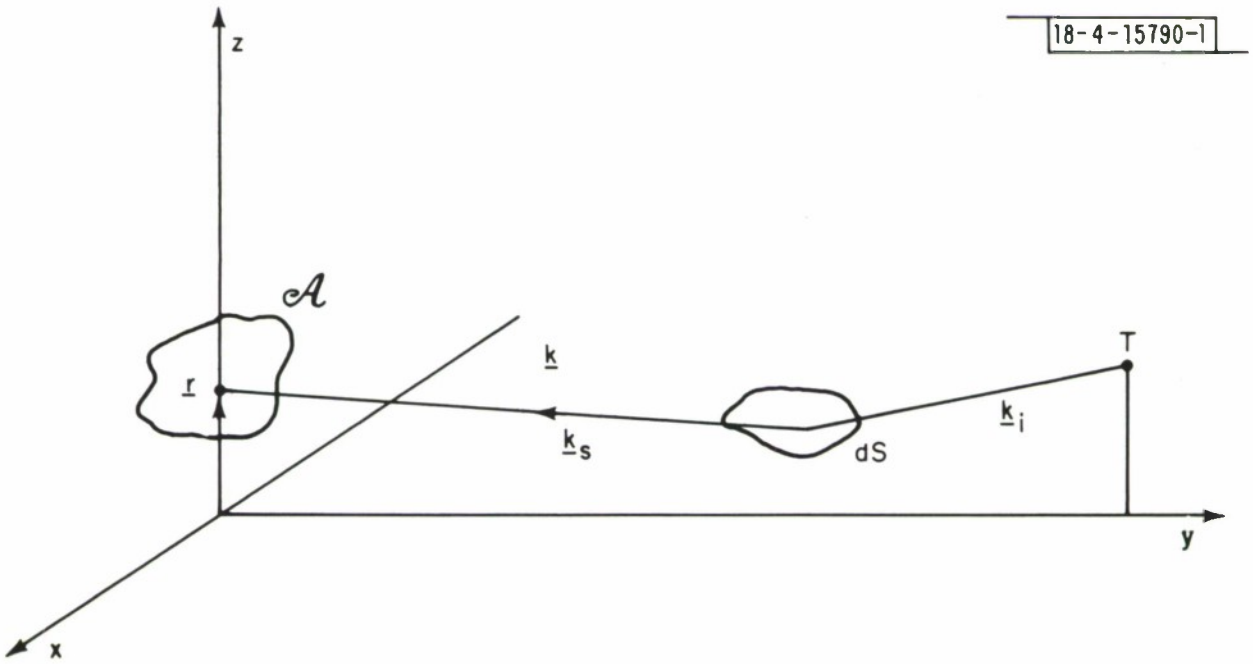

Fig. 1. Geometry of receiving aperture.

with respect to f_c so that r(t) can be represented in what is termed as complex envelope form. Namely

$$r(t) = \sqrt{2}\ \underline{\mathrm{Re}}\left[\tilde{r}(t)\exp\left(j2\pi f_c t\right)\right] \tag{2.1}$$

where

$\tilde{r}(t)$ is the complex envelope or r(t).

$\tilde{r}(t)$ is a slowly varying time function (e. g., a pulse) that represents the baseband modulation of the carrier. It is therefore sufficient to deal with only the complex envelope, $\tilde{r}(t)$.

The first portion of the received signal, the free space portion, is given in the following.

$$\tilde{s}_F(t) = \sqrt{E_0}\,\tilde{f}(t - R/c)\tilde{b}\exp\left(jk_0\underline{\mu}\cdot\underline{r}\right) \tag{2.2}$$

where

E_0 is the energy in the signal when transmitted

$\tilde{f}(t)$ is the complex envelope of the time variation

$\tilde{b}$ is the complex amplitude and phase variations due to path propagation

R is the range from the source to the sensor

c is the propagation velocity

k_0 is the wave number

$\underline{\mu}$ is the direction cosine vector indicating the incident direction of the wave front

The time variation has the property that over an interval (0, T), it is normalized such that

$$\int_0^T \tilde{f}(t)\,\tilde{f}^{*}(t)dt = 1 \qquad (2.3)$$

where

$*$ represents complex conjugate

The second portion of the received signal is the specular multipath return and is given by

$$\tilde{s}_S(t) = \sqrt{E_0}\,\tilde{f}(t - R'/c)\tilde{b}\tilde{\rho}\,\exp\,(jk_0\underline{\mu}'\cdot\,\underline{r}) \qquad (2.4)$$

where

$\tilde{\rho}$ is the complex reflection coefficient that results from the wave having been reflected from the earth's surface and also possibly being altered by an antenna gain change at the source

R' is the path length over the new path

$\underline{\mu}'$ is the direction cosine vector of the multipath wave.

The diffuse signal can also be characterized using this format. However, it must first be noted that the diffuse field is assumed to come from a continuum of directions and not just one as the free space and specular returns. To represent this continuum, we use an integral representation in the following form

$$\tilde{s}_D(t) = \sqrt{E_0}\iint \tilde{f}(t - R(\mu')/c)\tilde{b}(\mu')\exp\,(jk_0\underline{\mu}'\cdot\,\underline{r})d\mu' \qquad (2.5)$$

where

$R(\mu')$ now represents the path length from source to sensor over the diffuse multipath source arriving at the sensor from direction μ'

$\tilde{b}(\mu')$ is the amplitude and phase dependence of that particular direction.

To fully characterize the diffuse term, a complete description of $\tilde{b}(\mu)$ must be made. Since the reflecting surface giving rise to the surface is random, then so too is $\tilde{b}(\mu)$. Furthermore, since the field coming from direction μ may most likely arise from many points independently radiating in that direction (as will be shown in the next section), then using standard limiting arguments, one can show that $\tilde{b}(\mu)$ is a complex Gaussian random variable for each μ. Furthermore, it can also be shown to be zero mean. To fully characterize it, all that is needed is the covariance. Experience indicates that spatially the diffuse field is a homogeneous random field (see Capon) so that for the spectral (wave number) portion, we obtain the following. For a source whose free space direction is $\underline{\mu}$, we have

$$E[\tilde{b}(\mu')\tilde{b}^{*}(\mu'')] = K(\mu, \mu')\delta(\mu' - \mu'') \qquad (2.6)$$

where

$\delta(\mu)$ is the delta function.

This covariance states that radiation coming from different directions is independent. The term $K(\mu, \mu')$ represents the spectral density from direction μ' for a source at μ. This function is called the channel spread function (CSF) because it represents the spreading of the signal due to the diffuse field.

The fourth and final term in the received signal is the noise, a zero mean narrow band white Gaussian noise process $\tilde{w}(t)$. For this process we have

$$E[\tilde{w}(t)\tilde{w}^{*}(t+\tau)] = N_0\,\delta(\tau) \tag{2.7}$$

Thus the received signal at point $\underline{r}$ is given by

$$\tilde{r}(t) = \tilde{s}_F(t) + \tilde{s}_S(t) + \tilde{s}_D(t) + \tilde{w}(t) \tag{2.8}$$

It is often more convenient to deal with the demodulated form of $\tilde{r}(t)$ at each sensor. This is obtained by

$$\tilde{r} = \int_{R/c}^{T+R/c} \tilde{r}(t)\tilde{f}^{*}(t - R/c)dt \tag{2.9}$$

where

$\tilde{r}(t)$ is demodulated by the delayed complex envelope of the signal. The result will be to eliminate the envelope variations in both the direct and specular paths and introduce a known term in the diffuse path. The demodulated diffuse term is

$$\tilde{s}_D = \sqrt{E_0} \int\int \tilde{g}(\mu')\,\tilde{b}(\mu')\exp(jk_0\underline{\mu}' \cdot \underline{r})d\mu' \tag{2.10}$$

where

$$\tilde{g}(\mu') = \int_{R/c}^{T+R/c} \tilde{f}(t - R(\mu')/c)\tilde{f}^{*}(t - R/c)dt \tag{2.11}$$

Now over most viewing directions, $\tilde{g}(\mu')$ is almost unity by the nature of $\tilde{f}(t)$ so it can be neglected.

We can now relate this signal model to the field incident on the sensor. Let us first consider the diffuse field only. Let $\tilde{f}(t)\, dE(\theta,\phi)$ be the field coming from the solid angle θ, $\theta + d\theta$, ϕ, $\phi + d\phi$ at time t. Since this represents the diffuse field it is random. Assume that the sensor is a dipole with cross section $\lambda^2/4\pi$, where λ is the wavelength. Then in terms of the electric field, the mean square voltage output can be written as

$$\frac{\lambda^2}{4\pi} E\left[\left| \int_0^{2\pi} \int_0^{\pi} dE(\theta,\phi)\right|^2\right] \tilde{f}(t)\tilde{f}^*(t)T = E_0\, \tilde{f}(t)\tilde{f}^*(t) \int_{-1}^{1} \int_{-1}^{1} K(\mu,\mu')d\mu' \tag{2.12}$$

where we have equated it to the mean square of the voltage output using the diffuse model developed in this section, and define θ and ϕ as shown in Fig. 2. Now if we also assume the electric field to be independent from direction to direction, we define

$$E[dE(\theta,\phi)\, dE^{\dagger}(\theta',\phi')] = \begin{cases} 0 & ;\ \theta \neq \theta',\ \phi \neq \phi' \\ \tilde{K}(\theta,\phi)d\theta d\phi; & \theta = \theta',\ \phi = \phi' \end{cases} \tag{2.13}$$

where

$\dagger$ is the complex conjugate transponse.

The units of $\tilde{K}(\theta,\phi)$ are in volts^2/m^2-steradian. Using this definition and equating terms in the mean square voltage output we find that

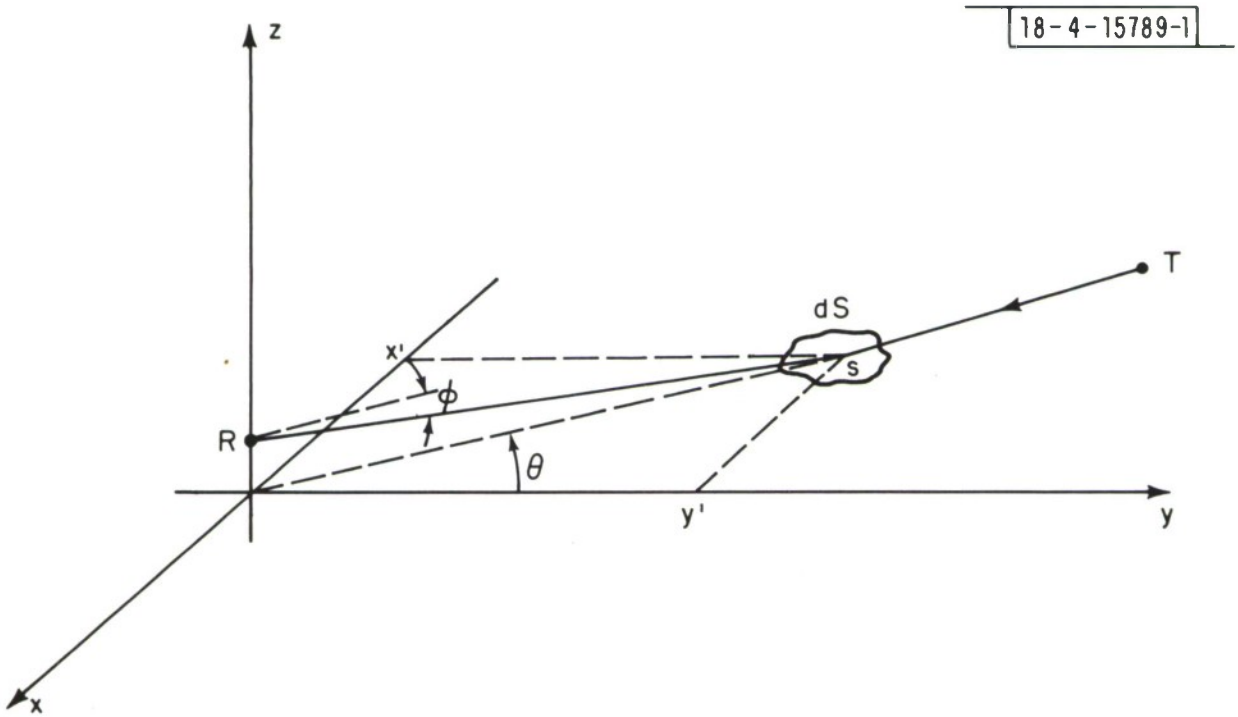

Fig. 2. Diffuse multipath geometry.

$$K(\mu,\mu') = \frac{\lambda^2 T}{4\pi E_0}\,\tilde{K}(\theta,\phi)\,\frac{d\theta d\phi}{d\mu'} \tag{2.14}$$

Thus if from the geometry and propagation equations we can find the electric field and its statistics, then $\tilde{K}(\theta,\phi)$ is obtained and concurrently $K(\mu,\mu')$. It is the purpose of the next section to show how this term is obtained.

In general, when dealing with arrays, the total demodulated received signal is represented by the output of N sensors located at positions $\underline{r}_i$, $i = 1,\ldots,N$. If we introduce an N x 1 vector $\underline{\tilde{m}}(\mu)$, called the delay vector, given by

$$\underline{\tilde{m}}(\underline{\mu}) = \begin{bmatrix} \exp\,(jk_0\underline{\mu}\cdot\underline{r}_1) \\ \vdots \\ \exp\,(jk_C\underline{\mu}\cdot\underline{r}_N) \end{bmatrix} \tag{2.15}$$

then we can easily write the total output of an array in vector form. Specifically, if we let $\tilde{r}_i$ be the demodulated output at location $\underline{\tilde{r}}_i$, then define $\underline{\tilde{r}}$ as the N x 1 vector of such outputs then

$$\underline{\tilde{r}} = \sqrt{E_0}\,\tilde{b}\underline{\tilde{m}}(\mu) + \sqrt{E_0}\,\tilde{b}\tilde{\rho}\,\underline{\tilde{m}}(\mu') + \sqrt{E_0}\int_{-1}^{1}\int_{-1}^{1}\underline{\tilde{m}}(\mu')\,\tilde{b}(\mu')d\mu' + \underline{\tilde{w}} \tag{2.16}$$

where

$\underline{\tilde{w}}$ is now an N x 1 zero mean Gaussian random vector with covariance $\tilde{K}_w$.

With this model for a received signal, one can now ask how to estimate the direction cosines μ, or equivalently the azimuths and elevations. For the purposes of this report we are interested in only azimuth so that μ will be a scalar. However, the general or canonical form of the received signal is still of use.

The model we have developed has provided the following.

1. A description of the received signal in terms of a free space path, a specular multipath, a diffuse multipath, and noise
2. A time demodulated waveform
3. A model for the diffuse component that shows it to be a zero mean homogeneous Gaussian random field
4. A relationship between the model and the electromagnetic field incident on a dipole yielding the measured output voltage
5. A canonical form for an array output useful for estimating arrival angles.

With this model, in the next section we shall analytically obtain $K(\mu, \mu')$ from first principles, and in Section 4 evaluate various processors to estimate θ the azimuth, or μ the direction cosine.

SECTION 3

THE CHANNEL SPREAD FUNCTION

The channel spread function is a measure of how the diffusely scattered radiation is distributed in azimuth and elevation with respect to the aperture of a receiving antenna. In this section we shall derive this expression in some detail showing how it arises from the random nature of the surface and the laws of propagation. In order to solve the equations, certain assumptions must be made and the implications and limitations of these assumptions will be discussed.

In this section we first obtain the CSF in terms of a certain set of parameters and show how it arises naturally as a result of surface scattering. The parameters needed in the definition are the scattering cross section per unit area, and suitable Jacobian and shadowing effects. In the remainder of this section these effects are evaluated.

3.1 The CSF

In the previous section we evaluated the relationship between the model of the received voltage at the output of a dipole and the electric field incident on the dipole. This field was described as having come from a continuum of azimuth (θ) and elevation (ϕ) directions with respect to the dipole. Consider the geometry in Fig. 3. A source of radiation is at point T and it is

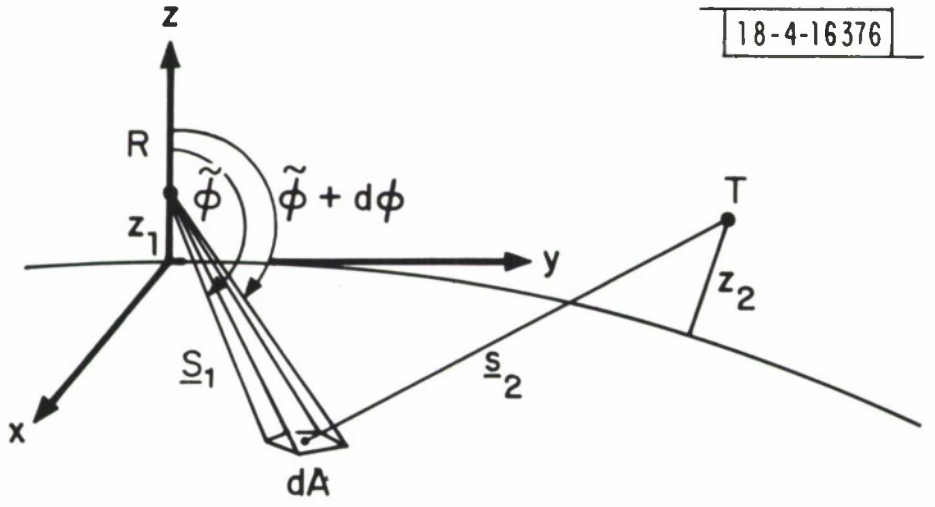

Fig. 3. Geometry of incremental scattering surface.

received at point S. The source has power P_s and an antenna with gain $G_T(\theta_i, \phi_i)$ where θ_i and ϕ_i are the azimuth and elevation, respectively, with respect to the radiated energy. These two points are located over a spherical earth of radius R_E. The transmitter is at a height z_2, and the sensor at height z_1. Now consider radiation coming to the sensor S from solid angle ϕ, $\phi + d\phi$ and θ, $\theta + d\theta$. In the figure we show that if we let $\tilde{\phi} = \phi + \pi/2$, then this solid angle generates a surface area dA from which power must be scattered so as to be received from this direction. Let $\underline{s}_1$ be a vector from the sensor at S to the center of dA, and $\underline{s}_2$ a vector from T to the center of dA. A coordinate system is centered below S on the surface of the earth. Also assume the radiation has wavelength λ.

Let θ_i and ϕ_i represent the azimuth and elevation at the surface dA to the transmitter at T. The transmitter radiates a power density (watts/m^2) of $(P_0/4\pi R^2)\, G_T(\theta_i, \phi_i)$ at a range R and in direction θ_i, ϕ_i. Then the power density on dA is $(P_0/4\pi|\underline{s}_2|^2)\, G_T(\theta_i, \phi_i)$. The surface has area dA so that the total power can be evaluated. Let $\underline{k}_i$ represent the wave vector defining the direction of radiation coming from T at dA, and let $\underline{k}_s$ represent the wave vector defining propagation from dA to S. To find how much of the incident power is scattered from $\underline{k}_i$ to $\underline{k}_s$ on dA, namely from transmitter to receiver, we need to define a scattering cross section, $\sigma(\underline{k}_s, \underline{k}_i)$. This scattering cross section reflects how effective dA is in transmitting power from the incident direction into the scattered direction.

Having the power scattered toward the receiver S, it is then possible to obtain the power density (watts/m^2) at S as follows

$$\frac{P_0\, G_T(\theta_i, \phi_i)}{(4\pi)^2 |\underline{s}_1|^2 |\underline{s}_2|^2}\ \sigma(\underline{k}_i, \underline{k}_s)\, dA \ (\text{watts/m}^2) \tag{3.1}$$

To obtain $\tilde{K}(\theta, \phi)$, the mean square voltage density (volts^2/m^2-steradian), we use the radiation resistance of 120π ohms (see Friis and Lewis) and the solid angle, $d\theta d\phi$. Thus

$$\boxed{\tilde{K}(\theta, \phi) = \frac{P_0\, G_T(\theta_i, \phi_i)}{(4\pi)^2 |\underline{s}_1|^2 |\underline{s}_2|^2}\ \frac{\sigma(\underline{k}_i, \underline{k}_s)}{120\pi}\ \frac{dA}{d\theta d\phi}} \tag{3.2}$$

where θ and ϕ are the azimuth and elevation of dA with respect to S.

Once $\tilde{K}(\theta, \phi)$ is obtained the CSF, $K(\mu)$, follows directly from the evaluation in Section 2. It can be noted that in the definition of $\tilde{K}(\theta, \phi)$, the first term depends on the geometry of the two sensors, the second term on the nature of the scattering surface, and the third term, a Jacobian, on the relationship of the scattering surface mean value to the viewing angles. Each of these terms will now be evaluated starting with the scattering cross section.

3.2 Scattering Cross Section

Consider the geometry as described above and let $\underline{k}_s$ be a vector pointing from S to dA. If we define an arbitrary coordinate system centered in dA, then by using the Stratton-Chu formulation, we can obtain the field from this surface area at S. Let this field be given by $\underline{E}(\underline{r}_p)$ where $\underline{r}_p$ is a vector from the center of dA to S that is in the same direction as $\underline{k}_s$. Now

assume that the field incident on dA is a plane wave with a wave vector $\underline{k}_i$ with respect to the coordinate system defined at dA. Let the amplitude of the field be E_0 and assume it has an arbitrary polarization. Then the scattering cross section (in m^2) is defined as

$$\tilde{\sigma}(\underline{k}_i, \underline{k}_s) = 4\pi R^2 \frac{E\left[\left|\underline{E}(\underline{r}_\rho)\right|^2\right]}{E_0^2} \tag{3.3}$$

where R is the distance from S to dA, and E [ ] represents the expected value (see Kerr, p. 33).

The expectation is necessary because the surface is irregular and random in nature, so that the field scattered from it is random. Let $\xi(x, y)$ be the height of the surface at a specific x, y coordinate. For this analysis we assume that $\xi(x, y)$ is a Guassian random variable with zero mean

$$E[\xi(x, y)] = 0 \tag{3.4}$$

and a covariance of the form

$$E[\xi(x, y)\, \xi(x', y')] = \sigma_h^2 \exp(-r^2/\sigma_\ell^2) \tag{3.5}$$

where

σ_h is the r. m. s. surface height

σ_ℓ is the correlation length

also

$$r^2 = (x - x')^2 + (y - y')^2 \tag{3.6}$$

Thus over any incrementally small area dA, this planar description of the surface height holds for a coordinate system centered in dA. The correlation function for the surface has been chosen to satisfy certain regularity conditions mentioned by Barrick [2].

In order to solve the boundary value problem that arises from the Stratton-Chu formulations, we assume that the surface is a perfect conductor. Then, as shown in Appendix I, the resulting integral over the surface area is in a form that can be solved if stationary point approximations are valid. These approximations mean that the average radii of curvature of the surface are much larger than a wavelength so that points that lead to scattering do so in a specular manner. Thus with this approximation, we have a specular point theory valid for high frequencies, generally at UHF and above.

The net result of this approximation is that $\tilde{\sigma}(\underline{k}_i, \underline{k}_s)$ can be written as

$$\tilde{\sigma}(\underline{k}_i, \underline{k}_s) = \pi n_T \mathscr{R} R^2(\underline{k}_i, \underline{k}_s) \tag{3.7}$$

where

n_T = the average number of specular reflectors

$\mathscr{R}$ = the average of the product of the radii of curvature

$R^2(\underline{k}_i, \underline{k}_s)$ = the reflection coefficient giving the depolarization loss from a tilted surface.

If we let dA become incrementally small, then we can equivalently define the scattering cross section per unit area as

$$\sigma(\underline{k}_i, \underline{k}_s) = \pi n_A \mathcal{R} R^2(\underline{k}_i, \underline{k}_s) \tag{3.8}$$

where

n_A = the average number of specular points per unit area

The average of both the specular points and the product of the radii of curvature can be obtained using the hypothesized statistical distribution of the surface. This has been done by Barrick [1] and is

$$\boxed{n_A = \frac{7.255}{\pi^2 \sigma_\ell^2} \exp\left(-\frac{\tan^2\gamma}{s^2}\right)} \tag{3.9}$$

where

$s^2 = \frac{4\sigma_h^2}{\sigma_\ell^2}$; the square of the rms surface slope

and

$$\tan\gamma = \frac{\sqrt{\sin^2\phi_i - 2\sin\phi_i \sin\phi_s \cos\theta_s + \sin^2\phi_s}}{\cos\phi_i + \cos\phi_s} \tag{3.10}$$

where

γ is the angle between the local normal on dA and the local surface normal of the specular point.

The angles ϕ_i and ϕ_s are the angles between the local normal on dA and the propagation vectors $\underline{k}_i$ and $\underline{k}_s$. θ_s is the angle of scattering in the local x, y plane between $\underline{k}_i$ and $\underline{k}_s$ (see Fig. 4).

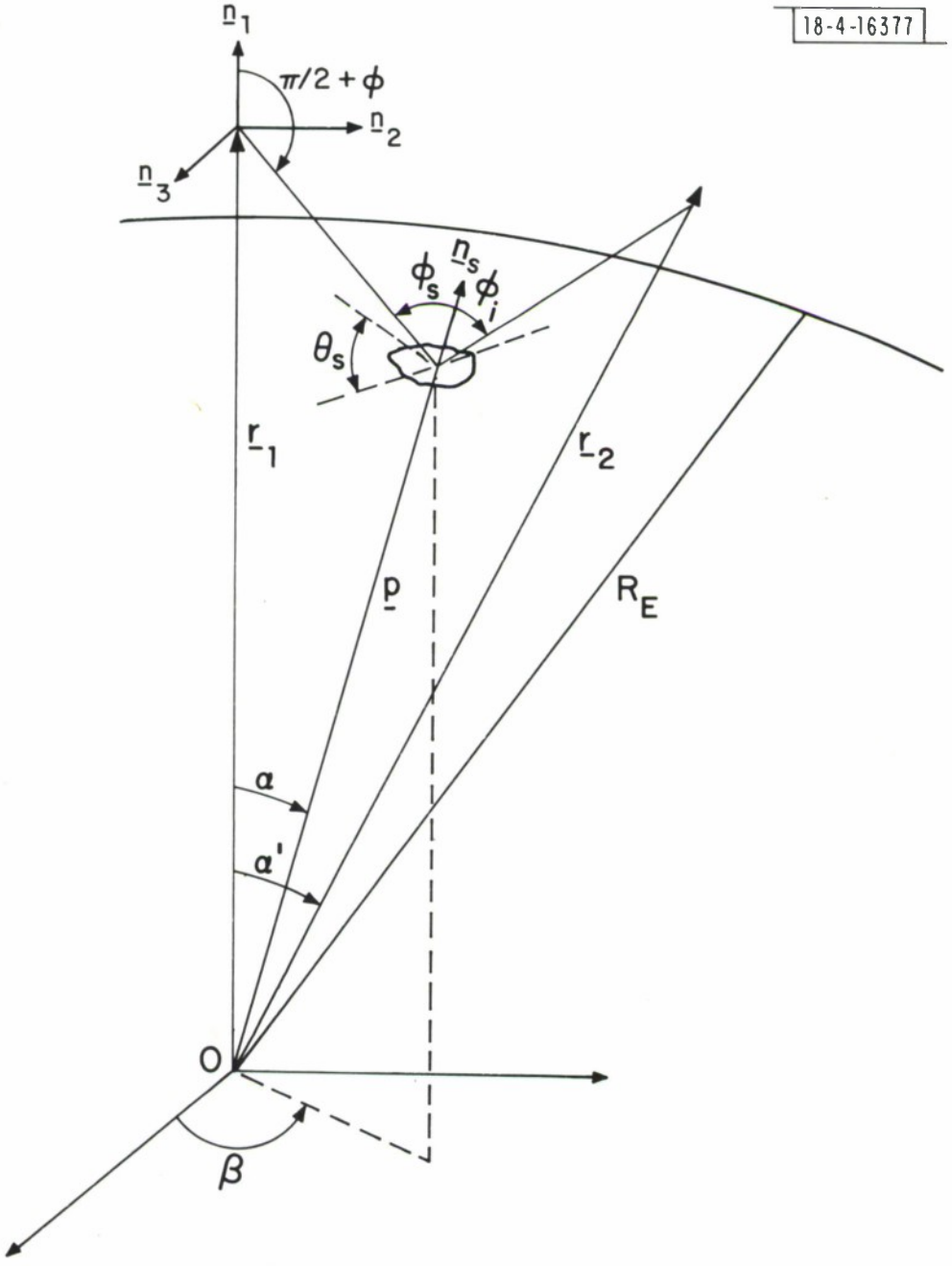

Fig. 4. Spherical earth scattering geometry.

Note that n_A represents a density of specular scatterers per unit area and it depends upon the location of the surface and the statistical characteristics of the surface. For surfaces with large rms slopes, s, n_A can tend to be large.

Barrick has also evaluated the average product of the radii of curvature. It is

$$\boxed{\mathscr{R} = 0.1378\pi \frac{\sigma_\ell^2}{s^2} \sec^4\gamma} \tag{3.11}$$

Combining these we obtain the scattering cross section

$$\boxed{\sigma(\underline{k}_i, \underline{k}_s) = \frac{\sec^4\gamma}{s^2} \exp\left(-\frac{\tan^2\gamma}{s^2}\right) R^2(\underline{k}_i, \underline{k}_s)} \tag{3.12}$$

The result shows that $\sigma(\underline{k}_i, \underline{k}_s)$ depends upon γ, s and $R^2(\underline{k}_i, \underline{k}_s)$, and is independent of σ_h and σ_ℓ separately, i.e., it depends upon the rms surface slope and it is independent of wavelength.

The wavelength independence results from the fact that we used the specular point approximation. Thus it is truly wavelength independent only if $\mathscr{R}$ is greater than λ^2. From the dependence of $\mathscr{R}$ on σ_ℓ, s and γ, we see that this assumption depends upon the surface statistics and the geometry of the scattering point.

The reflection coefficient has been evaluated by Mitzner. For horizontal to horizontal or vertical to vertical polarization we have

$$R^2(\underline{k}_i, \underline{k}_s) = \left[\frac{-\sin\phi_i \sin\phi_s \sin^2\theta_s + a_2 a_3}{4 \sin^2\xi \cos^2\xi}\right] \qquad (3.13)$$

with

$$\cos\xi = \sqrt{\frac{1 - \sin\phi_i \sin\phi_s \cos\theta_s + \cos\phi_i \cos\phi_s}{2}} \qquad (3.14a)$$

$$a_z = \cos\phi_i \sin\phi_s + \sin\phi_i \cos\phi_s \cos\theta_s \qquad (3.14b)$$

$$a_3 = \sin\phi_i \cos\phi_s + \cos\phi_i \sin\phi_s \cos\theta_s \qquad (3.14c)$$

Similar results apply for cross and circular polarization.

The fundamental constraint or assumption using this method is that the reflectors are quasi-specular which assumes that the wavelength of the radiation is small with respect to the radii of curvature. Thus, the results are valid on the short wavelength limit. Beckmann and Spizzichino (p. 89) also evaluate a mean power reflection coefficient, which when suitably normalized, is identical to (3.7) but without the reflection coefficient term. They state that their result is valid for very rough surfaces where

$$g = \left[2\pi \frac{\sigma_h}{\lambda} (\cos\phi_i + \cos\phi_s)\right]^2 \gg 1 \quad . \qquad (3.15)$$

This agrees with the limitation on the Rayleigh criterion for rough surfaces, which states that a surface can be considered smooth if

$$\sigma_h < \frac{\lambda}{8 \cos \phi} \tag{3.16}$$

Thus, for low angle scattering ($\phi \rightarrow \pi/2$) we have the constraint that the model we are considering is valid for

$$\frac{\sigma_h}{\lambda} \gg \frac{1}{8\psi} ; \quad \psi = \pi/2 - \phi \quad . \tag{3.17}$$

For example, at $\psi = 3^{\circ}$, this means that σ_h/λ must be greater than 2.5. Thus, for $\lambda = 1$ foot, for example, the surface heights for diffuse multipath are on the order of 8 ft or more. Such heights are common in hilly terrain. It furthermore states that at such angles small rocks, etc., appear smooth.

Thus, the model that we are considering is valid under the following constraints:

1. The radius of curvature is large compared to a wavelength. This means that the specular point approximation can be used. This implies that diffraction can be neglected from each independent reflector.
2. Multiple scattering can be neglected. The problems associated with multiple scattering are significant and are discussed in McGarty [3]. It basically relates to the closure property associated with solving for the moments of random integral equations.
3. That ϕ_i is such that the surface cannot be considered smooth. This implies (3.15) is valid. This allows for the scatterers to be added incoherently.

The first assumption is the short wavelength approximation, while that for (3) implies a very rough surface. Now as (3.12) demonstrates, $\sigma(\underline{k}_i, \underline{k}_s)$ depends only on the ratio s^2 and not on σ_h or σ_ℓ independently. However, this dependence is implicit under assumption (3).

We can attempt to extend the model by augmenting the saddle point integration with other techniques (see Felsen and Marcuvitz, Chpt. 4). However, the intuitive expression for the scattering cross section breaks down. In conclusion then, the expression for the scattering cross section should be adequate for a wide range of surfaces found in operational environments.

3.3 Surface Jacobian

The third portion of the channel spread function relates the incremental surface area to the solid angle that generates it. This is in effect a Jacobian transforming surface area to solid angle. This function can be evaluated for various surfaces such as planar, spherical and others. The first portion of the CSF also depends upon the geometry with respect to a given θ, ϕ viewing angle. In this section we will relate θ and ϕ to the sensor and source locations and the scattering angles at the specular points. Specifically we shall consider the geometry for a spherical earth, that for a flat earth having been done elsewhere (see McGarty [2]).

Consider a receiver as shown in Fig. 4 with azimuth θ and elevation ϕ to a scattering surface. Let $\underline{n}_s$ be the local normal on the scattering surface, and $\underline{k}_i, \underline{k}_s$ be defined as before. Let the source be at an angle α' from the receiver referenced to the center of the earth. The ground range to the

transmitter is $R = \alpha' R_E$. Let the receiver be at height z_1 and the transmitter at z_2. In this case also assume that the transmitter and receiver are coplanar.

Now let α be the angle to the center of the scattering surface. It is readily shown that given ϕ, α can be obtained from the relationship

$$\tan \phi = \frac{z_1 + R_E(1 - \cos\alpha)}{R_E \sin\alpha} \quad . \tag{3.18}$$

Thus, to obtain $K(\theta, \phi)$, we have for each θ, ϕ, a defined incremental surface at an angle α relative to a spherical coordinate system centered at the earth's core. Similarly, the surface is also defined by a β given by

$$\theta = \frac{\pi}{2} - \beta \quad . \tag{3.19}$$

From the results of the previous subsection we saw that ϕ_i, ϕ_s and θ_s must be defined for each θ, ϕ surface. In the Appendix, we show that

$$\phi_s = \frac{\pi}{2} - \phi + \alpha \tag{3.20}$$

and ϕ_i and θ_s are rather complicated but readily evaluated functions of θ and ϕ.

Similarly $|\underline{s}_1|$ and $|\underline{s}_2|$ are given by

$$|\underline{s}_1|^2 = R_E^2 \sin^2\alpha + (R_E(1 - \cos\alpha) + z_1)^2 \tag{3.21}$$

$$|\underline{s}_2|^2 = \cos^2\beta \sin^2\alpha \; R_E^2 + ((z_2 + R_E) \sin\alpha' - \sin\beta \sin\alpha \, R_E)^2$$

$$+ ((z_2 + R_E) \cos\alpha' - \cos\alpha \, R_E)^2 \quad . \tag{3.22}$$

Finally, from the geometry we note that

$$dA = R_E^2 \sin\alpha \, d\alpha \, d\beta \quad . \tag{3.23}$$

Using the functional relationships, dA can be shown to reduce to (see Appendix II)

$$dA = \frac{|\underline{s}_1|^2}{\left[\csc^2\alpha - \csc\alpha \cot\alpha\left(\frac{z_1}{R_E} + 1\right)\right]} \frac{d\theta \, d\phi}{\sin\alpha} \quad . \tag{3.24}$$

Thus the spatial spectrum of the field is

$$\tilde{K}(\theta, \phi) = \frac{P_0 \, G_T(\theta_i, \phi_i)}{(4\pi)^2 \, |\underline{s}_2|^2} \, \sigma(\theta_s, \phi_s; \phi_i) \left| \frac{\sin\alpha}{1 - \cos\alpha\left(1 + \frac{z_1}{R_E}\right)} \right| \tag{3.25}$$

where ϕ_i, ϕ_s, θ_s and α all are defined in terms of θ and ϕ.

Before continuing we must consider the limiting factors on α and β. Clearly, restrictions on β are the same as those on θ; consequently they are not important. However, α can only be so large since we must consider the effect of the horizon. Consider the geometry in Fig. 5. Here we show the largest value of α, α_*, and the corresponding ϕ value. This occurs when the ray from the source just touches the surface of the earth. Thus

$$\cos\alpha_* = \frac{R_E}{R_E + z_1} \tag{3.26}$$

18-4-16411

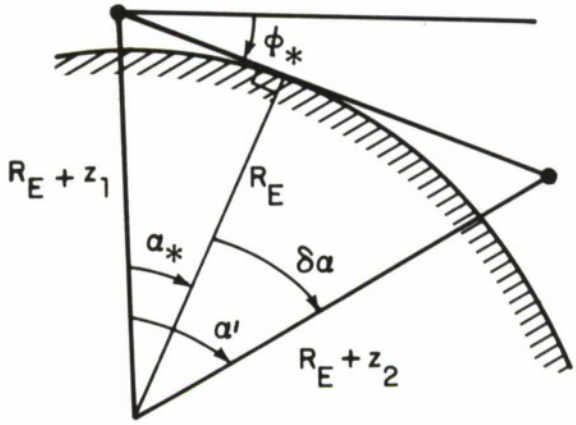

Fig. 5. Horizon cutoff.

is the maximum α_*. Thus all acceptable α are those such that

$$\cos \alpha > \frac{R_E}{R_E + z_1} \tag{3.27}$$

which implies

$$1 - \left(1 + \frac{z_1}{R_E}\right) \cos \alpha < 0 \quad . \tag{3.28}$$

For the case where $z_1 << R_E$

$$\alpha_* \approx \sqrt{\frac{2z_1}{R_E}} \quad . \tag{3.29}$$

To find the ground range to the target at this maximum angle we note that

$$\cos \delta\alpha = \frac{R_E}{R_E + z_2} \tag{3.30}$$

and the maximum ground range is

$$R_{max} = R_E \alpha' = R_E(\alpha_* + \delta\alpha) \quad . \tag{3.31}$$

In general, $z_2 << R_E$ so that

$$\delta\alpha \approx \sqrt{\frac{2z_2}{R_E}} \tag{3.32}$$

and the maximum range is

$$R_{max} \approx \sqrt{2z_2 R_E} + \sqrt{2z_1 R_E} \quad . \tag{3.33}$$

The corresponding minimum ϕ value is given by ϕ_*, where,

$$\phi_* = \tan^{-1}\left[\frac{\sqrt{z_1^2 + 2z_1 R_E}}{R_E}\right] \quad . \tag{3.34}$$

Then for $R_E \gg r_1$ we have

$$\boxed{\phi_* \approx \sqrt{\frac{2z_1}{R_E}}} \tag{3.35}$$

which is identical to α_*. This, of course, follows directly from the geometry in Fig. 5. We shall use this model in the next subsection to include the effects of shadowing.

3.4 Shadowing Effects

The evaluation of the incident power density upon a given aperture, as developed in the last two subsections, did not take into account the possibility that not all of the surface is irradiated. When the surface is rough, then the very nature of the roughness acts as a shadowing mechanism that prevents the incident radiation from falling on a reflecting surface. Furthermore, when the radiation is scattered, it may also find itself shadowed from the receiving point as a result of the same phenomenon.

Assume that we have some arbitrary surface with height, $\xi(x, y)$, which is a random field. Now consider the geometry shown in Fig. 6. A wave incident at angle ϕ_i at point x_s, y_s is scattered at angle ϕ_s. If this is a specular type of scattering, then the ray in the ϕ_s direction is the specular reflection. The normal $\underline{n}$ is the normal to the surface (x, y). The height of the surface is given by $\xi(x_s, y_s)$ at the point of scattering. Now we want to ask the question, what is the probability that the surface $\xi(x_s, y_s)$ is irradiated? What chance is there that the ray may be blocked by some large surface perturbation? The same question can also be asked about the scattered ray. To answer this question we shall follow the work of Wagner.

Wagner has derived a function, $S(\phi_i, \phi_s)$, which is the probability that a ray incident from angle ϕ_i does not get blocked and generate a scattered ray in direction ϕ_s, which is also not blocked. This function, called the shadowing function, is given by

$$S(\phi_i, \phi_s) = [1 - \exp(-2(B_i + B_s))] \cdot [\operatorname{erf}(v_i) + \operatorname{erf}(v_s)]/(4(B_i + B_s)) \tag{3.36}$$

where

$$B_k = \left[\exp\left(-v_k^2\right) - \sqrt{\pi}\, v_k \operatorname{erfc}(v_k)\right]/(4\sqrt{\pi}\, v_k) \tag{3.37}$$

$$v_k = |\cot \phi_k| / \sqrt{2s^2} \tag{3.38}$$

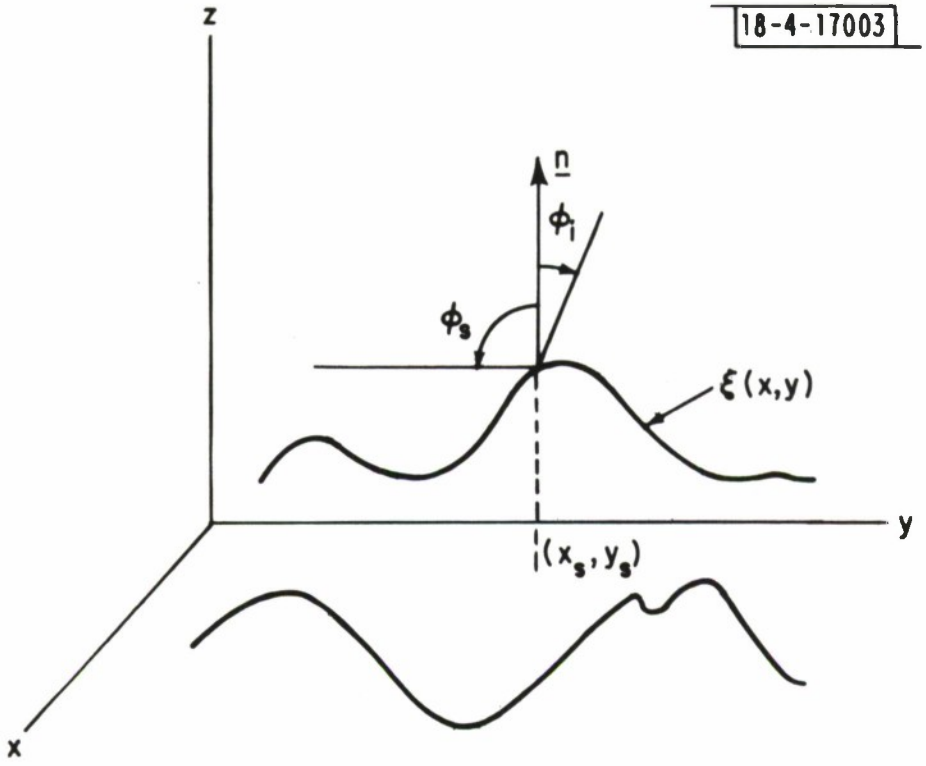

Fig. 6. General geometric scheme for shadowing.

where k = i or s and

$$\mathrm{erf}(x) = \int_{-\infty}^{x} \frac{1}{\sqrt{2\pi}} \exp(-x^2/2)\, dx \tag{3.39}$$

$$\mathrm{erfc}(x) = 1 - \mathrm{erf}(x) \quad . \tag{3.40}$$

Now note that for ϕ_i, ϕ_s close to $\pi/2$, we have that $\cot \phi_i$ and $\cot \phi_s$ are close to zero. Thus, v_i and v_s are close to zero. Therefore,

$$B_k \approx \exp\left(-v_k^2\right)/(4\sqrt{\pi}\, v_k) \tag{3.41}$$

so that

$$S(\phi_i, \phi_s) \approx \frac{1 - \exp\left(-\frac{1}{2\sqrt{\pi}\, v_i} - \frac{1}{2\sqrt{\pi}\, v_s}\right)}{\frac{1}{2\sqrt{\pi}\, v_i} + \frac{1}{2\sqrt{\pi}\, v_s}}$$

$$\approx \frac{2\sqrt{\pi}\, v_i\, v_s}{v_i + v_s} \tag{3.42}$$

which is itself quite small. Thus, at low angles, the shadowing is quite great. Furthermore, even if just one of the $\phi(s)$ is small, the corresponding B_k will be quite large so that $S(\phi_i, \phi_s)$ will be dominated by that term as expected.

As we shall note in the next subsection, these results will be important in modifying the channel spread function, particularly at angles away from the specular points where ϕ_i or ϕ_s approach $\pi/2$. Furthermore, this theory is also useful for modifying the ideas in specular multipath theory.

A more recent study of this effect has been made by Lynch and Wagner who considered both multiple scattering and energy conservation in the shadowing process. Their resulting functions show a 3-dB difference at lower angles (1°) and would probably be more appropriate at grazing angles. Their work is based upon that of Wagner and also Sancer.

3.5 Example of Channel Spread Functions

In the previous sections, we developed the theory to describe the statistical characteristics of the scattered field as viewed at a receiving aperture from both a flat surface and a spherical earth. Extensions to other arbitrary surfaces are possible and follow as a direct application of the theory. In this section, we evaluate the spread function for several different geometries and comment on the limitations of the theory as imposed by the approximation used.

The spread function $K(\theta, \phi)$ was evaluated for a spherical earth as given in Equation 3.25. In Figs. 7 through 11, we have plotted the function

$$10 \log_{10} \frac{K(\theta, \phi)}{(P_0/4\pi d^2)}$$

where d is the free space distance between transmitter and receiver. All plots are for sources at a height of 1 km above the earth's surface, and

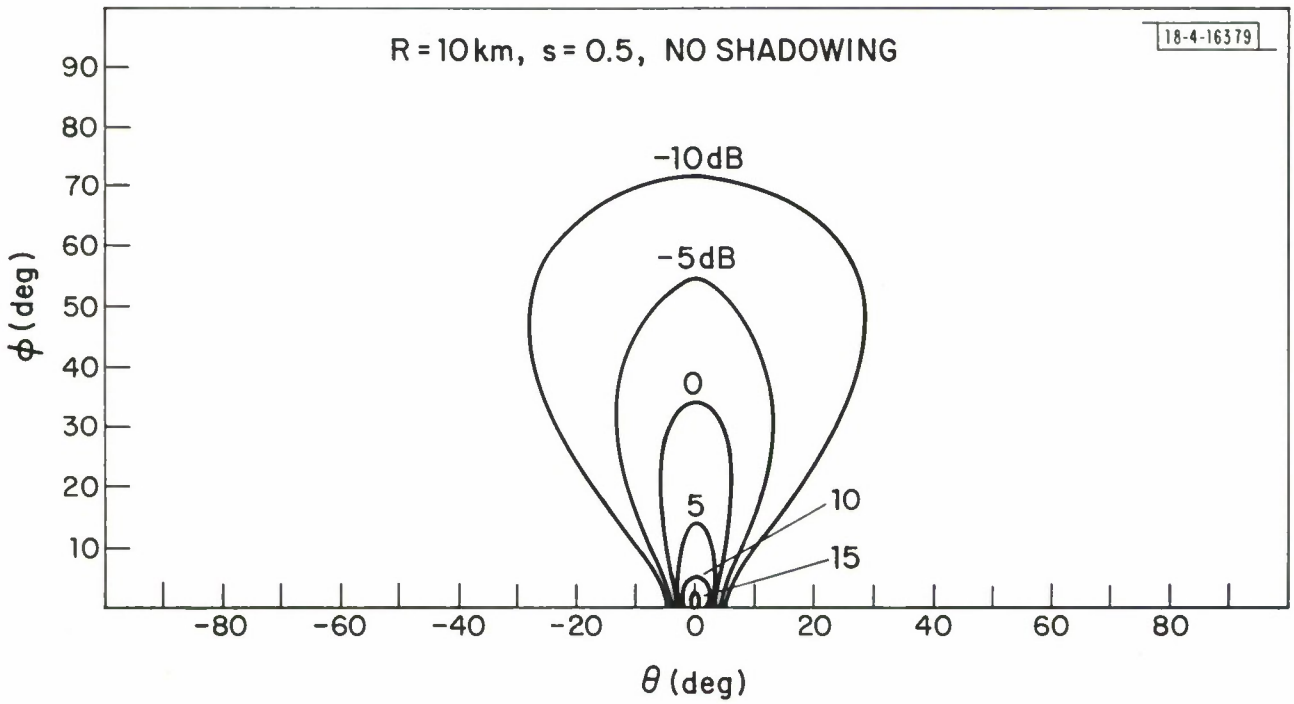

Fig. 7. Channel spread (R = 10 km, s = 0.5, no shadowing).

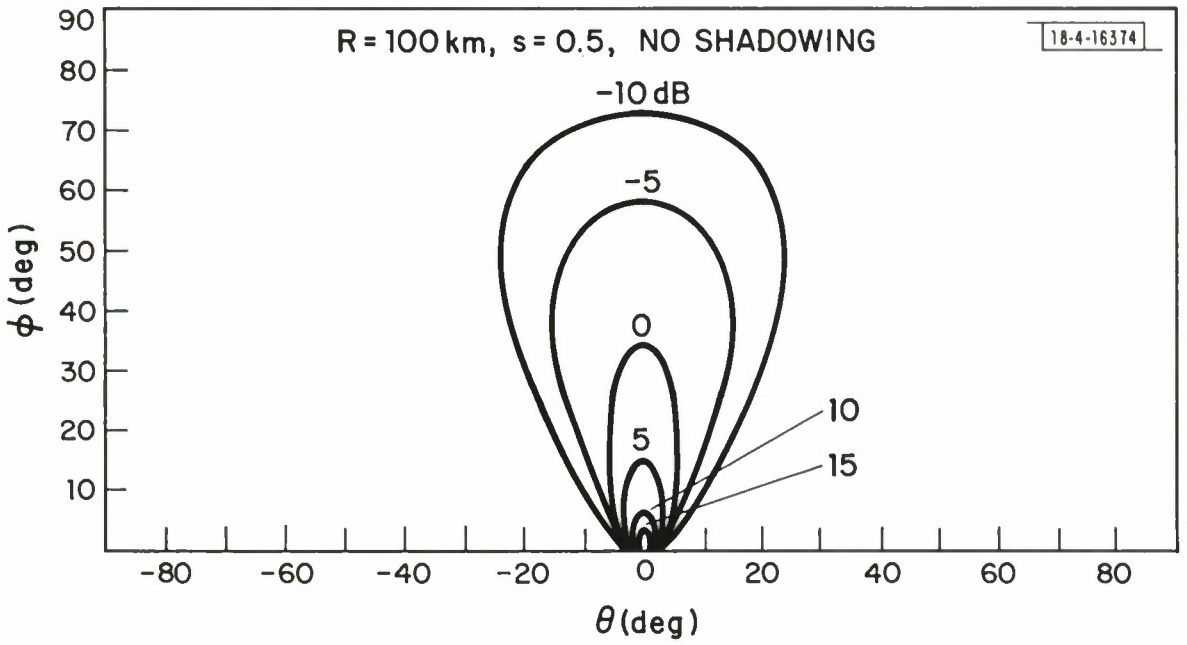

Fig. 8. Channel spread (R = 100 km, s = 0.5, no shadowing).

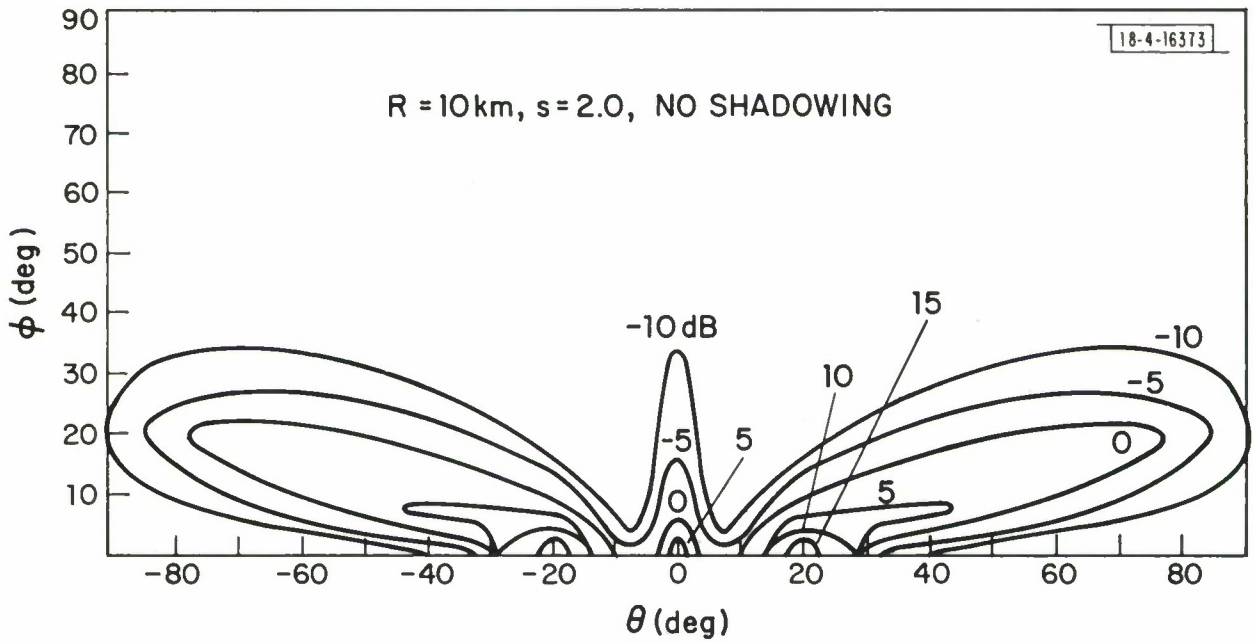

Fig. 9. Channel spread (R = 10 km, s = 2.0, no shadowing).

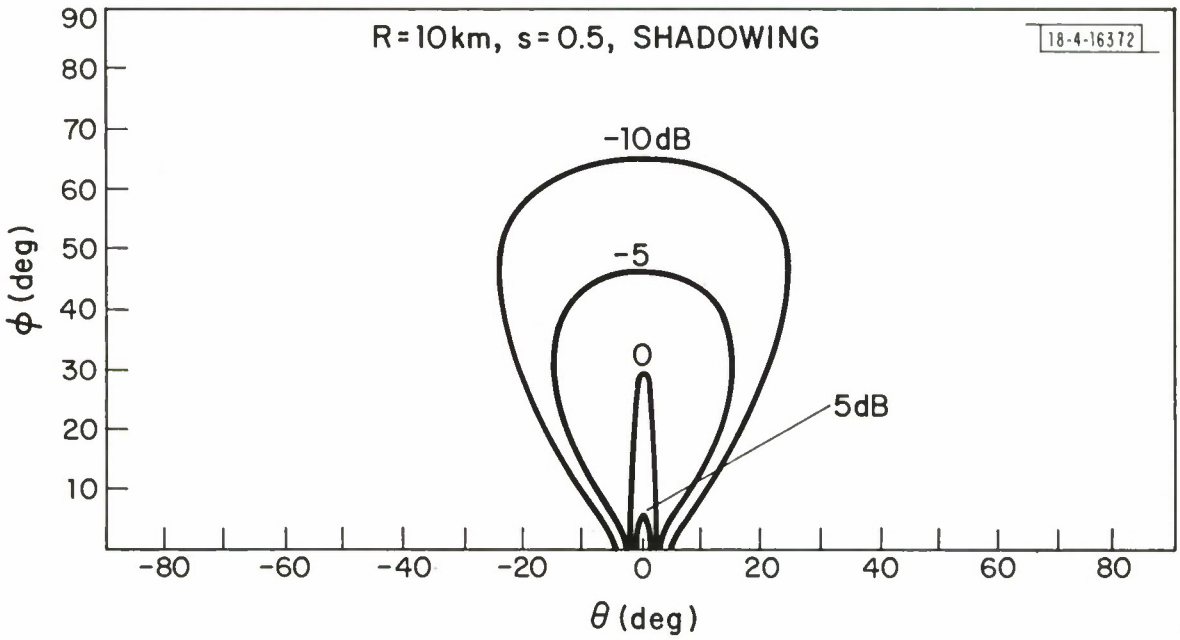

Fig. 10. Channel spread (R = 10 km, s = 0.5, shadowing).

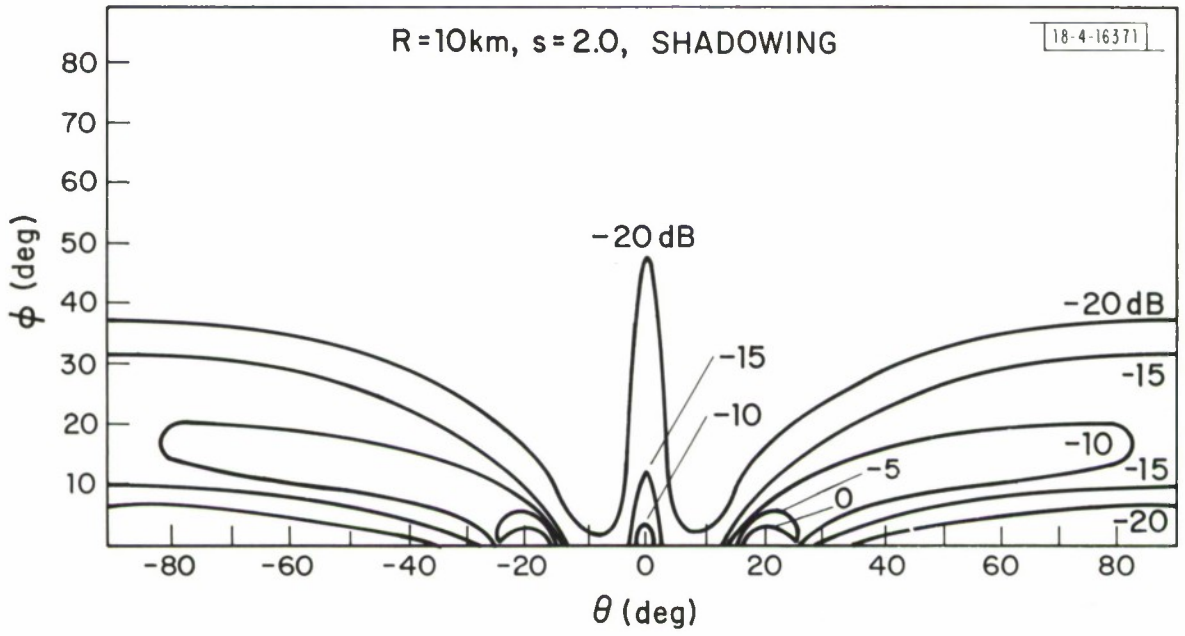

Fig. 11. Channel spread (R = 10 km, s = 2.0, shadowing).

receivers at a height of 10 m. For all the curves, we have assumed vertical polarization for the transmitter and receiver.

Figures 7 through 9 are for the case of no shadowing. In Fig. 7, the spread was evaluated for s = 0.5 and a range of 10 km. It can be noticed that most of the energy is concentrated close to the horizon (low elevation angles) and symmetrically about the boresight between transmitter and receiver. As the range of the transmitter (source) increases to 100 km, the profiles narrow. There is also some redistribution of the energy density not directly noticeable in these contours. As the slope increases to s = 2.0 in Fig. 9, a surprising effect occurs. The concentration of the energy in the central area disappears, and sidelobe behavior arises. This effect is due to the increased radius of curvature term in the scattering cross section.

In Appendix I, the average radius of curvature is given by

$$\begin{aligned} &< R_1 R_2 >_\ell \\ &= \frac{1}{|\hat{\underline{q}}|^2 D_\ell (\underline{n}_\ell \cdot \underline{e}_z)^4} \\ &= \frac{1}{k^2 |\underline{q}|^2 D_\ell (\underline{n}_\ell \cdot \underline{e}_z)^4} \end{aligned} \tag{3.43}$$

However, the integral, I_ℓ, used in the method of stationary phase was

$$I_\ell = \int\int \exp\left[j\frac{q_z}{2}\left(A_\ell (x - x_\ell)^2 + 2B_\ell (y - y_\ell)(x - x_\ell) + C_\ell (y - y_\ell)^2\right)\right] dx\, dy$$

$$= \frac{2\pi j}{|\underline{q}| D_\ell^{1/2} (\underline{n}_\ell \cdot \underline{e}_z)} \quad . \tag{3.44}$$

This integral was obtained by assuming that the distance to the receiver from the scattering surface was much larger than the dimensions of the scattering surface. Thus using Equation 3.44 in 3.43, we find

$$< R_1 R_2 >_\ell = |I_\ell|^2 \frac{(\underline{n}_\ell \cdot \underline{e}_z)^2 k^2}{(2\pi)^2} \tag{3.45}$$

which means that $|I_\ell|^2$ should be small compared to the distance between it and the receiver. Therefore, as $< R_1 R_2 >_\ell$ gets large and becomes comparable to this distance, the basic assumption begins to break down and the analysis will no longer hold. Therefore, for very large s values, the value of $\mathcal{R}$, the average radius of curvature can become excessive for certain values of γ, the angle between the z axis and the normal at the specular point. Thus it may be appropriate to actually limit the value of γ.

Recall that $\mathcal{R}$ is

$$\mathcal{R} = 0.1378\,\pi \frac{\sigma_\ell^2}{s^2} \sec^4 \gamma$$

$$= 0.1378\,\pi \frac{\sigma_\ell^4}{4\sigma_h^2} \sec^4 \gamma \tag{3.46}$$

Now for small γ, those close to the line-of-sight line between source and receiver, sec γ is almost unity. Then

$$\mathcal{R} \approx 0.1378\,\pi \frac{\sigma_\ell^4}{4\sigma_h^2} \quad . \tag{3.47}$$

If the average slope, s, is unity, then for large correlation lengths, σ_ℓ, $\mathcal{R}$ can be comparable to the distance squared between source and receiver, clearly a violation of the assumptions.

When shadowing is introduced, the profiles show a drastic change. Their basic shape is the same, but there is a 10-dB loss in amplitude due to shadowing. This effect is shown in Figs. 10 and 11.

The effects of shadowing can best be seen by evaluating the ratios of power densities received as a function of range. Specifically, the power density (watts/m^2) due to diffuse multipath is given by

$$\int_{-\pi/2}^{\pi/2} \int_{-\pi}^{\pi} K(\theta, \phi)\, d\theta d\phi$$

while that due to the free space propagation is $P_0/4\pi\, d^2$. Thus, in Figs. 12 and 13 we have plotted the ratio, P_r

$$P_r = 10 \log_{10} \left[\frac{\int_{-\pi/2}^{\pi/2} \int_{-\pi}^{\pi} K(\theta, \phi)\, d\theta d\phi}{P_0/(4\pi d^2)} \right] \qquad (3.48)$$

as a function of range. Here we have assumed an isotropic receiving antenna. This is in effect the ratio of diffuse to direct power. In Fig. 12, we have plotted this as a function of range for s = 2.0 and s = 0.5. Note that the rougher surface, s = 2.0, has a higher power level by about 1 dB. There is also some increase as the range decreases. The difference between the

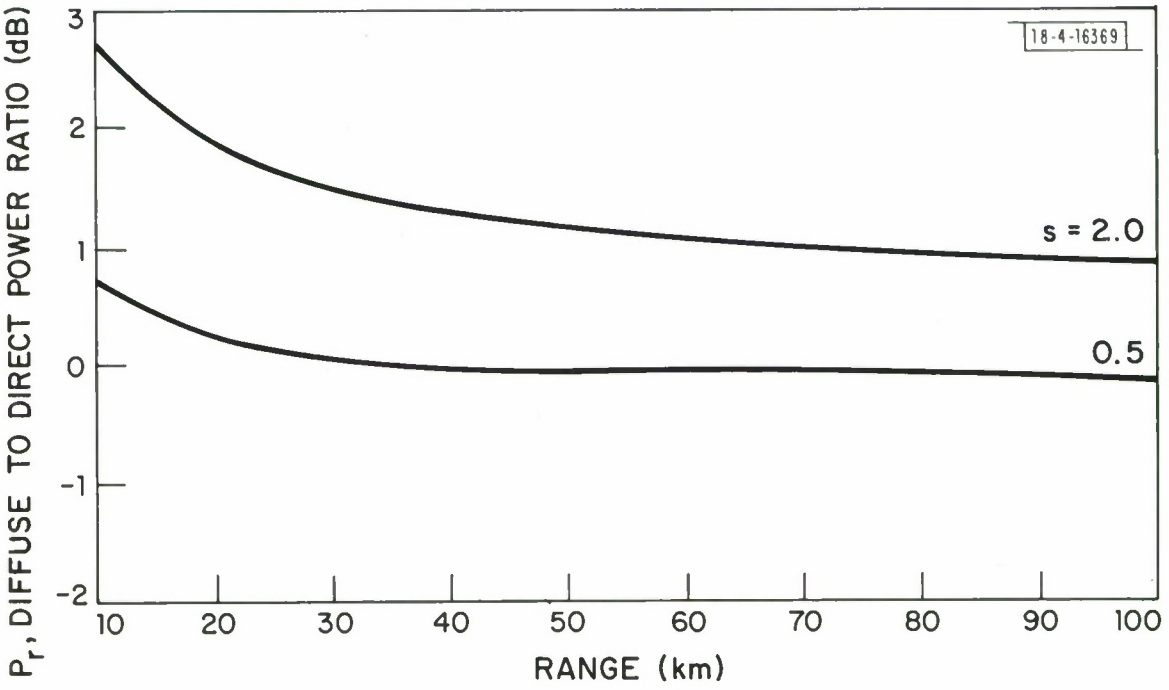

Fig. 12. Ratio of diffuse to direct power; no shadowing.

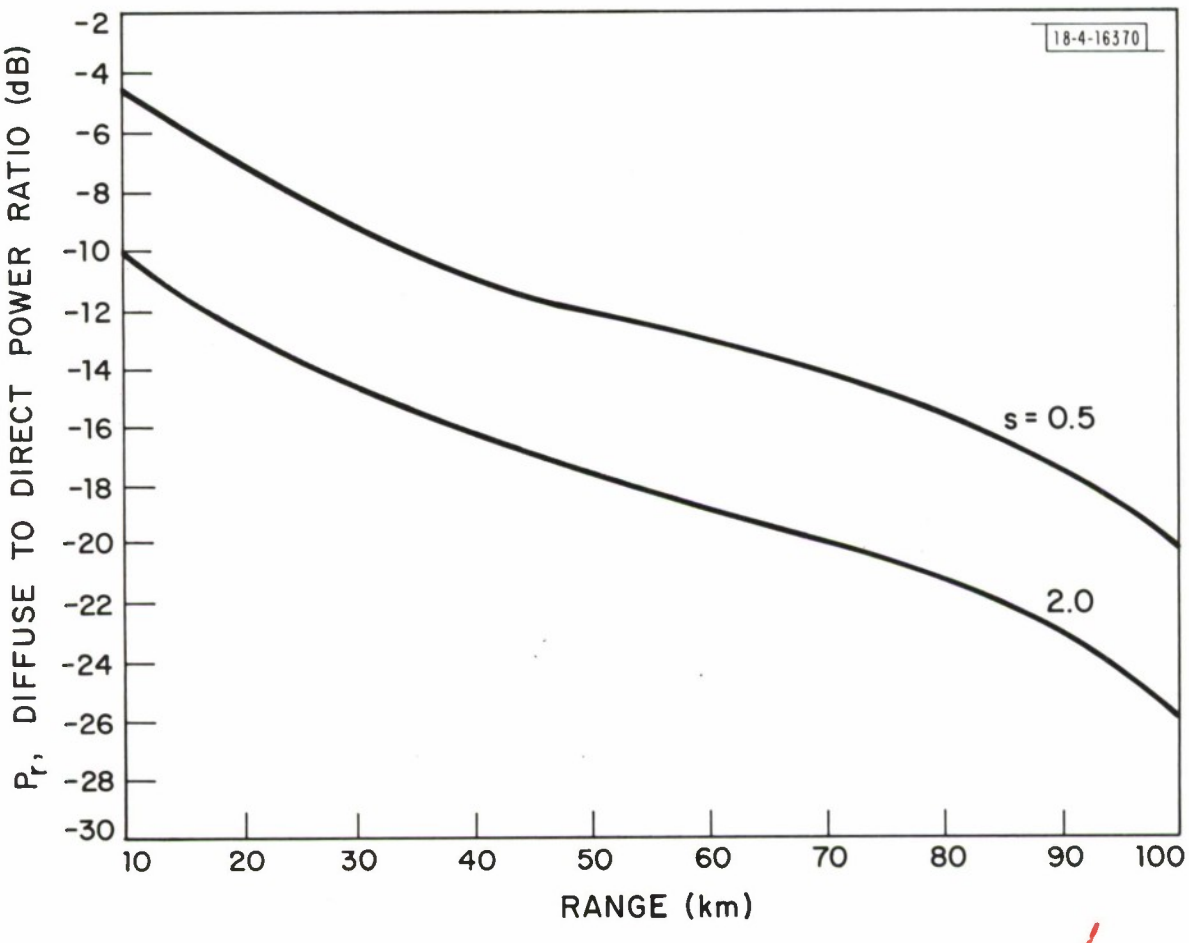

Fig. 13. Ratio of diffuse to direct power; shadowing.

two is accounted for by the sidelobe nature of the s = 2.0 case. In Fig. 13, we have plotted the ratio for the case where shadowing has been included. Now note the drastic difference. First, the levels are 10 to 20 dB lower. Second, there is a significant change with range as expected, i.e., at far ranges the incident rays are close to the surface and have high probabilities of being blocked. Third, the curves for s = 0.5 and s = 2 have been reversed. Now s = 0.5 is generally 6 dB higher than that for s = 2.0. This is a result of the shadowing occurring in the sidelobe region. In Fig. 14, we have separately considered P_r vs range for a slope of 0.3. This is a rough sea surface value as discussed by Barton. Again note the significant difference between the nonshadowed and shadowed case. Also note the peak in the nonshadowed case at 20-km range.

These curves clearly indicate that for these surface slopes and sensor geometries the diffuse multipath will in general be below the direct path level and, as will be shown in the next section, have little effect on position estimation accuracy. Moreover, when other surface slopes are considered, the levels of diffuse to direct power levels are about the same. For example, in Fig. 15 we have plotted P_r vs the rms surface slope s(s = 0.1 - 1.0) for z_1 = 10 m, z_2 = 1 km, and R = 30 km. These curves are for both shadowing and nonshadowing surfaces. Clearly for low values of s(s = 0.1), the diffuse power is greatest. This result is in agreement with Barton's recent work. For the case of no shadowing, the difference between s = 0.1 and s = 1 is 5.2 dB.

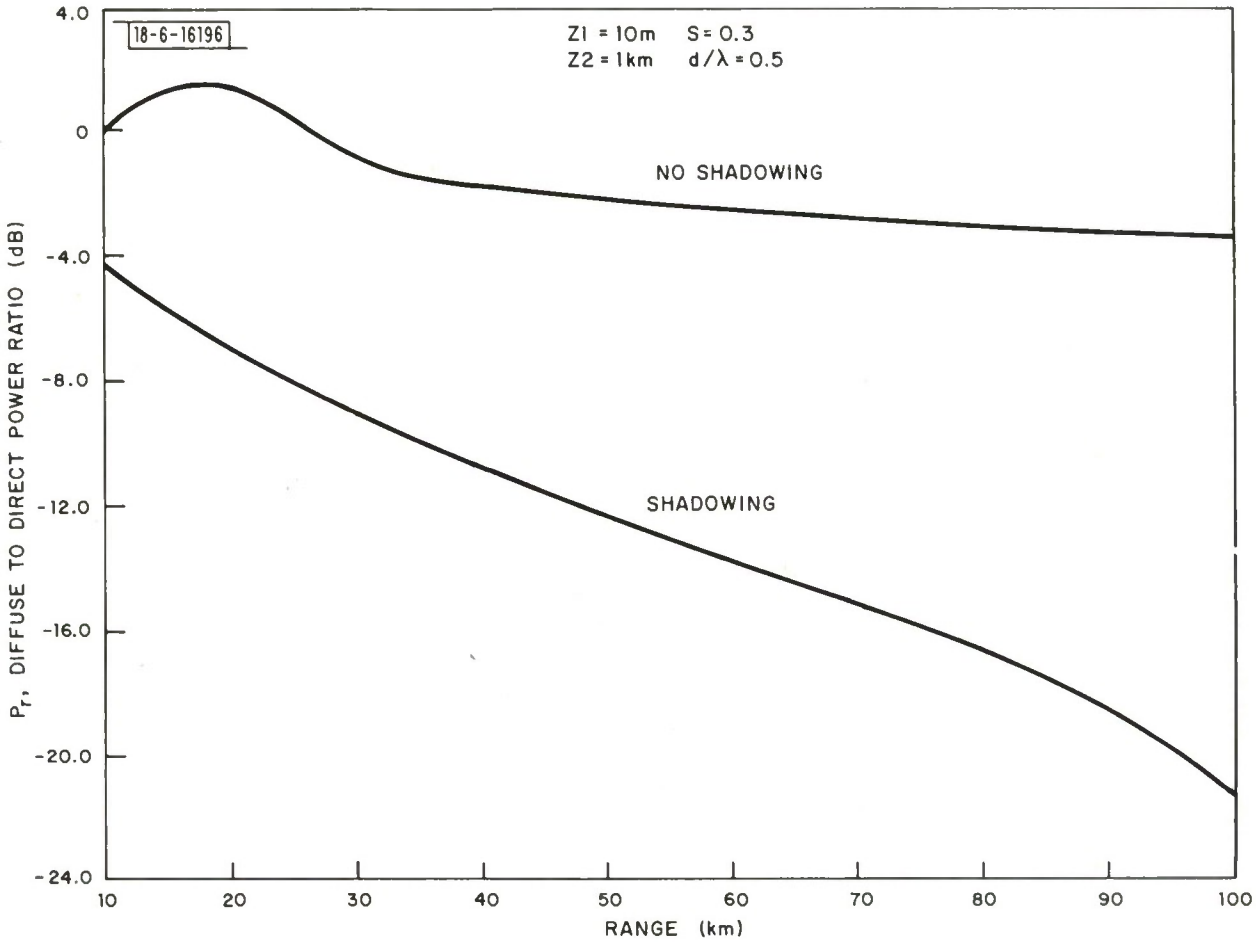

Fig. 14. Ratio of diffuse to direct power (z_1 = 10 m, z_2 = 1 km, s = 0.3).

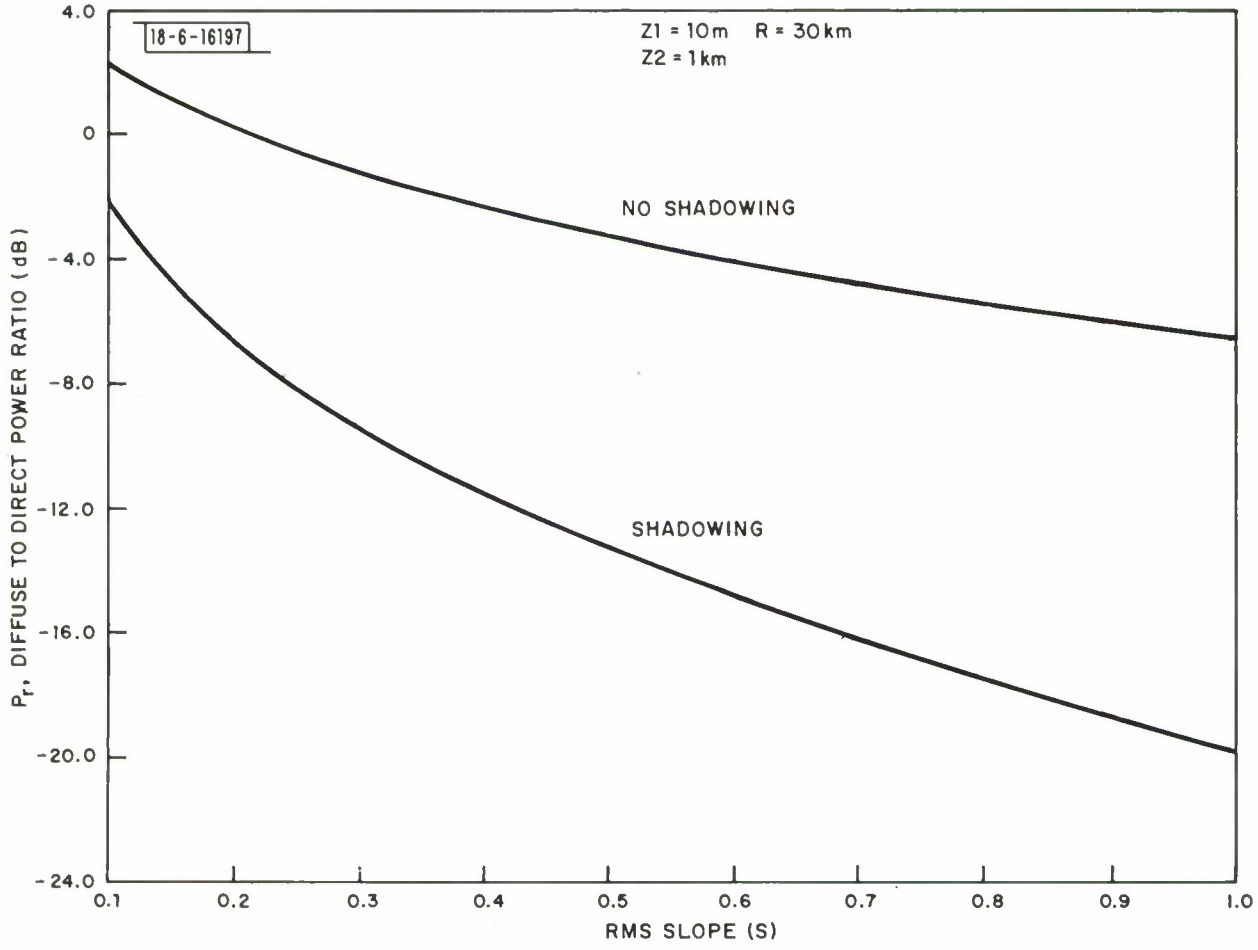

Fig. 15. P_r vs rms surface slope.

Section 4

ANTENNA PERFORMANCE EVALUATION

Diffuse multipath acts as a source of interference to angle estimation processors by presenting to them false sources of energy from directions other than the true one. Different processors have different performance characteristics. In this section we consider various forms of processors that result from different models for the received signals. Basically there are three models that we consider: Gaussian signal in Gaussian noise, an unknown but nonrandom signal, and a known signal. Each signal model results in a different processor. We also consider suboptimum schemes such as monopulse and compare it to the optimum schemes.

The purpose of this section is to consider how diffuse multipath affects the ability of an array to determine the angular location of a source of radiation. By considering a wide variety of processors from the optimum minimum mean square error estimator to monopulse, it is possible to see what one gives up for processor simplicity. We evaluate both processor form and performance for a wide variety of channel models.

In this section we will consider eight different processors that are used to estimate μ, the angle of arrival. Each of these processors results from a different model for the signal $\underline{\tilde{r}}$, that results from the time processing of the r-f outputs of the N sensors of the receiving antenna. Specifically we assume that the received signal at r-f has the form

$$\underline{r}(t) = \sqrt{2}\ \mathrm{Re}[\underline{\tilde{r}}(t)\ \exp(j\ 2\pi f_c t)] \tag{4.1}$$

where f_c is the carrier frequency and $\underline{\tilde{r}}(t)$ is the N x 1 vector of complex envelopes of the outputs (in phase and quadrature) of the N sensors. The N x 1 vector $\underline{\tilde{r}}$ is given by

$$\underline{\tilde{r}} = \frac{1}{\sqrt{T}} \int_0^T \underline{\tilde{r}}(t)\ dt \tag{4.2}$$

which represents matched filter detection of r-f burst signals. Other more complex time variations are possible and have been discussed elsewhere (see Van Trees [2]). The N x 1 vector $\underline{\tilde{r}}$ can be decomposed into three possible components as follows

$$\underline{\tilde{r}} = \sqrt{E_s}\ \tilde{b}\ \underline{\tilde{m}}(\mu) + \underline{\tilde{n}}_D + \underline{\tilde{w}} \tag{4.3}$$

where

$\tilde{b}\ \underline{\tilde{m}}(\mu)$ = the signal component due to the direct and specular path. μ is the angular location of the source of the radiation, and $\tilde{b}$ is a scalar complex envelope

$\underline{\tilde{n}}_D$ = the diffuse signal component. This is an N x 1 complex Gaussian zero mean random vector

$\underline{\tilde{w}}$ = the sensor noise. This also is an N x 1 complex zero mean Gaussian random vector

and E_s is the signal energy.

This model for the received signal is a canonical one. The variations in processors result from the varying assumptions that are made on the nature of $\tilde{b}$. Specifically $\tilde{b}$ may be a complex Gaussian random variable, an unknown but nonrandom constant or a known deterministic constant. Furthermore, processors may be structured with and without $\tilde{n}_D$ being present. When $\tilde{n}_D$ is absent the result is a nonspread processor.

The covariance matrices for $\underline{\tilde{n}}_D$ and $\underline{\tilde{w}}$ are

$$\tilde{K}_n(\mu) = E[\underline{\tilde{n}}_D \underline{\tilde{n}}_D^{\dagger}] \tag{4.4}$$

$$\tilde{K}_w = E[\underline{\tilde{w}} \underline{\tilde{w}}^{\dagger}] \quad . \tag{4.5}$$

In both cases they are Hermitian. We further assume that (see McGarty [4]) $\tilde{K}_w^{-1}$ can be factored as

$$\tilde{K}_w^{-1} = \tilde{W}^{\dagger} \tilde{W} \tag{4.6}$$

where $\tilde{W}$ is an N x N complex matrix called a whitening matrix.

To determine the optimum processor for each possible variation we first need to determine the likelihood function. This is determined from the binary hypothesis problem where under H_1 and H_0 we have

$$H_1: \underline{\tilde{r}} = \sqrt{E_s}\, \tilde{b}\, \underline{\tilde{m}}(\mu) + \underline{\tilde{n}}_D + \underline{\tilde{w}} \tag{4.7}$$

$$H_0: \underline{\tilde{r}} = \underline{\tilde{w}} \quad . \tag{4.8}$$

Note that the dummy or H_0 hypothesis contains only noise. This results from the assumption that $\underset{\sim}{n}_D$ arises as a direct result of the presence of the specular signal. Thus, when that portion is absent, so too is the diffuse component. Note also that $\tilde{K}_n(\mu)$ is a function of μ, the source direction.

The likelihood ratio $\Lambda(\underset{\sim}{r}, \mu)$ is given by

$$\Lambda(\underset{\sim}{r}, \mu) = \frac{p(\underset{\sim}{r} \mid H_1)}{p(\underset{\sim}{r} \mid H_0)} \quad . \tag{4.9}$$

The maximum likelihood processor for μ then is the one that uses $\Lambda(\underset{\sim}{r}, \mu)$ and finds that value of μ to yield the maximum. The log likelihood function is similarly defined as

$$\ell(\underset{\sim}{r}, \mu) = \ell n\, \Lambda(\underset{\sim}{r}, \mu) \quad . \tag{4.10}$$

Finally for unbiased estimates we have for the Cramer-Rao bound on σ_μ^2,

$$\sigma_\mu^2 \geq \frac{-1}{E\left[\frac{\partial^2}{\partial \mu^2} \ell(\underset{\sim}{r}, \mu)\right]} \quad . \tag{4.11}$$

In the following subsections we shall use this canonical model and provide statistics on $\tilde{b}$ so that $\ell(\underset{\sim}{r}, \mu)$ and the C-R bound can be evaluated.

4.1 The Gauss-in-Gauss Problem

The first case assumes that $\tilde{b}$ is a zero mean complex Gaussian random variable with

$$\sigma_b^2 = E[\tilde{b}\,\tilde{b}^*] \quad . \tag{4.12}$$

The likelihood function for this processor has been derived by McGarty [1 - 5], and is

$$\boxed{\Lambda(\underline{\tilde{r}}, \mu) = \frac{|\tilde{K}_T|}{|\tilde{K}_w|} \exp\left[\frac{1}{2}\,\underline{\tilde{r}}^{\dagger}\,\tilde{K}_w^{-1}\,\tilde{K}_b\,[\tilde{K}_b + \tilde{K}_w]^{-1}\,\underline{\tilde{r}}\right]} \tag{4.13}$$

where

$$\tilde{K}_b = E_s\,\sigma_b^2\,\underline{\tilde{m}}(\mu)\,\underline{\tilde{m}}^{\dagger}(\mu') + \tilde{K}_n(\mu) \tag{4.14}$$

$$\tilde{K}_T = \tilde{K}_b[\tilde{K}_b + \tilde{K}_w]^{-1}\,\tilde{K}_w \quad . \tag{4.15}$$

It has been shown elsewhere that $\tilde{K}_b[\tilde{K}_b + \tilde{K}_w]^{-1}\,\tilde{r}$ is the minimum mean square error (MMSE) estimate of the N x 1 vector $\tilde{b}\,\underline{\tilde{m}}(\mu) + \underline{\tilde{n}}_D$. In Fig. 16, we have used this fact to sketch the maximum likelihood estimator in the estimator-correlator form. The processor works in the following fashion. The vector $\underline{\tilde{r}}$ is received and then whitened through $\underline{\tilde{W}}$. Then for each value of μ, an estimate of the direct signal plus diffuse multipath signal is made and cross correlated with the whitened signal (denoted as $\underline{\tilde{r}}_w$). As μ is scanned

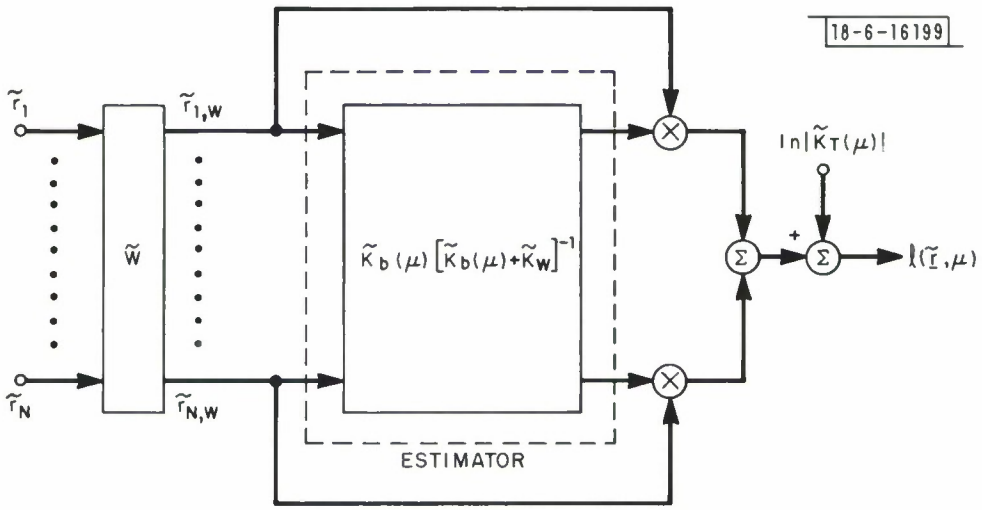

Fig. 16. Gauss-in-Gauss; optimum spread.

through all values, $\ell(\underset{\sim}{\tilde{r}}, \mu)$ is recorded and that value of μ maximizing $\ell(\underset{\sim}{\tilde{r}}, \mu)$ is the estimate. In general for practical applications, fixed beams are formed and suboptimum processing follows.

The performance of this processor could in theory be evaluated. No known exact calculations exist due to the dependence of $\tilde{K}_b(\mu)$ on μ. Parallels with continuous time results can be made (see Van Trees [2], Chpt. 7).

In a similar fashion we can consider the case of an unspread channel. For this case we set $\underset{\sim}{\tilde{n}}_D$ identically to zero (letting $\underset{\sim}{\tilde{K}}_n = 0$). The resulting likelihood function has been evaluated by McGarty [1] and is

$$\boxed{\Lambda(\underset{\sim}{\tilde{r}}, \mu) = \frac{\sigma_T^2}{\sigma_b^2} \exp\left[\frac{\sigma_T^2}{2} \underset{\sim}{\tilde{r}}^\dagger \tilde{K}_w^{-1} \tilde{m}(\mu) \tilde{m}^\dagger(\mu) K_w^{-1} \underset{\sim}{\tilde{r}}\right]} \tag{4.16}$$

where

$$\sigma_T^2 = \frac{E_s \sigma_b^2}{1 + E_s \sigma_b^2 \underset{\sim}{\tilde{m}}(\mu) \tilde{K}_w^{-1} \underset{\sim}{\tilde{m}}(\mu)} \quad . \tag{4.17}$$

This form can be put into the estimator-correlator form by noting that the MMSE estimate of the scalar $\tilde{b}$, $\hat{\tilde{b}}$, is given by

$$\hat{\tilde{b}} = \sigma_T^2 \underset{\sim}{\tilde{m}}^\dagger(\mu) \tilde{K}_w^{-1} \underset{\sim}{\tilde{r}} \quad . \tag{4.18}$$

Thus $\Lambda(\tilde{\underline{r}}, \mu)$ becomes

$$\Lambda(\tilde{\underline{r}}, \mu) = \frac{\sigma_T^2}{\sigma_b^2} \exp\left[\frac{\hat{\tilde{b}}}{2} \tilde{\underline{r}} \ \underline{W}^\dagger \underline{W} \ \underline{m}(\mu)\right] \quad . \tag{4.19}$$

This processor is diagrammed in Fig. 17. Note now that the covariance does not depend on μ. Thus, the performance bound is readily determined. Specifically

$$E\left[\frac{\partial^2}{\partial \mu^2} \ell(\tilde{\underline{r}}, \mu)\right]$$

$$= E_s^2 \sigma_T^2 \sigma_b^2 \left[\left(2 + \frac{\sigma_T^2}{\sigma_B^2}\right)\left(\frac{\partial}{\partial \mu} B(\mu; 0)\right)^2 \right.$$

$$\left. - \frac{1}{E_s \sigma_T^2} \frac{\partial^2}{\partial \mu^2} B(\mu; 0) + \frac{\partial^2}{\partial \mu^2} \left| B(\mu, \mu') \right|^2 \Big|_{\mu' = 0}\right] \tag{4.20}$$

where

$$B(\mu, \mu') = \tilde{\underline{m}}(\mu) \ \tilde{K}_w^{-1} \ \tilde{\underline{m}}(\mu + \mu') \quad . \tag{4.21}$$

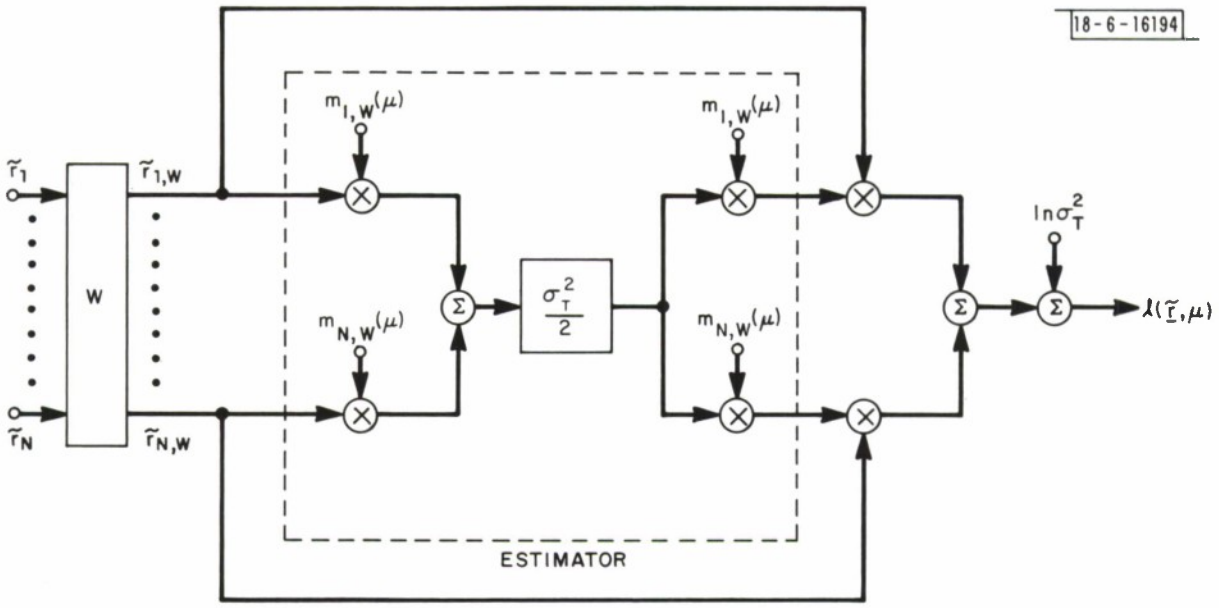

Fig. 17. Gauss-in-Gauss; optimum unspread.

In general K_w^{-1} is Toeplitz, and the inversion follows the simplified Levinsion algorithm (see McGarty [4]). This model is useful for describing interference environments in the ATC context. The bound on σ_μ^2 follows directly from the CR inequality.

In the preceding processor, it was seen that the dependence of K_w on μ was not present and the result was a simplified processor. A suboptimum processor can be generated by assuming that the specular and diffuse components were scalar random variables. The resulting processor would be one that would be used in the case of an unspread channel where merely a power or energy increase was observed. Specifically if we let

$$\tilde{K}_w = N_0 I \tag{4.22}$$

where I is the N x N identity matrix and N_0 the noise spectral height, then the suboptimum processor would be

$$\boxed{\Lambda(\tilde{r}_1, \mu) = \frac{\frac{N_0}{2}}{\frac{\sigma_B^2}{N} + \frac{N_0}{2}} \exp\left[\frac{1}{2}\left|\tilde{r}_1\right|^2\right]} \tag{4.23}$$

where

$$\tilde{r}_1 = \left[\frac{\sigma_B^2/N}{\frac{N_0}{2}\left(\frac{\sigma_B^2}{N} + \frac{N_0}{2}\right)}\right]^{1/2} \underline{\tilde{m}}^\dagger(\mu)\, \underline{\tilde{r}} \tag{4.24}$$

$$\sigma_B^2 = N^2 E_s \sigma_b^2 + E_s \int_{-1}^{1} K(\mu, \mu')\, B(\mu - \mu')\, d\mu' \quad . \tag{4.25}$$

Careful comparison with the preceding processor indicates that this sub-optimum processor is identical to that of the nonspread Gauss-in-Gauss problem discussed above. Thus, the processor is diagrammed exactly as in Fig. 17 with the appropriate changes. The performance of this processor is given by the bound

$$\sigma_\mu^2 \geq -\left[C\left[\frac{\partial^2}{\partial\mu^2} B(\mu)\Big|_{\mu=0} + \sigma_i^2 \int_{-1}^{1} K(\mu') \frac{\partial^2}{\partial\mu'^2} B(\mu')\, d\mu'\right]\right]^{-1} \tag{4.26}$$

which is valid only for azimuth estimation. Also

$$C = \frac{1 + \dfrac{\sigma_i^2}{N^2} \displaystyle\int_{-1}^{1} K(\mu')\, B(\mu')\, d\mu'}{N\sigma_n^2\left[1 + \dfrac{\sigma_i^2}{N^2} \displaystyle\int_{-1}^{1} K(\mu')\, B(\mu')\, d\mu' + \dfrac{\sigma_n^2}{N}\right]} \tag{4.27}$$

and $K(\mu)$ is given by the transformation

$$K(\mu) = \frac{\displaystyle\int_{-\pi/2}^{\pi/2} G(\phi)\, K(\theta, \phi)\, d\phi \frac{1}{\sqrt{1-\mu^2}}}{\displaystyle\int_{-\pi/2}^{\pi/2}\int_{0}^{2\pi} G(\phi)\, K(\theta, \phi)\, d\theta\, d\phi} \tag{4.28}$$

where $G(\phi)$ is the antenna gain in elevation. The function $1/\sqrt{1-\mu^2}$ is a Jacobian resulting from the transformation, $\mu = \cos\theta$. The function $K(\mu)$ is normalized to have unit area.

The remaining function is the array ambiguity function given by the expression

$$B(\mu) = \left| \underline{\tilde{m}}(\mu') \, \underline{\tilde{m}}^{\dagger}(\mu' + \mu) \right|^2 \tag{4.29}$$

with σ_i^2 the interference-to-signal ratio, σ_n^2 the noise-to-signal ratio per dipole, k_0 the wave number $(2\pi/\lambda_0)$, and d_i the distance from the array phase center to the ith sensor (dipole), and $\dagger$ denoting the complex conjugate transpose. Furthermore, we can relate σ_θ^2, the azimuth variance, to σ_μ^2 by

$$\sigma_\theta^2 = \tan^2 \theta \left[-1 + \sqrt{1 + \frac{2 \cot^2 \theta}{\sin^2 \theta} \sigma_\mu^2} \right] . \tag{4.30}$$

These are the three classes of processors used for the Gauss-in-Gauss problem. They all entail whitening arguments and, except for the first, the performance can be obtained directly.

A special case of interest in the Gauss-in-Gauss problem is the unspread channel with

$$\tilde{K}_w = \sigma_n^2 I \tag{4.31}$$

and a linear array with spacing d_0 between sensors. For this case it is easily shown that

$$\boxed{\sigma_\mu^2 \geq \frac{12}{\left(\frac{E_s \sigma_b^2}{\sigma_n^2}\right)\left(\frac{2\pi d_0}{\lambda}\right)^2 N(N^2 - 1)} \left[1 + \frac{\sigma_n^2}{N E_s \sigma_b^2} \right]} . \tag{4.32}$$

This represents a performance benchmark for the Gauss-in-Gauss problem.

4.2 Unknown but Nonrandom

A second model for the specular source, $\tilde{b}$, is as an unknown but nonrandom complex variable, i.e., we let

$$\tilde{b} = Ae^{j\varphi} \tag{4.33}$$

where A is the amplitude and φ the phase. Since both are unknown, the likelihood estimate of both A and φ are obtained and used in the likelihood ratio. Using this, the likelihood ratio is obtained using the generalized likelihood ratio. Specifically,

$$\Lambda(\underline{r}, \mu) = \max_{A, \varphi} \frac{p(\tilde{\underline{r}} | H_1, A, \varphi)}{p(\tilde{\underline{r}} | H_0)} \quad . \tag{4.34}$$

This technique has been used by Hofstetter and DeLong in their study of amplitude comparison monopulse. We define

$$\tilde{K}_1 = \tilde{K}_n + \tilde{K}_w \tag{4.35}$$

$$\tilde{K}_0 = \tilde{K}_w \quad . \tag{4.36}$$

Then N beams are formed by taking the received vector $\underset{\sim}{r}$ and projecting it onto vectors $\underset{\sim}{g}_i(\mu')$. The beam gains $G_i(\mu - \mu')$ for the ith beam are defined as

$$G_i(\mu - \mu') = \underset{\sim}{g}_i^{\dagger}(\mu')\, \underline{m}(\mu) \tag{4.37}$$

where μ' represents the known pointing directions of the ith beam. We further require that the $\underset{\sim}{g}_i(\mu')$ are orthogonal, i.e.,

$$\underset{\sim}{g}_i^{\dagger}(\mu')\, \underset{\sim}{g}_j(\mu') = \begin{cases} N & i=j \\ 0 & i\neq j \end{cases} . \tag{4.38}$$

We shall demonstrate shortly how this can be interpreted in the sense of sum-difference monopulse. Using these beams we obtain M complex measurements $\underset{\sim}{r}_i$ where

$$\underset{\sim}{r}_i = Ae^{j\varphi} G_i(\mu) + \underset{\sim}{n}_{gi} + \underset{\sim}{w}_{gi} \quad i = 1, \ldots, M \tag{4.39}$$

where

$$\underset{\sim}{n}_{gi} = \underset{\sim}{g}_i^{\dagger}\, \underline{n} \tag{4.40}$$

$$\underset{\sim}{w}_{gi} = \underset{\sim}{g}_i^{\dagger}\, \underline{w} \quad . \tag{4.41}$$

Using the orthogonality of $\tilde{\underline{g}}_i$, it can be shown that for independent $\tilde{\underline{w}}$, the corresponding

$$\tilde{w}_g = \begin{bmatrix} \tilde{w}_{g1} \\ \vdots \\ \tilde{w}_{gM} \end{bmatrix} = \tilde{G}\,\tilde{w} \tag{4.42}$$

where

$$\tilde{G} = \begin{bmatrix} \tilde{\underline{g}}_1^{\dagger} \\ \vdots \\ \tilde{\underline{g}}_M^{\dagger} \end{bmatrix} . \tag{4.43}$$

Then define

$$\tilde{K}_{g1} = \tilde{G}\,\tilde{K}_1\,\tilde{G}^{\dagger} \tag{4.44}$$

$$\tilde{K}_{g0} = \tilde{G}\,\tilde{K}_0\,\tilde{G}^{\dagger} . \tag{4.45}$$

Using this we can obtain the log likelihood ratio $\ell(\tilde{\underline{r}}, \mu)$ as

$$\boxed{\ell(\tilde{\underline{r}}, \mu) = \max_{A,\varphi} \left[-\frac{1}{2} (\tilde{\underline{r}} - Ae^{j\varphi}\,\tilde{\underline{g}})^{\dagger}\ \tilde{K}_{g1}^{-1} (\tilde{\underline{r}} - Ae^{j\varphi}\,\tilde{\underline{g}}) + \frac{1}{2}\,\tilde{\underline{r}}^{\dagger}\,\tilde{K}_{g0}^{-1}\,\tilde{\underline{r}} + \ell n\left|\tilde{K}_{g1}\right| - \ell n\left|\tilde{K}_{g0}\right| \right]} \tag{4.46}$$

where $\underset{\sim}{\tilde{r}}$ is the M x 1 vector of beam projections and

$$\underset{\sim}{\tilde{g}} = \begin{bmatrix} G_1 \\ \cdot \\ \cdot \\ \cdot \\ G_M \end{bmatrix} = \tilde{G}\, \underset{\sim}{\tilde{m}}(\mu) \quad . \tag{4.47}$$

or

$$\underset{\sim}{\tilde{g}} = \tilde{G}\, \underset{\sim}{\tilde{m}}(\mu) \quad . \tag{4.48}$$

Following Hofstetter and Delong we obtain for $\hat{A}$

$$\hat{A} = \frac{\mathrm{Re}\left[e^{j\varphi}\, \underset{\sim}{\tilde{r}}^{\dagger}\, \tilde{K}_{g1}^{-1}\, \underset{\sim}{\tilde{g}}\right]}{\underset{\sim}{\tilde{g}}^{\dagger}\, \tilde{K}_{g1}^{-1}\, \underset{\sim}{\tilde{g}}} \tag{4.49}$$

and

$$\hat{\varphi} = -\arg\left[\underset{\sim}{\tilde{r}}^{\dagger}\, \tilde{K}_{g1}^{-1}\, \underset{\sim}{\tilde{g}}\right] \quad . \tag{4.50}$$

Using these in the likelihood ratio we obtain

$$\ell(\underset{\sim}{\tilde{r}}, \mu) = -\frac{1}{2}\, \underset{\sim}{\tilde{r}}^{\dagger} (\tilde{K}_{g1}^{-1} - \tilde{K}_{g0}^{-1})\, \underset{\sim}{\tilde{r}} + \frac{1}{2} \frac{\left|\underset{\sim}{\tilde{r}}\ \tilde{K}_{g1}^{-1}\, \underset{\sim}{\tilde{g}}\right|^2}{\underset{\sim}{\tilde{g}}^{\dagger}\, \tilde{K}_{g1}^{-1}\, \underset{\sim}{\tilde{g}}} + \ln\left|\tilde{K}_{g1}\right| - \ell n\left|\tilde{K}_{g0}\right| \quad . \tag{4.51}$$

Now recall that $\tilde{\underline{g}}$ and K_{g1} depend upon μ. Thus the processor as shown in Fig. 18 performs as other processors by scanning through all μ directions.

The performance of processors of this form is quite involved and have been discussed at length by Hofstetter and DeLong.

4.3 Known Signal

When the complex number $\tilde{b}$ is known, a different set of processors occurs. Let us again consider the case where $\tilde{r}$ is the N x 1 sensor outputs. Define

$$\tilde{\underline{s}}_0 = \tilde{\underline{b}}\,\tilde{\underline{m}}(\mu) \tag{4.52}$$

and $\tilde{K}_1$ and $\tilde{K}_0$ as before. Then

$$\ell(\tilde{\underline{r}},\mu) = \ell n \frac{|\tilde{K}_0|}{|\tilde{K}_1|} - \frac{1}{2}(\tilde{\underline{r}} - \tilde{\underline{s}}_0)^{\dagger}\,\tilde{K}_1^{-1}(\tilde{\underline{r}} - \tilde{\underline{s}}_0)$$

$$+ \frac{1}{2}\,\tilde{\underline{r}}\;K_0^{-1}\;\tilde{\underline{r}} \quad . \tag{4.53}$$

Recalling that the MMSE estimate of $\tilde{\underline{n}}$ can be given by

$$\hat{\tilde{\underline{n}}} = \tilde{\underline{K}}_n(\tilde{\underline{K}}_n + \tilde{\underline{K}}_w)^{-1}\,\tilde{\underline{r}} \quad . \tag{4.54}$$

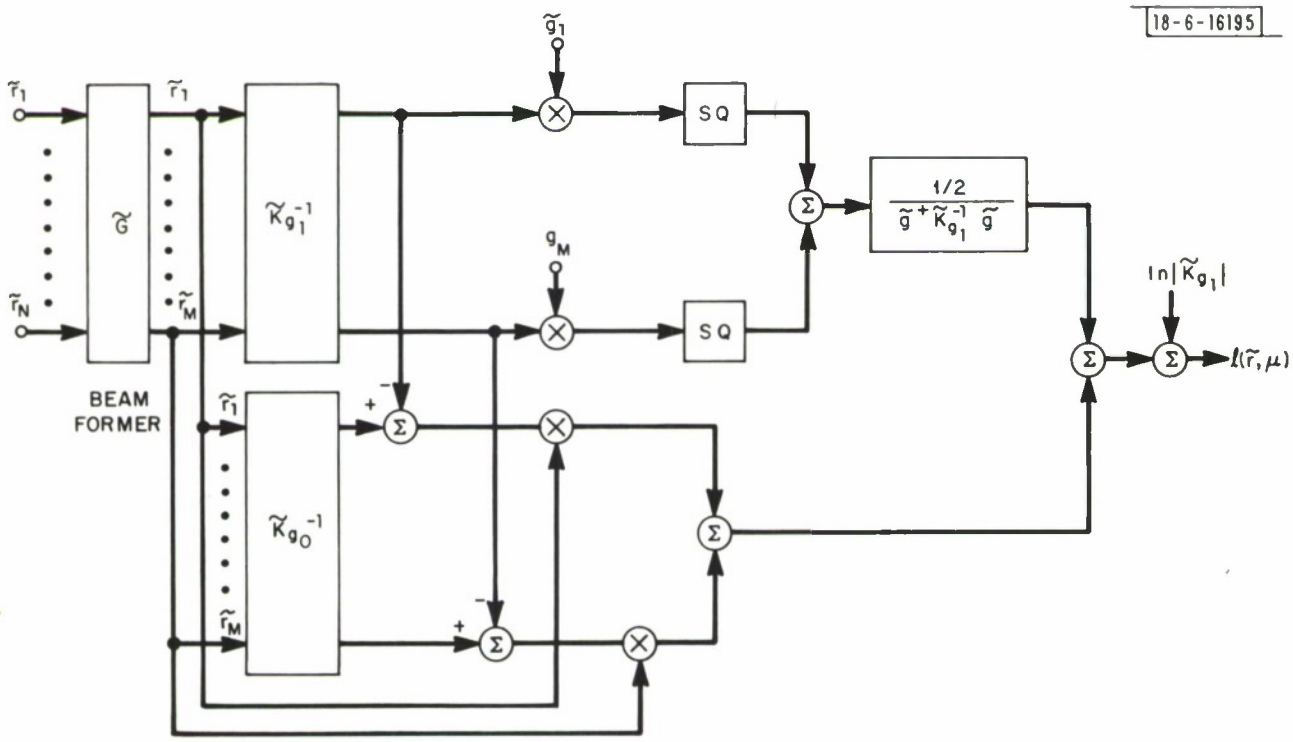

Fig. 18. Unknown but nonrandom.

Then $\ell(\underline{\tilde{r}}, \mu)$ can be obtained

$$\ell(\underline{\tilde{r}}, \mu) = \ell n \frac{|\tilde{K}_1|}{|\tilde{K}_0|} + \frac{1}{2} (\underline{\tilde{r}} - \underline{\tilde{s}}_0)^\dagger \tilde{K}_0^{-1} \underline{\hat{\tilde{n}}} + \frac{1}{2} \underline{\tilde{r}}^\dagger \tilde{K}_0^{-1} \underline{\tilde{s}}_0 + \frac{1}{2} \underline{\tilde{s}}_0^\dagger \tilde{K}_0^{-1} \underline{\tilde{r}} - \frac{1}{2} \underline{\tilde{s}}_0^\dagger \tilde{K}_0^{-1} \underline{\tilde{s}}_0 \quad . \tag{4.55}$$

Using the whitening decompositions of $\tilde{K}_0^{-1}$ and defining

$$\underline{\tilde{s}}_{0,w} = \tilde{W} \underline{\tilde{s}}_0 \tag{4.56}$$

the resulting processor is shown in Fig. 19. The first portion is for colored noise estimations, and the second portion is for known signal correlation.

The evaluation of the performance follows directly from other cases, however, since $\underline{\hat{\tilde{n}}}$ is a complex function of μ via the $\tilde{K}_1$ matrix, an exact formulation becomes quite cumbersome.

A special case worth considering for the known signal case is for

$$\tilde{K}_n = 0 \tag{4.57}$$

$$\tilde{K}_w = \sigma_n^2 I \quad . \tag{4.58}$$

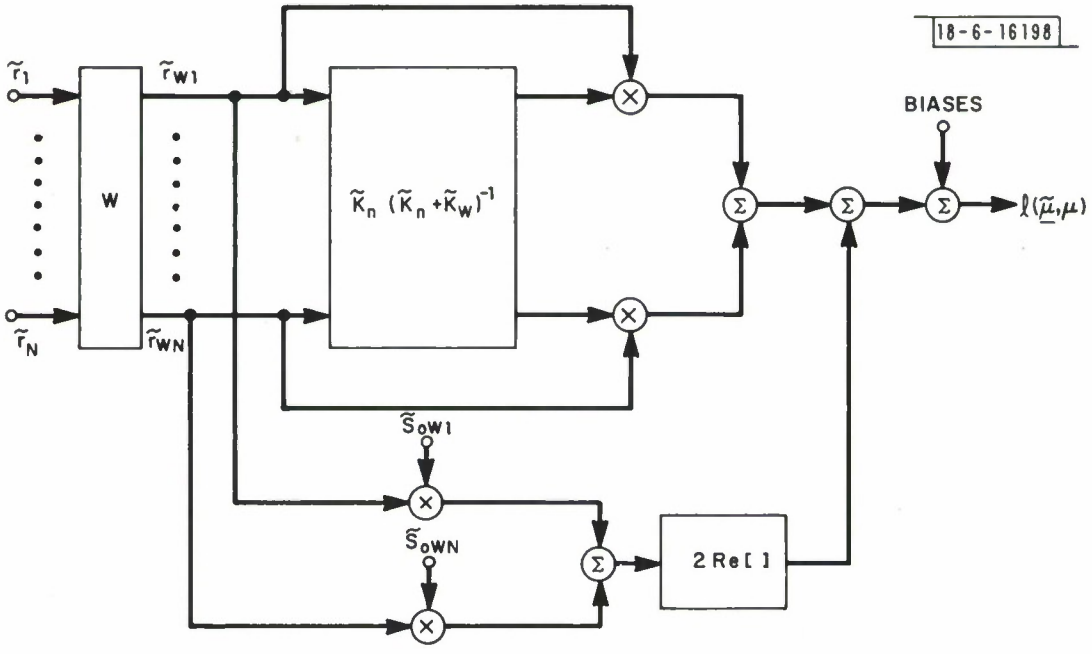

Fig. 19. Known signal; spread.

For this case, $\ell(\tilde{r}, \mu)$ becomes

$$\ell(\underset{\sim}{\tilde{r}}, \mu) = \frac{1}{2\sigma_n^2} \underset{\sim}{\tilde{r}}^{\dagger} \underset{\sim}{\tilde{m}}(\mu) \tilde{b} + \frac{1}{2\sigma_n^2} b^* \underset{\sim}{m}^{\dagger}(\mu) \underset{\sim}{\tilde{r}}$$

$$- \frac{1}{2\sigma_n^2} \tilde{b} \tilde{b}^* \underset{\sim}{\tilde{m}}^{\dagger}(\mu) \underset{\sim}{\tilde{m}}(\mu)$$

$$\approx \frac{\mathrm{Re}[\underset{\sim}{\tilde{r}}^{\dagger} \underset{\sim}{\tilde{m}}(\mu) \tilde{b}]}{\sigma_n^2} \quad . \tag{4.59}$$

This is the classic beam steered case found in radar and sonar. To evaluate the C-R bound, we first note that

$$E\left[\frac{\partial^2}{\partial \mu^2} \ell(\underset{\sim}{\tilde{r}}, \mu)\right] = - \frac{E_s}{\sigma_n^2} \sum_{k=1}^{N} \left(\frac{2\pi d_k}{\lambda}\right)^2 \tag{4.60}$$

where $E_s = \tilde{b} \tilde{b}^*$, and d_k is the position of the kth sensor. Let us further assume that we have a linear array with spacing d_0 between elements. Let d_M be the arbitrary starting point on the array so that

$$d_k = k d_0 + d_M \quad . \tag{4.61}$$

Substituting into the expectation sum in Equation 4.60 we find

$$\sum_{k=1}^{N} \left(\frac{2\pi d_k}{\lambda}\right)^2 = \left(\frac{2\pi d_0}{\lambda}\right)^2 \sum_{k=1}^{N} k^2$$

$$+\left(\frac{2\pi}{\lambda}\right)^2 N d_M[(N+1)\, d_0 + d_M] \quad . \qquad (4.62)$$

Now d_M is a free parameter that we can use to tighten the C-R bound. We want to choose d_M so that the sum is minimized. This yields

$$\boxed{\sigma_\mu^2 \geq \frac{12}{\frac{\sigma_b^2 E_s}{\sigma_n^2}\left(\frac{2\pi d_0}{\lambda}\right)^2 N(N^2-1)}} \quad . \qquad (4.63)$$

This should be compared to the bound for the unspread case of the Gauss-in-Gauss problem that had the additional term which, for high E_s/σ_n^2, vanished.

4.4 Monopulse

Monopulse is a special case of known signal or unknown but nonrandom signal with only two outputs being provided. To evaluate the performance of monopulse we first consider the unspread channel. The two outputs, $\tilde{r}_D$ and $\tilde{r}_\Sigma$, represent difference and sum beams respectively. Let $\underset{\sim}{\tilde{g}}_\Sigma(\mu')$ and $\underset{\sim}{\tilde{g}}_\Delta(\mu')$ be two orthogonal N x 1 vectors. Then define

$$\tilde{r}_{\Delta} = \tilde{\underline{g}}_{\Delta}^{\dagger}(\mu')\,\tilde{\underline{r}}$$

$$= \tilde{b}\,\tilde{\underline{g}}_{\Delta}^{\dagger}(\mu')\,\tilde{\underline{m}}(\mu) + \tilde{\underline{g}}_{\Delta}^{\dagger}(\mu')\,\tilde{\underline{n}} \qquad (4.64)$$

and

$$\tilde{r}_{\Sigma} = \tilde{\underline{g}}_{\Sigma}^{\dagger}(\mu')\,\tilde{\underline{r}}$$

$$= \tilde{b}\,\underline{g}_{\Sigma}^{\dagger}(\mu')\,\tilde{\underline{m}}(\mu) + \tilde{\underline{g}}^{\dagger}(\mu')\,\tilde{\underline{n}} \quad . \qquad (4.65)$$

Further

$$\tilde{\underline{g}}_{\Delta}(\mu') = \tilde{G}_{\Delta}\,\tilde{\underline{m}}(\mu') \qquad (4.66)$$

$$\tilde{\underline{g}}_{\Sigma}(\mu') = \tilde{G}_{\Sigma}\,\tilde{\underline{m}}(\mu') \qquad (4.67)$$

where $\tilde{G}_{\Delta}$ and $\tilde{G}_{\Sigma}$ are beam steering or distribution networks. To ensure even and odd beams, we assume N to be an even number. For a uniformly illuminated array, $\tilde{G}_{\Sigma}$ is $\underline{I}$ and

$$\tilde{G}_{\Delta} = \begin{bmatrix} -1 & 0 & 0 \ldots 0 \\ 0 & -1 & \\ \vdots & & \\ \vdots & & -1 \ldots \\ \vdots & & +1. \\ \vdots & & \\ 0. \ldots & \ldots & +1 \end{bmatrix} \begin{matrix} 1 \\ \vdots \\ \vdots \\ N/2 \\ N/2+1 \\ \vdots \\ N \end{matrix} \quad . \qquad (4.68)$$

The estimate of $\hat{\mu}$ is

$$\hat{\mu} = \frac{1}{k} \operatorname{Re}\left[\frac{\tilde{r}_{\Delta}}{\tilde{r}_{\Sigma}}\right] \tag{4.69}$$

where

$$k = \frac{\partial}{\partial(\mu - \mu')} \left. \frac{\underline{\tilde{g}}^{\dagger}_{\Delta}(\mu')\, \underline{\tilde{m}}(\mu)}{\underline{\tilde{g}}^{\dagger}_{\Sigma}(\mu')\, \underline{\tilde{m}}(\mu)} \right|_{\mu = \mu'} . \tag{4.70}$$

The constant k is called the monopulse slope. For a uniformly illuminated linear array with spacing d_0, we find the slope to be

$$k = \frac{2\pi\, d_0}{\lambda} \frac{N}{4} . \tag{4.71}$$

For values of $\mu - \mu' << 1$ (small off-boresight positions, μ' is the boresight angle) we have following Sharenson:

$$\boxed{\sigma^2_{\mu,\,\text{mono}} = \frac{16}{\left(\frac{2\pi\, d_0}{\lambda}\right)^2 N^3 \frac{E_s \sigma_b^2}{\sigma_b^2}}} \tag{4.72}$$

The first thing to note is that

$$\sigma^2_{\mu,\ \text{mono}} > \sigma^2_{\mu,\ \text{optimum}} \tag{4.73}$$

i.e., the monopulse error is greater than that for the optimum processor. For large N, the difference is

$$\frac{\sigma^2_{\mu,\ \text{mono}}}{\sigma^2_{\mu,\ \text{optimum}}} = 1.333\ldots \quad . \tag{4.74}$$

In general this is insignificant, but it does show that monopulse is not asymptotically optimum.

The final case of interest is to evaluate monopulse performance for a spread channel. If we define the difference and sum gain as

$$G_\Delta(\mu - \mu') = \underset{\sim}{\tilde{g}}^{\dagger}_\Delta(\mu')\, \underline{\tilde{m}}(\mu) \tag{4.75}$$

$$G_\Sigma(\mu - \mu') = \underset{\sim}{\tilde{g}}^{\dagger}_\Sigma(\mu')\, \underline{\tilde{m}}(\mu) \tag{4.76}$$

and the noiseless sum and difference signals as

$$\tilde{\Sigma} = \tilde{b}\ G_\Sigma(\mu - \mu') \tag{4.77}$$

$$\tilde{\Delta} = \tilde{b}\ G_\Delta(\mu - \mu') \tag{4.78}$$

then we have the following

$$\tilde{r}_{\Delta} = \tilde{\Delta} + \int \tilde{G}_{\Delta}(\mu' - \mu'')\, \tilde{b}(\mu'')\, d\mu'' + \underline{\tilde{g}}_{\Delta}^{\dagger}(\mu')\, \underline{\tilde{w}} \qquad (4.79)$$

$$\tilde{r}_{\Sigma} = \tilde{\Sigma} + \int \tilde{G}_{\Sigma}(\mu' - \mu'')\, \tilde{b}(\mu'')\, d\mu'' + \underline{\tilde{g}}_{\Sigma}^{\dagger}(\mu')\, \underline{\tilde{w}} \quad . \qquad (4.80)$$

Defining the two noise terms on $\tilde{r}_{\Delta}$ and $\tilde{r}_{\Sigma}$ as $\tilde{n}_{\Delta}$ and $\tilde{n}_{\Sigma}$, respectively, we have

$$\tilde{r}_{\Delta} = \tilde{\Delta} + \tilde{n}_{\Delta} \qquad (4.81)$$

$$\tilde{r}_{\Sigma} = \tilde{\Sigma} + \tilde{n}_{\Sigma} \quad . \qquad (4.82)$$

If we denote $n_{\Delta c}$ and $n_{\Sigma c}$ as the in phase (with $\tilde{\Delta}$ and $\tilde{\Sigma}$) components of these two noises, then we can use Sharenson's results directly to prove that

$$\sigma_{\mu}^2 = \frac{1}{k^2}\left[\frac{\sigma_{\Delta c}^2}{|\tilde{\Sigma}|^2} + \frac{|\tilde{\Delta}|^2}{|\tilde{\Sigma}|^4}\,\sigma_{\Sigma c}^2 - \frac{2|\tilde{\Delta}|}{|\tilde{\Sigma}|^3}\,\rho\right] \qquad (4.83)$$

where

$$\sigma_{\Delta c}^2 = E[n_{\Delta c}^2] \qquad (4.84)$$

$$\sigma_{\Sigma c}^2 = E[n_{\Sigma c}^2] \tag{4.85}$$

$$\rho = E[n_{\Delta c}\, n_{\Sigma c}] \quad . \tag{4.86}$$

Furthermore, for $|\mu - \mu'| << 1$ we have

$$|\tilde{\Sigma}|^2 = N^2 E_s^2 \tag{4.87}$$

$$\frac{|\tilde{\Delta}|}{|\tilde{\Sigma}|} = k(\mu - \mu') \quad . \tag{4.88}$$

By straightforward calculations we can show that

$$\rho = \mathrm{Re}\left[\int_{-1}^{1} K(\mu - \mu'')\, G_{\Delta}(\mu' - \mu'')\, G_{\Sigma}^{*}(\mu' - \mu'')\, d\mu''\right] \tag{4.89}$$

$$\sigma_{\Delta c}^2 = \int_{-1}^{1} K(\mu - \mu'')\, |G_{\Delta}(\mu' - \mu'')|^2\, d\mu'' + N\sigma_n^2 \tag{4.90}$$

$$\sigma_{\Sigma c}^2 = \int_{-1}^{1} K(\mu - \mu'')\, |G_{\Sigma}(\mu' - \mu'')|^2\, d\mu'' + N\sigma_n^2 \quad . \tag{4.91}$$

Using these in the value for σ_μ^2 we obtain

$$\sigma_\mu^2 = \frac{1}{k^2}\left[\frac{\int_{-1}^{1} K(\mu - \mu'')\left|G_\Delta(\mu' - \mu'')\right|^2 d\mu'' + N\sigma_n^2}{N^2 E_s}\right]$$

$$+ \frac{(\mu - \mu')^2}{N^2 E_s}\left[\int_{-1}^{1} K(\mu - \mu'')\left|G_\Sigma(\mu' - \mu'')\right|^2 d\mu'' + N\sigma_n^2\right]$$

$$- 2\frac{(\mu - \mu')}{k E_s N^2}\,\mathrm{Re}\left[\int_{-1}^{1} K(\mu - \mu'')\, G_\Delta(\mu' - \mu'')\, G_\Sigma^*(\mu' - \mu'')\, d\mu''\right] . \qquad (4.92)$$

Generally for $|\mu - \mu'| << 1$, we can neglect the last term and also the next to the last term. Also

$$\left|G_\Delta(\mu' - \mu'')\right|^2 \approx N^2 k^2 (\mu' - \mu'')^2 . \qquad (4.93)$$

Using these approximations we have for the case of small channel spread, with respect to the beam width

$$\sigma_\mu^2 = \sigma_{\mu,\,\mathrm{noise}}^2 + \frac{\int_{-1}^{1} K(\mu')\,\mu'^2\, d\mu'}{E_s} . \qquad (4.94)$$

Finally by normalizing $K(\mu')$ by the diffuse-to-direct signal ratio

$$\rho_D^2 = \frac{\int_{-1}^{1} K(\mu')\, d\mu'}{E_s} \tag{4.95}$$

and defining the rms diffuse multipath spread as

$$\theta_{da}^2 = \frac{\int_{-1}^{1} K(\mu')\, \mu'^2\, d\mu'}{\int_{-1}^{1} K(\mu')\, d\mu'} \tag{4.96}$$

we obtain

$$\sigma_\mu^2 = \sigma_{\mu,\,\text{noise}}^2 + \sigma_{\mu,\,\text{diff}}^2 \tag{4.97}$$

with

$$\sigma_{\mu,\,\text{diff}}^2 = \rho_D^2\, \theta_{da}^2 \tag{4.98}$$

This expression corresponds to the expression given by Barton and Ward (p. 151), where we have included the $\overline{G}_{sr}$, average sidelobe ratio, already in $K(\mu)$. Thus θ_{da}^2 is evaluated directly from $K(\mu)$ and not approximately from the glistening surface approach. The reader should note that ρ_D^2 was obtained in the last chapter and was shown to be quite small (-10 dB or less) for most casses of interest.

Also one should note that θ_{da}^2 can be generalized to the cases where $K(\mu)$ is spread over the beam, i. e.,

$$\theta_{da}^2 = \frac{\int_{-1}^{1} K(\mu') \left| G_{\Delta}(\mu') \right|^2 d\mu'}{N^2 \int_{-1}^{1} K(\mu')\, d\mu'} \quad . \tag{4.99}$$

Barton has shown (see Barton [2]) that the $\sigma_{\mu,\,\text{diff}}^2$ is comparable to $\sigma_{\mu,\,\text{noise}}^2$. The essential factor here is that monopulse performs more poorly than the optimum processor; yet its total effect is small compared to specular errors noted in McGarty [1].

In Table 4. 1, we summarize all the processors and their corresponding performance values.

4. 5 Performance Comparisons

The analysis of the previous subsections determined the structure and performance of various processors that may be used as angle estimators. In this subsection we shall concentrate on two processors: the Gauss-in-Gauss suboptimum processor, and the monopulse processor. The suboptimum processor provides a convenient lower bound to array performance. It is a processor that scans over all angles and utilizes all angular information, and in so doing can use the diffuse field and extract positions information from it. The monopulse processor, however, is a single-hit, two-beam estimator for which it has already been shown that diffuse multipath will always degrade performance.

TABLE 4.1. PROCESSOR SUMMARY.

Case	Processor	Performance
1. Gauss-in-Gauss Optimum-Spread	$\underset{\sim}{\tilde{r}}^{\dagger} \tilde{K}_w^{-1} \tilde{K}_b [\tilde{K}_b + \tilde{K}_w]^{-1} \underset{\sim}{\tilde{r}}$ (Eq. 4.13)	See Van Trees [2], Chpt. 7
2. Gauss-in-Gauss Optimum-unspread	$\frac{\sigma_T^2}{2} \underset{\sim}{\tilde{r}}^{\dagger} \tilde{K}_w^{-1} \underset{\sim}{\tilde{m}}(\mu) \underset{\sim}{\tilde{m}}^{\dagger}(\mu) \tilde{K}_w^{-1} \underset{\sim}{\tilde{r}}$ (Eq. 4.16)	$\sigma_\mu^2 = \frac{12}{\left(\frac{E_s \sigma_b^2}{\sigma_n^2}\right)\left(\frac{2\pi d_0}{\lambda}\right)^2 (N^3 - N)} \cdot \left[1 + \frac{\sigma_n^2}{NE_s \sigma_b^2}\right]$ (Eq. 4.32) Also see McGarty [1] and Eq. 4.26
3. Gauss-in-Gauss Suboptimum-spread	Same as above (Eq. 4.23)	See Eq. 4.26
4. Unknown/nonrandom Optimum-spread	$-\frac{1}{2} \underset{\sim}{\tilde{r}}^{\dagger} \left(K_{g1}^{-1} - K_{g0}^{-1}\right) \underset{\sim}{\tilde{r}} + \frac{1}{2} \frac{\lvert \underset{\sim}{\tilde{r}}^{\dagger} K_{g1}^{-1} \underset{\sim}{\tilde{g}} \rvert^2}{\underset{\sim}{\tilde{g}}^{\dagger} K_{g1}^{-1} \underset{\sim}{\tilde{g}}}$ (Eq. 4.51)	See Hofstetter and DeLong
5. Known-signal Optimum-spread	$\frac{1}{2} (\underset{\sim}{\tilde{r}} - \underset{\sim}{\tilde{s}}_0)^{\dagger} K_0^{-1} \underset{\sim}{\hat{\tilde{n}}} + \frac{1}{2} \mathrm{Re}\left[\underset{\sim}{\tilde{r}}^{\dagger} K_0^{-1} \underset{\sim}{\tilde{s}}_0\right] - \frac{1}{2} \underset{\sim}{\tilde{s}}_0^{\dagger} K_0^{-1} \underset{\sim}{\tilde{s}}_0$ (Eq. 4.55)	See Van Trees [2], Chpt. 7

TABLE 4.1. PROCESSOR SUMMARY (cont.)

Case	Processor	Performance
6. Known-signal Optimum-spread	$\dfrac{\mathrm{Re}[\tilde{\underline{r}}^{\dagger}\,\underline{\underline{m}}(\mu)\,\tilde{b}]}{\sigma_n^2}$ (Eq. 4.59)	$\sigma_\mu^2 = \dfrac{12}{\left(\dfrac{\sigma_b^2 E_s}{\sigma_n^2}\right)\left(\dfrac{2\pi d_0}{\lambda}\right)^2 (N^3 - N)}$ (Eq. 4.63)
7. Monopulse unspread	$\hat{\mu} = \dfrac{1}{k}\,\mathrm{Re}\left(\dfrac{\tilde{r}_\Delta}{\tilde{r}_\Sigma}\right)$ (Eq. 4.77)	$\sigma^2_{\mu,\,\mathrm{noise}} = \dfrac{16}{\left(\dfrac{E_s \sigma_\mu^2}{\sigma_n^2}\right)\left(\dfrac{2\pi d_0}{\lambda}\right)^2 N^3}$ (Eq. 4.72)
8. Monopulse spread	Same as above	$\sigma_\mu^2 = \sigma^2_{\mu,\,\mathrm{noise}} + \rho_D^2\,\theta_{da}^2$ (Eq. 4.94) $\rho_D^2 = \dfrac{\int_{-1}^{1} K(\mu)\,d\mu}{\sigma_b^2 E_s}$ (Eq. 4.95) $\theta_{da}^2 = \dfrac{\int_{-1}^{1} K(\mu)\lvert G_\Delta(\mu)\rvert^2\,d\mu'}{N^2 \int_{-1}^{1} K(\mu)\,d\mu}$ (Eq. 4.99)

The suboptimum processor performance is given by Equation 4.26, and the monopulse performance by Equation 4.92. It should be noted that both variances depend upon integrals of the channel spread function with the array ambiguity pattern on the difference pattern. These integrations can be quite difficult, however, by introducing Fourier transforms they reduce to readily evaluated finite sums. This is done in Appendix IV, where, $\mathcal{K}$ (f), the Fourier transform of K(μ) is introduced. A specific example is shown in Figs. 20 and 21 where K(μ) for s = 0.5, R = 10 km, z_1 = 10 m, and z_2 = 1km are shown. In Fig. 21, we have plotted its transform $\mathcal{K}$(f). Note for this example, the transform is effectively zero for values of f greater than 10. In Appendix IV, we show that the necessary performance integrals are determined by evaluating $\mathcal{K}$(f) at only those points determined by the sensor array geometry. This means that in general, $\mathcal{K}$(f) need only be evaluated at discrete sets of points.

The behavior of the suboptimums and monopulse processors vary greatly. The general conclusion regarding the monopulse processor is that diffuse multipath always degraded performance. This, however, is not the case for the suboptimum processor. In particular by looking closely at Equation 4.26, we see that if the integral of the CSF is positive, then it is possible that the performance will be poorer with diffuse multipath. Yet if the integral is negative, then the diffuse multipath has information about the source location that will improve location accuracy. To see this in some detail, consider the following example.

Example: Let K(μ) be given by

$$K(\mu) = \begin{cases} \frac{1}{2\Delta} & |\mu| \leq \Delta \\ 0 & \text{elsewhere} \end{cases} . \qquad (4.100)$$

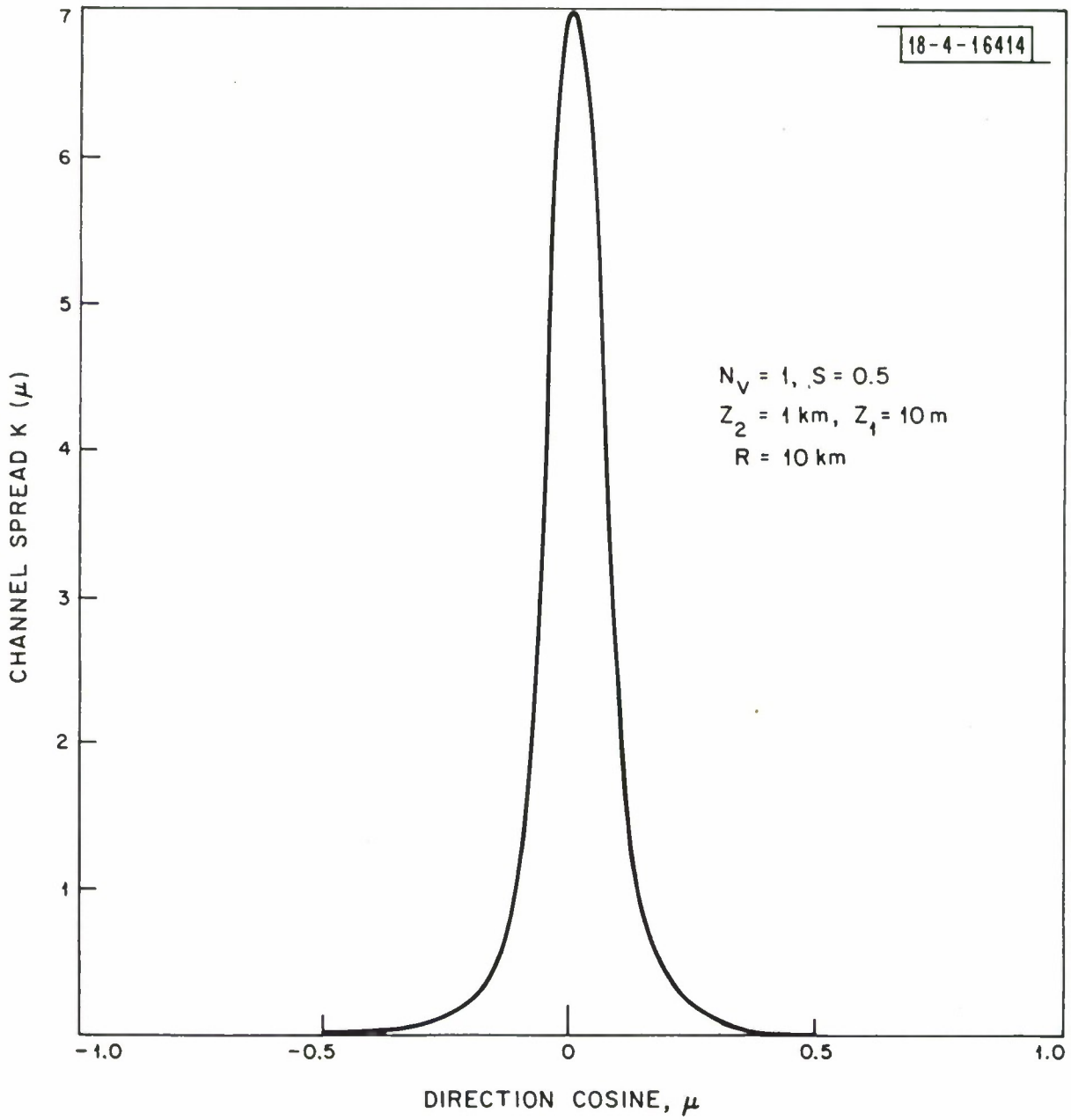

Fig. 20. Channel spread function, K(μ).

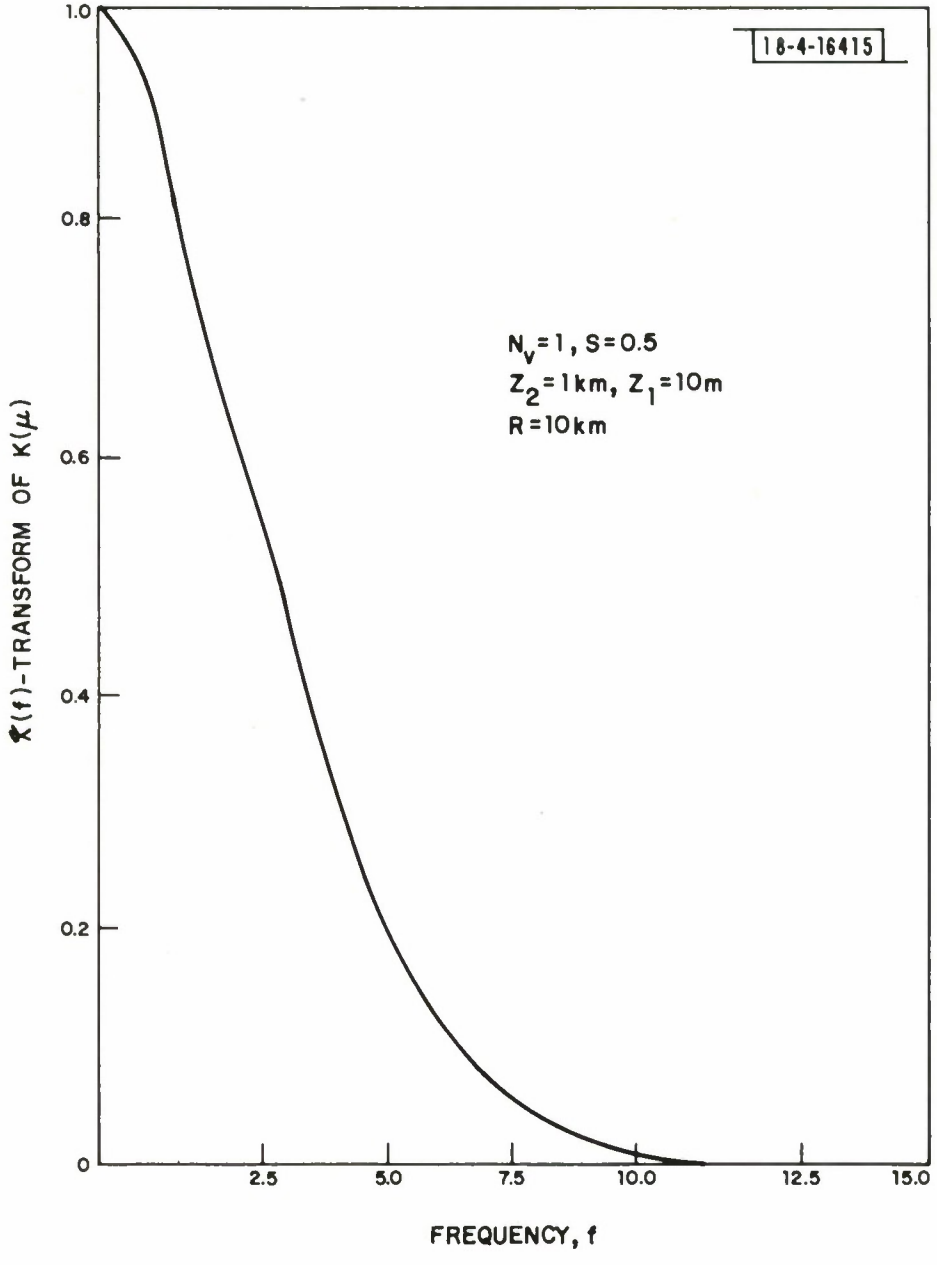

Fig. 21. Transform of K(μ); $\mathcal{K}(f)$.

Then the transform is given by

$$\chi(f) = \frac{\sin 2\pi\ f\Delta}{2\pi\ f\Delta} \tag{4.101}$$

and using the results from Appendix IV for a linear array we obtain

$$\int_{-1}^{1} K(\mu') \frac{\partial^2\ B(\mu')}{\partial \mu'^2}\ d\mu' = -2 \sum_{k=1}^{N} \left(\frac{2\pi\ kd}{\lambda}\right)^2 (N - |k|) \frac{\sin\left(2\pi \frac{kd}{\lambda} \Delta\right)}{\left(2\pi \frac{kd}{\lambda} \Delta\right)} \tag{4.102}$$

where we have used the symmetry to simplify the sum. Canceling and letting $x = kd_0/\lambda$, we define a function G(x) as follows

$$G(x) = \left(\frac{2\pi x}{\Delta}\right)\left(N - \frac{\lambda}{d}|x|\right) \sin(2\pi\ x\ \Delta) \quad . \tag{4.103}$$

Then the summation can be written as $-2 \sum_{k=1}^{N} G(x_k)$ where x_k equals x at the given k values. Now the sum in Equation 4.102 is evaluated at the values of x, which are the spacings of the dipoles normalized by the wavelength. In Fig. 22, we sketched G(x) for two different values of Δ. In (a), Δ is very small so that $K(\mu)$ is quite narrow and its transform is very broad. Thus, G(x) is broad and all the samples are positive so that Equation 4.102 is negative. Thus, σ_μ^2 can be reduced for such a channel by using the information in the diffuse energy because it is coming from the same azimuth. However, as

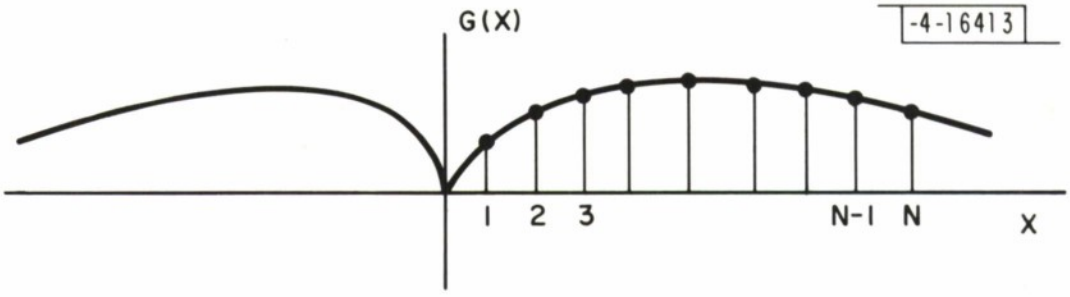

(a)

FOR $\Delta << 1/N$

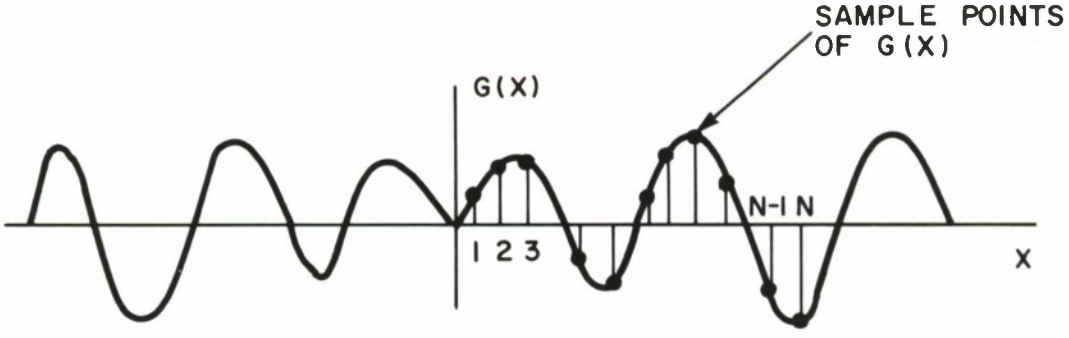

(b)

FOR $\Delta > 1/2N$

Fig. 22. Plot of G(x).

Δ increases we still sample at the same x values, but G(x) now oscillates so that Equation 4.102 becomes positive, thus increasing σ_μ^2. This can also be interpreted as the diffuse field coherently decoupling the array.

This example can also be applied to the monopulse processor with the result that performance will always be degraded. The basic purpose of the example was to show that the suboptimum processor does perform significantly different from monopulse. The cost, however, is that the suboptimum processor must scan all angles looking for the one to maximize the likelihood ratio.

In Figs. 23 to 25, σ_θ has been plotted for boresight pointing vs range for $s = 0.3$, $z_1 = 10$ m, $z_2 = 1$ km, $d/\lambda = 0.5$, and an SNR of 0 dB per element for both the suboptimum and monopulse processors. An isotropic vertical aperture gain was assumed for the first set of curves ($N_{VERT} = 1$). The σ_θ values have been plotted for three different array lengths N = 20, 30, and 40 elements. For each case we have plotted the noise limited values of σ_θ. Then σ_θ, with diffuse multipath, was plotted for a nonshadowed surface and a shadowed surface. For all cases, σ_θ, for the optimum processor with diffuse multipath present, is less than the noise limited value. This results from the fact that the optimum processor has used the information in the diffuse field. Note also the dip in σ_θ at 20 km coincides with the peaking in P_r in Fig. 14. The results for monopulse are also plotted. Note that they are consistently higher than the noise limited value. This is a result of the fact that they reflect the diffuse field as an increase in the background noise level.

In Figs. 23-25, we have also plotted performance vs range for the case where vertical aperture is being used. This has been done for both the optimum and monopulse processor. The performance curves for the optimum processor

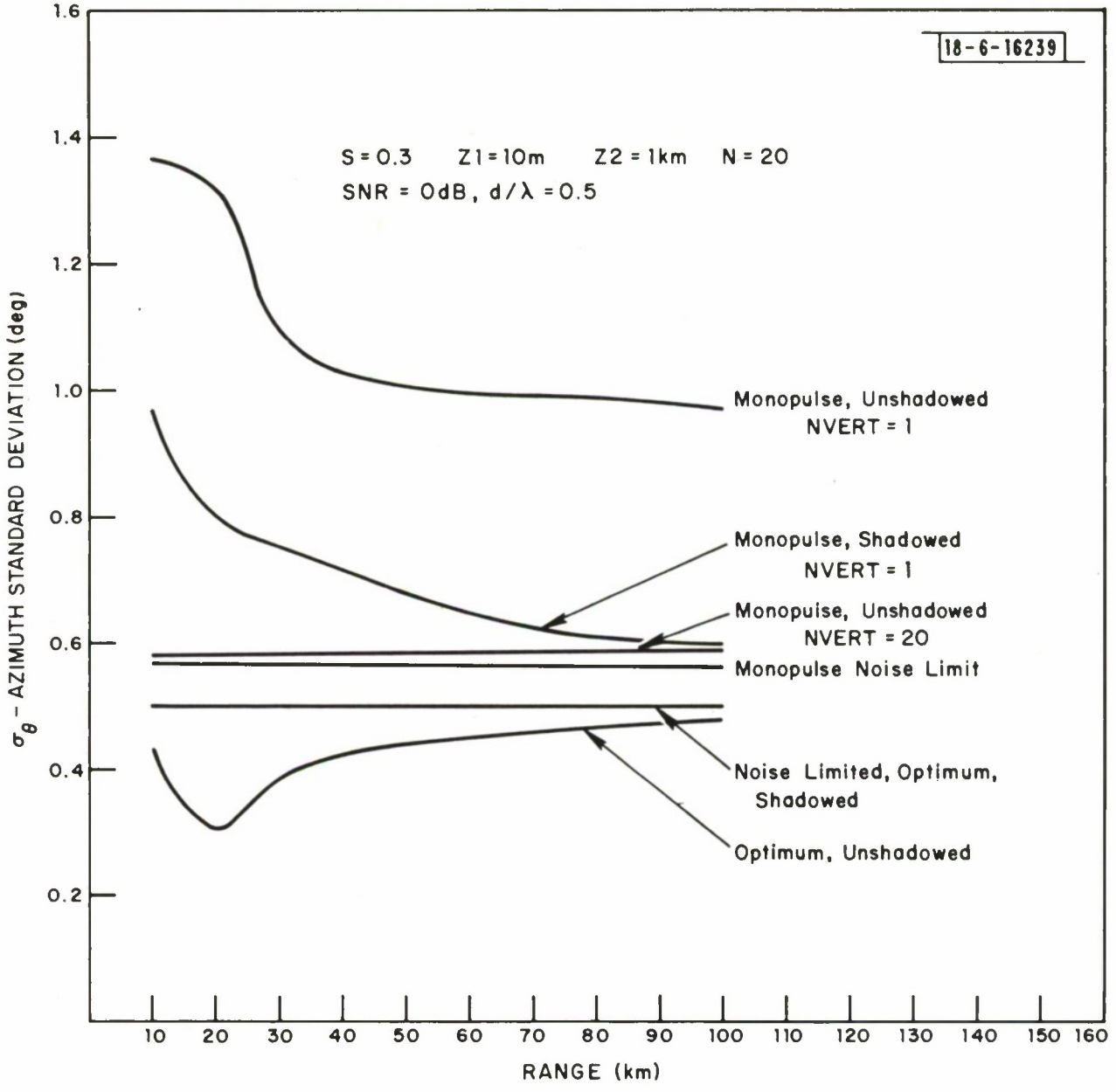

Fig. 23. Array performance vs range (S = 0.3, Z1 = 10 m, Z2 = 1 km, N = 20).

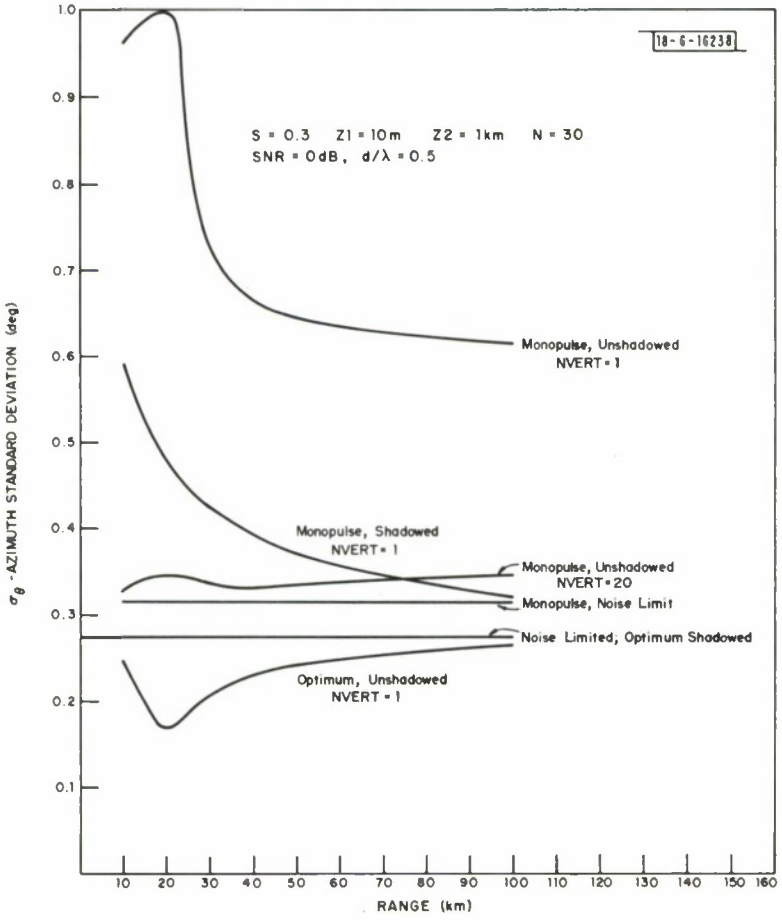

Fig. 24. Array performance vs range (S = 0.3, Z1 = 10 m, Z2 = 1 km, N = 30).

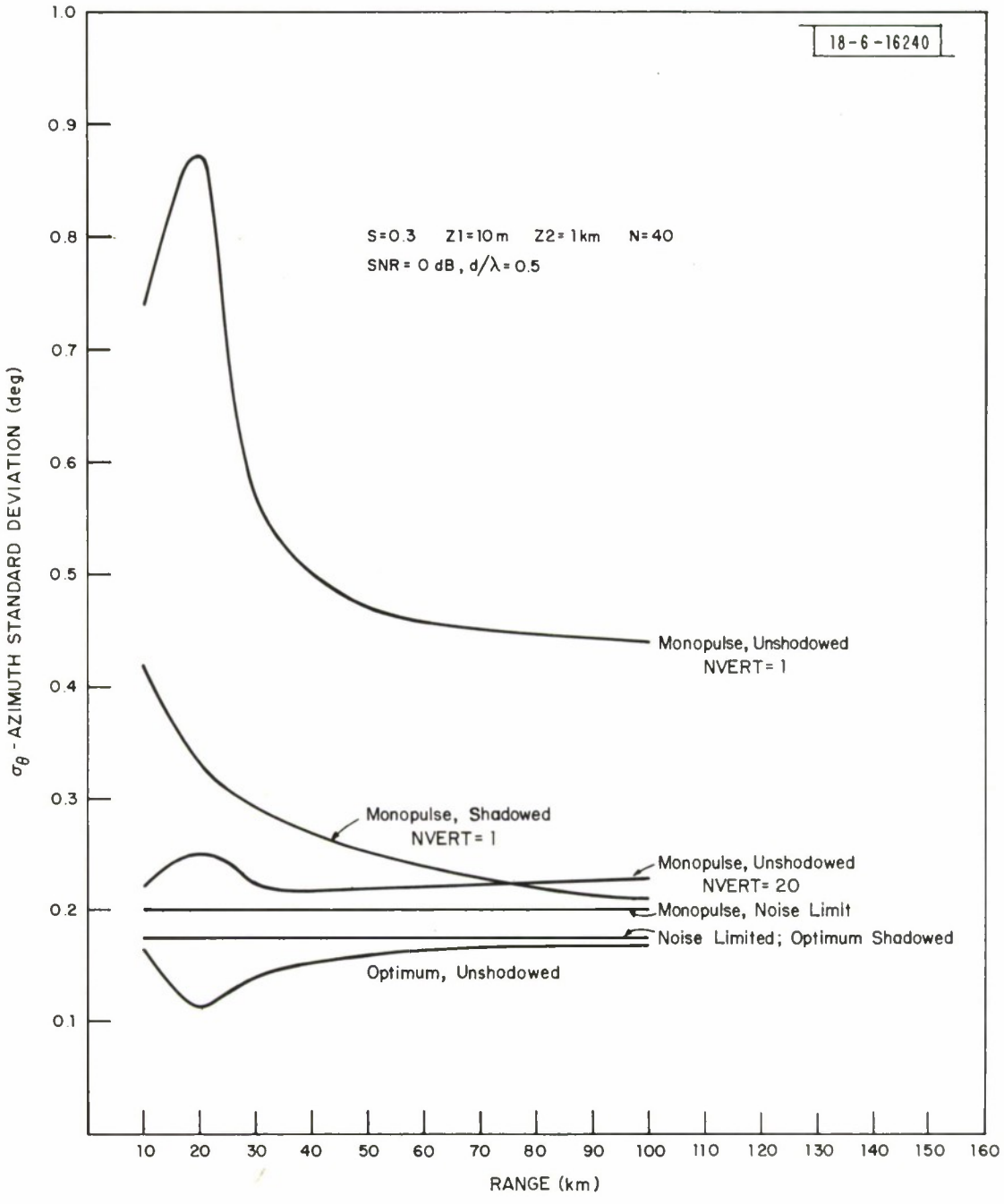

Fig. 25. Array performance vs range (S = 0.3, Z1 = 10 m, Z2 = 1 km, N = 40).

for both shadowed and unshadowed surfaces are equal to the noise limited value. The monopulse performance with vertical aperture and a shadowed surface equals the monopulse noise limited value. The vertical aperture contains twenty elements at half-wavelength spacings with a sector beam formed having a cutoff beginning at 5^{o} in elevation. The vertical pattern was formed using sin x/x beams. From the figures we can see how greatly the addition of vertical cutoff reduces the azimuth error. This is particularly true with the monopulse processor with unshadowed surfaces whose performance is now down to the noise limited value.

A final example is shown in Fig. 26 where we have plotted σ_{θ} vs s, the rms surface slope. As s increases, σ_{θ} increases for the suboptimum process because P_{r} decreases. The opposite would be true for the monopulse processor. It should also be noted that shadowing does play a significant role in performance.

To conclude, what we have done in this section was to compare the performance of the suboptimum processor with that of the monopulse processor. As a result of this comparison, the following observations can be made.

1. The suboptimum processor can have an order of magnitude performance improvement over monopulse. However, such improvement requires significant hardware and signal processing.
2. Performance calculations are most easily obtained by using the transform of the CSF. The transform is required at only N + 1 points.

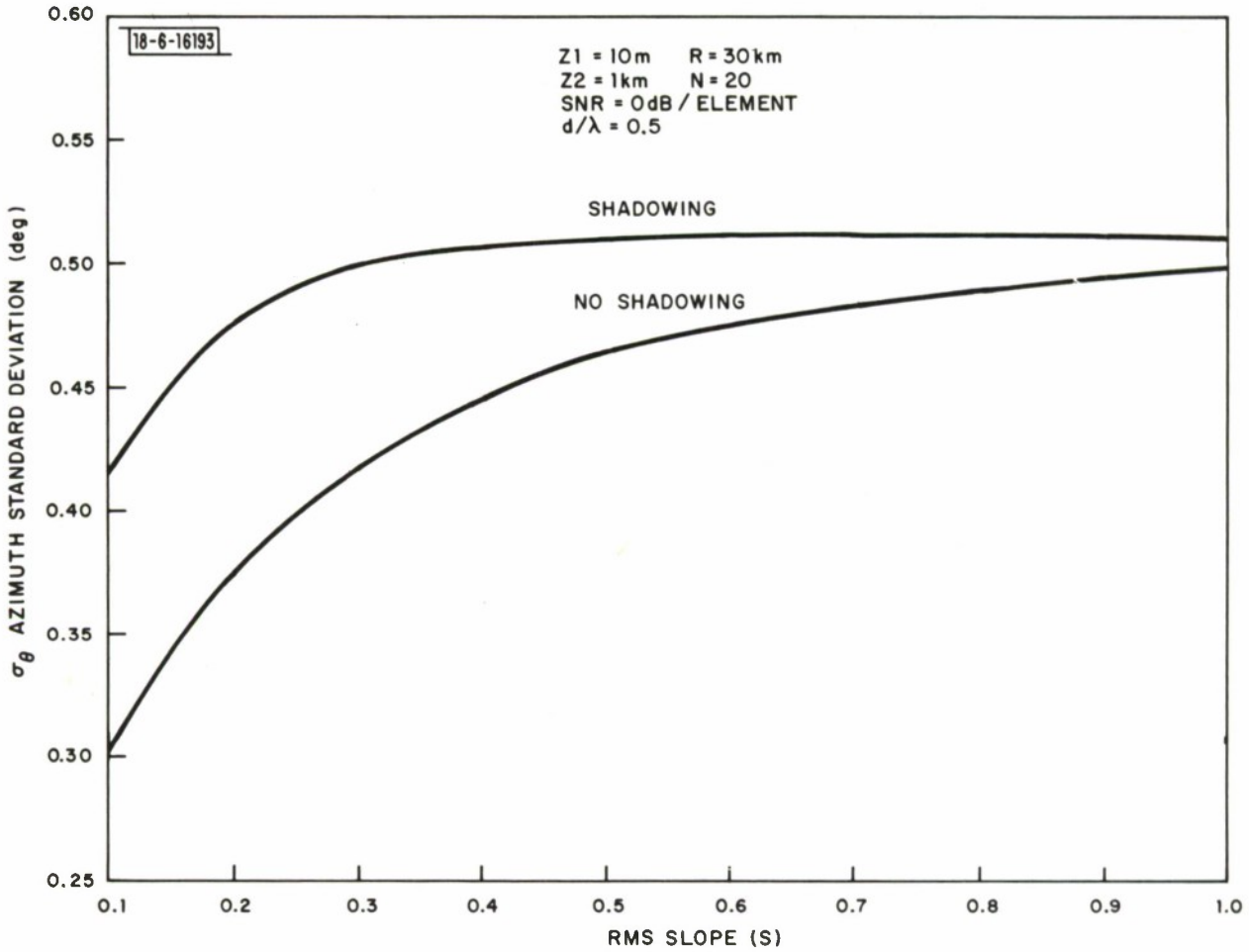

Fig. 26. Array performance vs rms slope.

3. The performance measures provide analytical means for comparing processors. Tradeoffs in sensor locations, weighting, and phasing can be made directly.
4. Surface roughness can degrade performance with the most serious degradation for monopulse being at $s \approx 0.1$.
5. Vertical aperture with vertical cutoff significantly reduces the effects of diffuse multipath and should be used where necessary. Even without vertical cutoff, a 20-foot array at L-band, with $s = 0.3$ experiences a maximum diffuse error of only 0.24°.

Experimental work has been performed at Lincoln Laboratory as part of the DABS program to evaluate the performance of monopulse of an off boresight mode. An experimental facility has been constructed (called DABSEF) to perform this measurement. A planar array of dipoles is used to form sum and difference beams. The diploes are at about half-wavelength spacings at L-band (1030 mHz and 1090 mHz) with 16 in the vertical direction and 32 in the horizontal direction. The horizontal spacing is 8.36 inches, and the vertical is 6.24 inches. The vertical aperture elevation pattern is shown in Fig. 27, and the sum and difference patterns in Figs. 28 and 29, respectively. Using this antenna, radial flights from DABSEF out to ranges of 50 nmi were flown, and on the inbound radial the azimuth estimates were recorded. Also position locations of azimuth, using a boresighted TV optical system, were recorded and used as the true values of azimuth. The difference between the monopulse

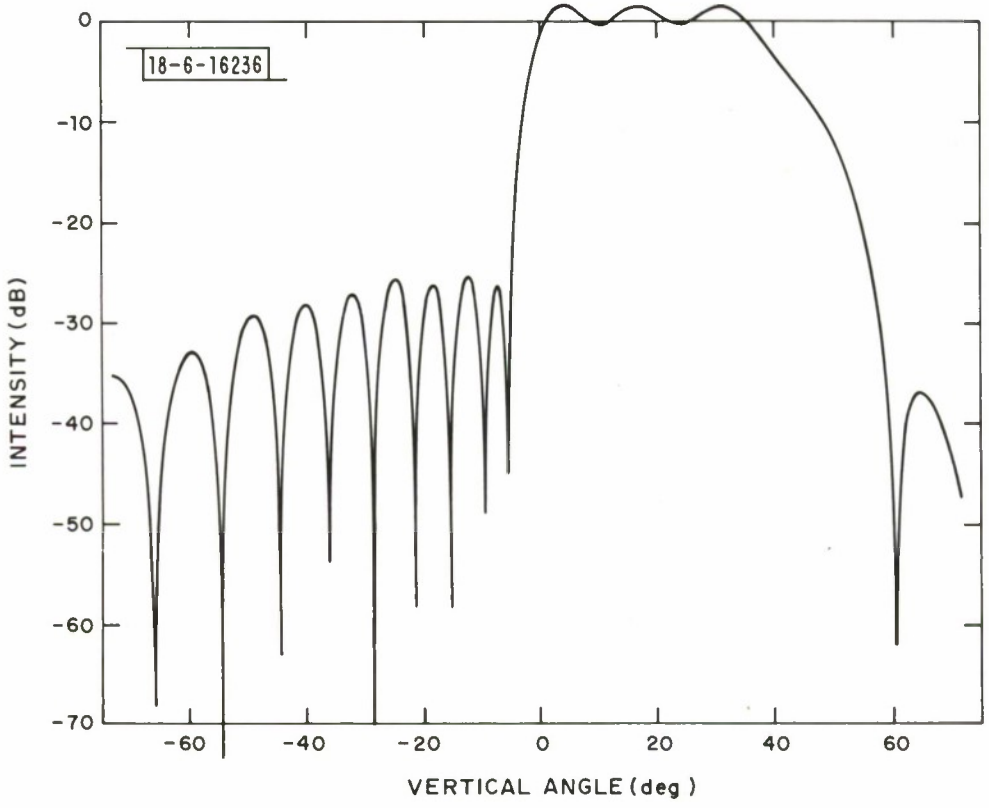

Fig. 27. Elevation patterns of DABSEF antenna through azimuth boresight.

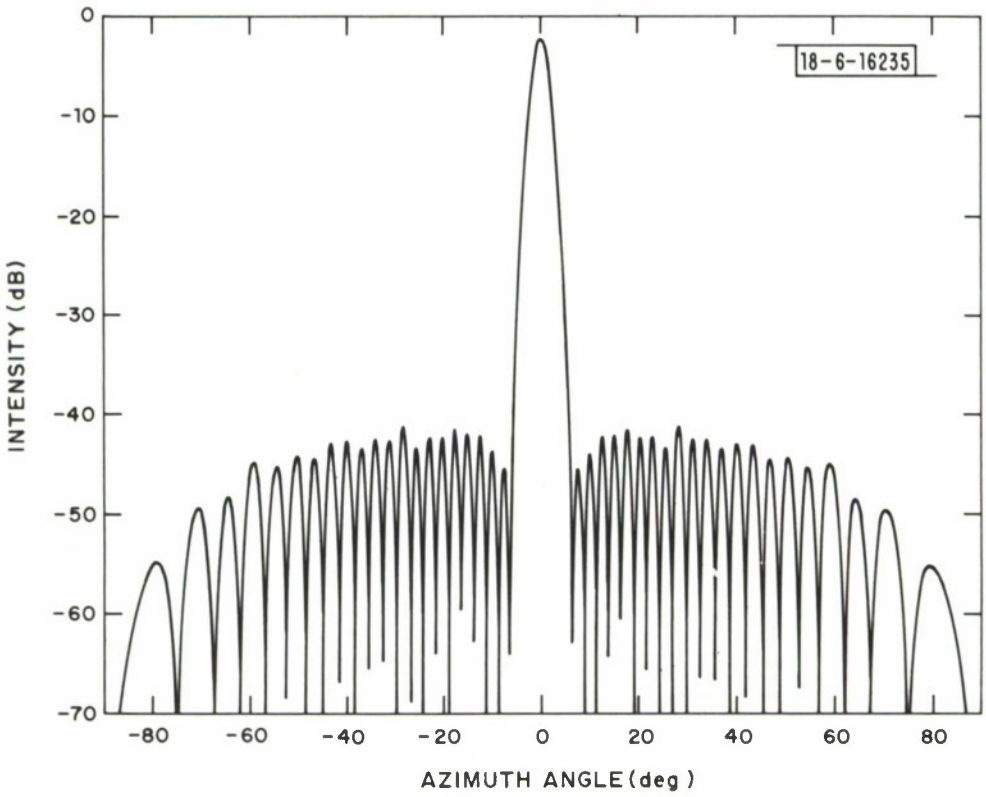

Fig. 28. Azimuth cut through free space sum pattern at elevation of 0.0 radian.

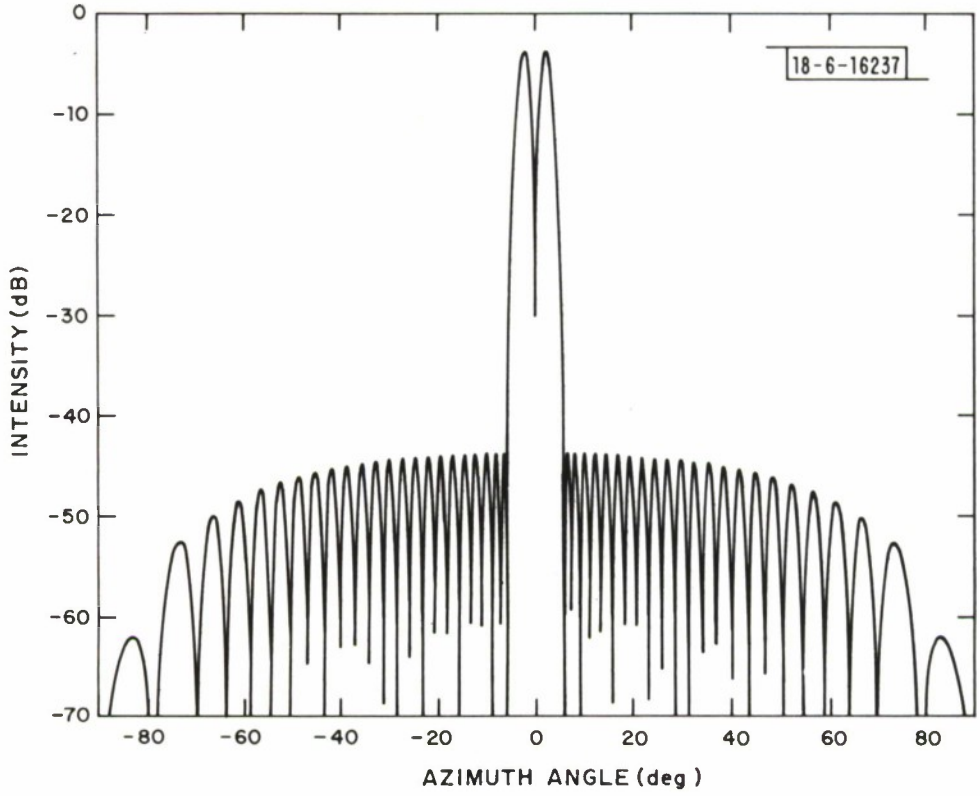

Fig. 29. Azimuth cut through free space difference pattern at elevation of 0.0 radian.

azimuth estimates and the optical estimates is the monopulse errors. These radials were flown under varying ground conditions (foliage, barren, snow, etc.) with similar results. Also the antenna could be tilted down 5^{o}, shifting the elevation pattern down by that amount. The result of this tilting was an increased illumination of the ground.

In Figs. 30 to 32, we present the results of several of these flights. They are all at an azimuth of 308.7^{o} from DABSEF over the airfield at L.G. Hanscom AFB. The aircraft heights are above sea level (ASL) values. The phase center of the receiving antenna was 332' ASL. The major reflecting surface in the first Fresnel zone was Hanscom Field at 130' ASL. The ground was clear of snow, and the visibility was in excess of 30 nmi. We have plotted both the power measured in the sum beam and the azimuth error as noted above. In Figs. 30 and 31, the antenna was tilted down so that the effects of the diffuse multipath were accentuated. In these two cases, the instantaneous azimuth errors can be seen to be large at closer ranges, (5 - 10 nmi) as predicted by the theory in Fig. 25. As the range increases, the errors decrease to the noise limited values. This is a result of the shadowing as well as spreading of the diffuse energy. In Fig. 32, however, the azimuth errors are of uniform distribution over the ranges presented. In this case the antenna was not tilted and the vertical cutoff attenuated the effect of diffuse multipath as predicted by theory (see Fig. 25). A careful examination indicates that diffuse errors are a factor of two to three times the noise limited case as predicted. The results presented here appear consistently on the 64 different radials flown during the experimental program. There thus seems to be a clear correlation between theory and experiment. Furthermore, the diffuse errors seem to be independent

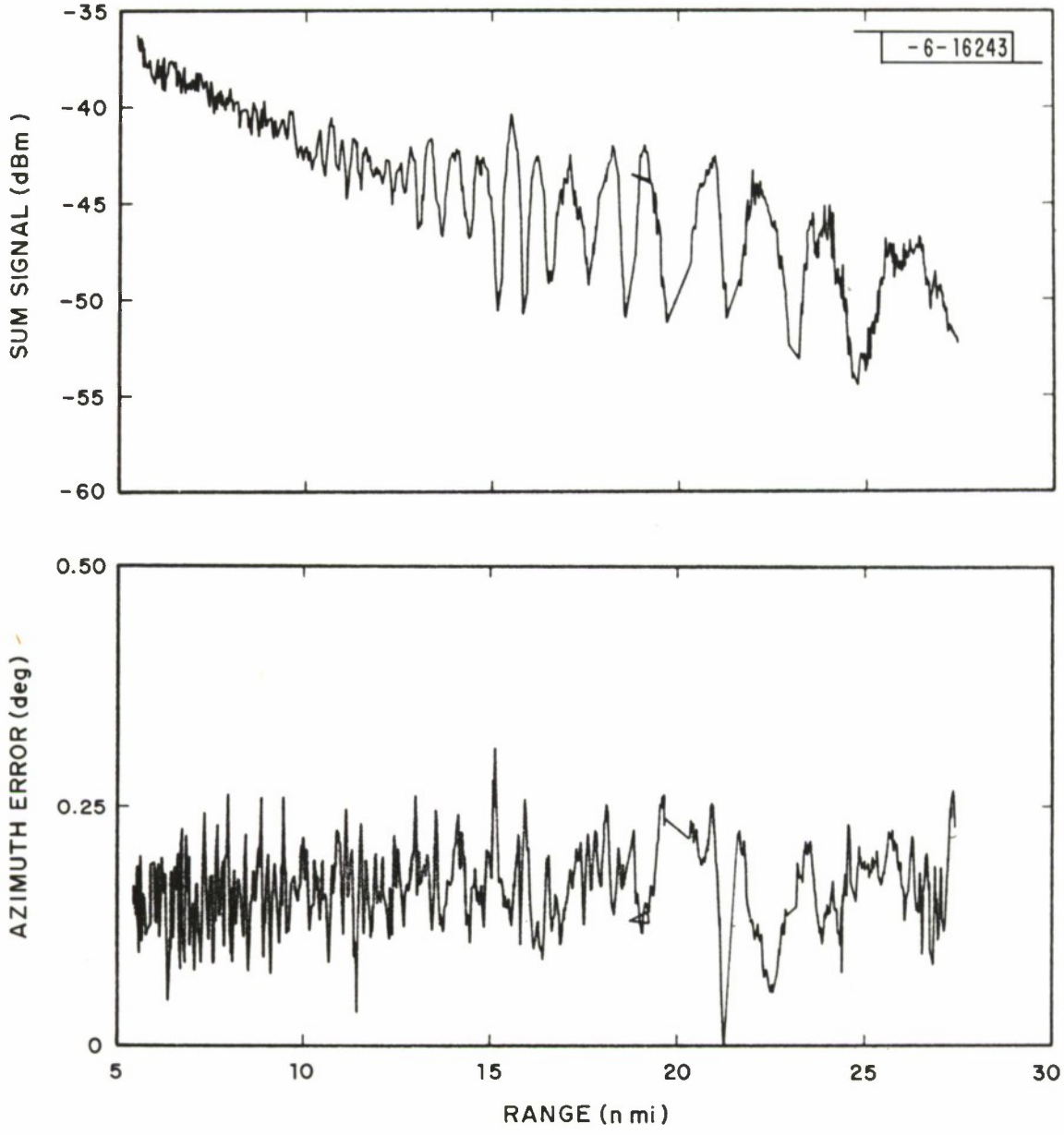

Fig. 30. DABSEF data (4K', 308.7°, antenna down).

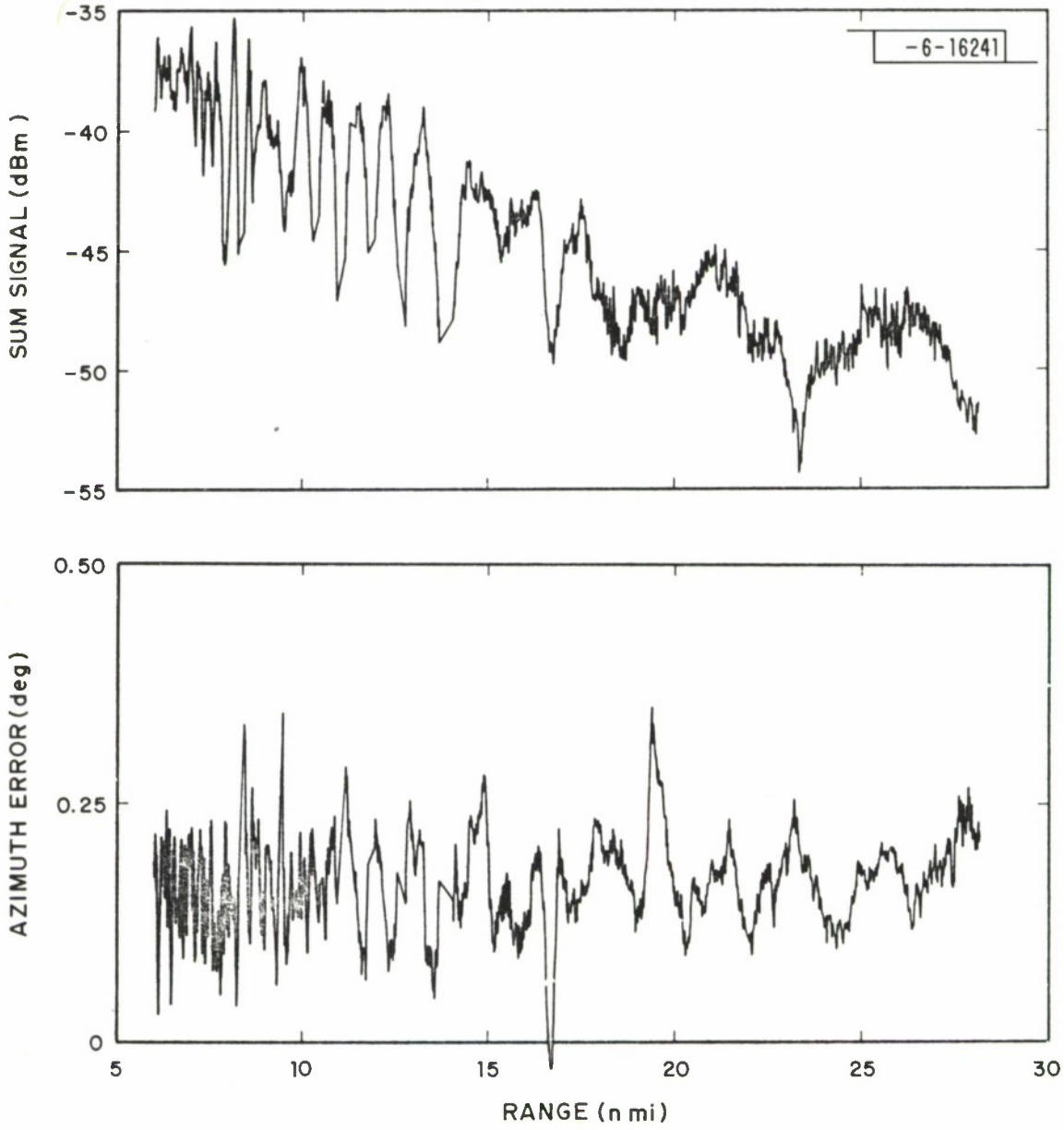

Fig. 31. DABSEF data (2K', 308.7°, antenna down).

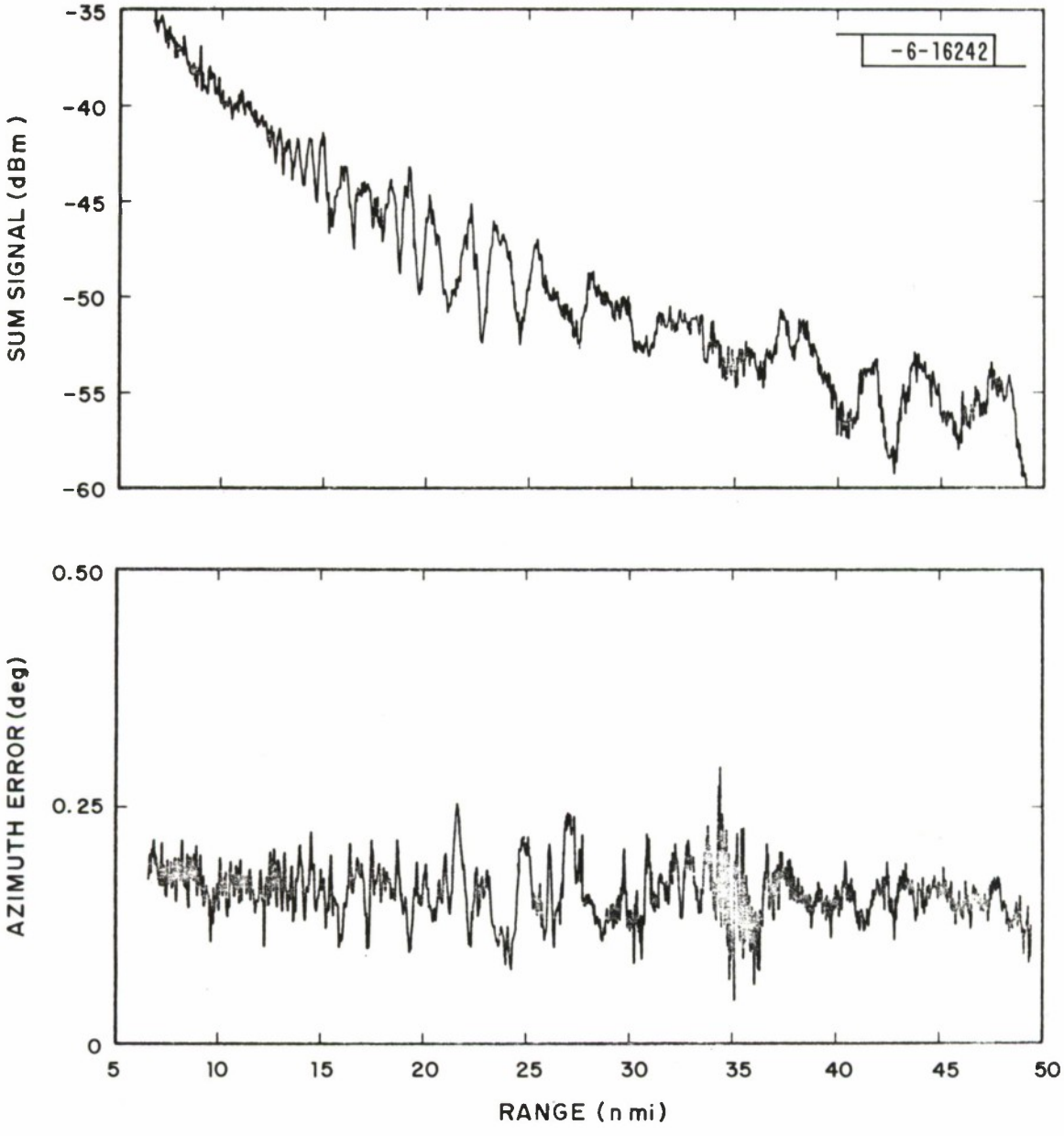

Fig. 32. DABSEF data (4K', 308.7°, antenna normal).

from sample to sample indicating that the diffuse field acts as white noise and comes from different locations at different ranges. This also is consistent with the theory of Section 3.

SECTION 5

CONCLUSIONS

Diffuse multipath has been characterized in detail, and its effect on the pointing accuracy of a planar array has been evaluated. The model used in this evaluation is one of many that are found useful in this area. It provides the antenna designer with a function that is readily used to evaluate array performance when such multipath is present. However, as discussed in the introduction, this is but one of several such models.

As a result of this study, the following conclusions and results were obtained

1. The Kodis-Barrick model is useful at L-band and higher frequencies because all the constraints that are required for the specular point approach are met.
2. The channel spread function was evaluated for a spherical earth. It was shown that this function was obtained directly from the scattering cross section. This function for a spherical earth extends the form developed for a flat earth as discussed in McGarty [2]. The spherical earth includes the effect of horizon cutoff.
3. Shadowing has been included in the model, and the resulting channel spread function shows a significant change. The shadowing effects developed are based on quasi-geometric optics that coincide with the scattering cross section analysis.

4. The evaluation of the channel spread function shows that diffuse energy is concentrated, as expected, along narrow strips. However, over very rough surfaces, sidelobes seem to appear.
5. Without including shadowing, the total power density arising from diffuse multipath is on the order of that from the direct path alone. When shadowing is included, this ratio changes significantly, i.e., diffuse power is from 4 to 24 dB below the direct power. This clearly indicates that diffuse power should, in the cases analyzed, have a minor affect on azimuth pointing accuracy.
6. Antenna pointing errors that result from diffuse multipath are small compared to noise induced errors when large vertical apertures are used to attenuate ground reflections. The analysis of pointing errors extended the present theory to include more complex surface models.

The numerical results used in this report are for aircraft at low elevation angles. At these angles, diffuse energy is small. However, at higher angles ($\phi > 10^{o}$), as may be found in satellite systems, the diffuse energy can increase significantly and the curves must be recalculated. Yet, the theory presented in this report extends readily to those cases.

APPENDIX I

THE SCATTERING CROSS SECTION

The evaluation of the scattering cross section depends upon an analysis of the scattering of an electromagnetic wave from some surface S as shown in Fig. I-1. First, center a coordinate system on the surface S. If we consider the point P, as in the figure, to be the observation point with coordinate $\underline{r}_p$, then Silver (p. 132) shows that the field at that point, due to reflections from the surface S, is given by

$$\underline{E}(\underline{r}_p) = \frac{-j}{4\pi\omega\epsilon} \int_S [(\underline{K} \cdot \nabla)\nabla + k^2 \underline{K}] \frac{\exp(-jkr)}{r} \, dA \qquad (I.1)$$

where S is the surface, $\underline{K}$ the current density on the surface, k the wave number. The differential area dA is the quantity dx' dy', where x', y' represents the coordinates of the scattering point $\underline{r}_s$. We have also assumed a monochromatic wave with frequency ω and that the surface has a dielectric constant ϵ. The ∇ operator operates on the x', y' coordinates. The range r is the distance between the scattering point and the observation point P, i. e.,

$$r = |\underline{r}_p - \underline{r}_s| \qquad (I.2)$$

and $\underline{r}_s$ has the coordinates x', y'. Thus ∇ operates on the $\underline{r}_s$ portion of r. To obtain the total field at the observation point, one must sum up all the fields coming from surfaces S that comprise the scattering plane.

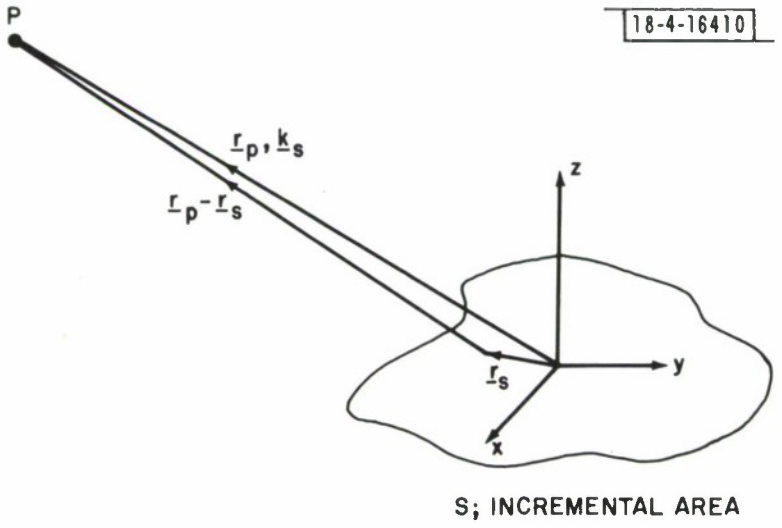

Fig. I. 1. Scattering surface.

Since the coordinate system is centered about the scattering surface as we are, in general, interested in the far field distribution, we can make the standard approximations for r. Namely,

$$r^2 = \underline{r}_p \cdot \underline{r}_p + \underline{r}_s \cdot \underline{r}_s - 2\underline{r}_p \cdot \underline{r}_s . \tag{I. 3}$$

Dividing through by $\underline{r}_p \cdot \underline{r}_p$ and assuming that $|\underline{r}_s| \ll |\underline{r}_p|$ we obtain

$$r^2 \cong |\underline{r}_p|^2 \left(1 - \frac{2\underline{r}_p \cdot \underline{r}_s}{|\underline{r}_p|^2}\right) \tag{I. 4}$$

What we are assuming is that S is some small bounded surface and the scattering points on this surface are at a distance small compared to the distance to the observation point. Taking the square root, we further approximate r by

$$r \approx |\underline{r}_p| - \frac{\underline{r}_p}{|\underline{r}_p|} \cdot \underline{r}_s \tag{I. 5}$$

For $|\underline{r}_s|$ small compared to $|\underline{r}_p|$, the vector $\underline{r}_p$ is almost collinear with $\underline{r}_p - \underline{r}_s$. Thus, the direction of observation is the direction determined by $\underline{r}_p$ from the point of scattering. We define this by the vector

$$\underline{k}_s \triangleq k \frac{\underline{r}_p}{|\underline{r}_p|} \tag{I. 6}$$

Thus, the field due to surface S is coming from direction $\underline{k}_s$. The total field at $\underline{r}_p$ is the sum of fields coming from all directions or equivalently from all surfaces S.

Using this simplification we can make the following approximation.

$$\frac{\exp(-jkr)}{r} \approx \frac{\exp\left(-j|\underline{r}_p| + j\,\underline{k}_s \cdot \underline{r}_s\right)}{|\underline{r}_p|} \tag{I.7}$$

Thus the term in Equation I.1 can be written as

$$(\underline{K} \cdot \nabla)\frac{\exp(-j\,k\,r)}{r}$$

$$= -(\underline{K} \cdot \underline{k}_s)\,\underline{k}_s \frac{\exp\left(-j\,k|\underline{r}_p|\right)}{|\underline{r}_p|} \exp(j\,\underline{k}_s \cdot \underline{r}_s) \tag{I.8}$$

Using this in Equation I.1, we obtain for the observed field

$$\underline{E}(\underline{r}_p) = \frac{j}{4\pi\omega\epsilon|\underline{r}_p|} \exp\left(-j\,k|\underline{r}_p|\right)$$

$$\int_S \left(\underline{k}_s\,\underline{k}_s^T - k^2\right)\underline{K} \exp\left(j\,\underline{k}_s^T\,\underline{r}_s\right) dA \tag{I.9}$$

The value of $\underline{K}$, the surface current density, must be known to obtain a solution to this equation. In general, such a solution is quite difficult, but if the Kirchoff conditions are used (see Jackson, p. 283), Equation I.9 can be readily simplified. These conditions use the field incident on S as the value for $\underline{K}$.

Now since we assumed that the reflecting surface has an infinite conductivity, we then have for a boundary condition

$$\underline{n} \times \underline{H}_{inc} = \underline{K} \tag{I.10}$$

where $\underline{n}$ is the normal at the surface, and $\underline{H}_{inc}$ the incident magnetic field vector. If we further assume that the incident field is a plane wave with electric field vector

$$\underline{E}_{inc} = E_0 \, \underline{e} \exp(-j \, \underline{k}_i \cdot \underline{r}) \tag{I.11}$$

where $\underline{e}$ is the polarization vector, and $\underline{k}_i$ the incident direction vector, then we can find $\underline{H}_{inc}(\underline{r})$ directly as

$$\underline{H}_{inc}(\underline{r}) = \frac{-j}{\omega\mu} (j \, \underline{k}_i \times \underline{e}) \, E_0 \exp(-j \, \underline{k}_i \cdot \underline{r}) \tag{I.12}$$

Using this in Equation I.9, we obtain

$$\underline{E}(\underline{r}_p) = \frac{-j}{4\pi\omega^2\epsilon\mu} E_0 \frac{\exp\left(-j \, k \left| \underline{r}_p \right|\right)}{\left| \underline{r}_p \right|}$$

$$\int_S \left(\underline{k}_s \, \underline{k}_s^T - k^2\right) \underline{n} \times (\underline{k}_i \times \underline{e}) \exp\left(j \, \underline{k}_s^T \, \underline{r}_s - j \, \underline{k}_i^T \, \underline{r}_s\right) dA \tag{I.13}$$

This can be simplified if we note that $k^2 = \omega^2 \epsilon\mu$.

We now want to evaluate this integral at each of its stationary points. That is, if we let

$$\underline{q} = \underline{k}_s - \underline{k}_i \tag{I.14}$$

then at the point $\underline{r}$, which has a normal such that for the given values of $\underline{k}_s$ and $\underline{k}_i$, the angles of incidence and reflection are equal, we have a stationary phase point. If we let $\underline{n}$ be the normal vector at that point and let $\xi(x, y)$ be the z value, then the scattering surface is defined by

$$f(x, y, z) = z - \xi(x, y) = 0 \tag{I. 15}$$

and $\underline{n}$ is given by

$$\underline{n} = \frac{\nabla f}{|\nabla f|} \tag{I. 16}$$

Using Equation I. 15 we obtain

$$\underline{n} = \frac{-\frac{\partial \xi}{\partial x}\underline{e}_x - \frac{\partial \xi}{\partial y}\underline{e}_y + \underline{e}_z}{\sqrt{1 + \left(\frac{\partial \xi}{\partial x}\right)^2 + \left(\frac{\partial \xi}{\partial y}\right)^2}} \tag{I. 17}$$

and $\underline{e}_x$, $\underline{e}_y$, $\underline{e}_z$ are the unit vectors. At the specular point, we know that the vector $\underline{q}$ points in the direction of $\underline{n}$ so that

$$\underline{q} = \underline{k}_i - \underline{k}_s = |k|\underline{n} \tag{I. 18}$$

We now seek to prove this fact using a stationary phase analysis on the integral appearing in Equation I. 13. It is easily seen that if $\underline{e}_z$ is the unit vector in the z-direction and $\underline{n}$ the normal of the surface at the point (x, y), then

$$dA\, \underline{n} \cdot \underline{e}_z = dx\, dy \tag{I. 19}$$

This is nothing more than the Jacobian of the transformation. Define the vector $\underline{h}$ as the vector cross product

$$\underline{h} = \underline{k}_i \times \underline{e} \tag{I. 20}$$

Then using Equations I. 19 and I. 20 and the definition of $\underline{q}$ in Equation I. 13, we obtain

$$\underline{E}(\underline{r}_p) = \frac{-j}{4\pi\, k^2}\, E_0 \frac{\exp\left(-j\, k |\underline{r}_p|\right)}{|\underline{r}_p|}$$

$$\int_S \left(\underline{k}_s\, \underline{k}_s^T - k^2\right) \underline{n} \times \underline{h} \exp\left(j\, \underline{q}^T\, \underline{r}_s\right) \frac{dx\, dy}{\underline{n} \cdot \underline{e}_z} \qquad \text{(I. 21)}$$

The vector $\underline{r}_s$ is given by

$$\underline{r}_s = x\, \underline{e}_x + y\, \underline{e}_y + \xi(x, y)\, \underline{e}_z \qquad \text{(I. 22)}$$

where $\xi(x, y)$ represents the height of the surface. Thus if we expand $\xi(x, y)$ about some particular point (x_ℓ, y_ℓ), then we have

$$\begin{aligned}
\underline{r}_s = {} & x\, \underline{e}_x + y\, \underline{e}_y + \xi(x_\ell, y_\ell)\, \underline{e}_z \\
& + \frac{\partial \xi}{\partial x}(x - x_\ell)\, \underline{e}_z + \frac{\partial \xi}{\partial y}(y - y_\ell)\, \underline{e}_z \\
& + \frac{1}{2} \frac{\partial^2 \xi}{\partial x^2}(x - x_\ell)^2\, \underline{e}_z + \frac{\partial^2 \xi}{\partial x\, \partial y}(x - x_\ell)(y - y_\ell)\, \underline{e}_z \\
& + \frac{1}{2} \frac{\partial^2 \xi}{\partial y^2}(y - y_\ell)^2\, \underline{e}_z \\
& + \ldots
\end{aligned} \qquad \text{(I. 23)}$$

For convenience, define the following constants

$$A_\ell = \frac{\partial^2}{\partial x^2} \xi(x, y) \Big|_{x_\ell,\ y_\ell} \tag{I. 24}$$

$$B_\ell = \frac{\partial^2}{\partial x \partial y} \xi(x, y) \Big|_{x_\ell,\ y_\ell} \tag{I. 25}$$

$$C_\ell = \frac{\partial^2}{\partial y^2} \xi(x, y) \Big|_{x_\ell,\ y_\ell} \tag{I. 26}$$

Then the product $\underline{q}^T \underline{r}_s$ will equal

$$\begin{aligned} \underline{q}^T \underline{r}_s = &\left(q_x + q_z \frac{\partial \xi}{\partial x}\right) x + \left(q_y + q_z \frac{\partial \xi}{\partial y}\right) y \\ &- q_z \frac{\partial \xi}{\partial x} x_\ell - q_z \frac{\partial \xi}{\partial y} y_\ell + q_z \xi(x_\ell, y_\ell) \\ &+ \frac{q_z}{2} \left[A_\ell (x - x_\ell)^2 + 2B_\ell (x - x_\ell)(y - y_\ell) + C_\ell (y - y_\ell)^2\right] \\ &+ \ldots \end{aligned} \tag{I. 27}$$

Now the method of stationary phase states that the integral in Equation I. 21 vanishes for all x, y values except those in and around the points where the coefficients of the x and y terms in Equation I. 27 vanish. At the point at which they vanish, the integral is nonzero and can be evaluated (see Born and Wolf). Thus, the stationary phase points are those x_ℓ and y_ℓ which are solutions to

$$q_x + q_z \frac{\partial \xi}{\partial x} = 0 \tag{I. 28}$$

$$q_y + q_z \frac{\partial \xi}{\partial y} = 0 \tag{I. 29}$$

Since the region where Equations I. 28 and I. 29 hold true is small for large values of $|\underline{q}|$, we evaluate the functions inside the integral at the points x_ℓ, y_ℓ. Thus, they are constant and independent and can be removed from the integral. The value of the integral in Equation I. 21 evaluated at the ℓth stationary phase point then is

$$\underline{E}(\underline{r}_p) = \frac{j}{4\pi k^2} E_0 \frac{\exp\left(-j\, k |\underline{r}_p|\right)}{|\underline{r}_p|}$$

$$\frac{\underline{F}_\ell}{\underline{n}_\ell \cdot \underline{e}_z} \exp\left(-j\, q_z \left(\frac{\partial \xi}{\partial x} x_\ell + \frac{\partial \xi}{\partial y} y_\ell - \xi(x_\ell, y_\ell)\right)\right)$$

$$\iint \exp\left(j \frac{q_z}{2} \left(A_\ell (x - x_\ell)^2 + 2B_\ell (y - y_\ell)(x - x_\ell)\right.\right.$$

$$\left.\left. + C_\ell (y - y_\ell)^2\right)\right) dx\,dy \tag{I. 30}$$

The term $\underline{F}_\ell$ is

$$\underline{F}_\ell = \left(\underline{k}_s \underline{k}_s^T - k^2\right) \underline{h} \times \underline{n}_\ell \tag{I. 31}$$

Where $\underline{n}_\ell$ is the normal at the point x_ℓ, y_ℓ. Using the fact that

$$\frac{\partial \xi}{\partial x} = -\frac{q_x}{q_z} \tag{I. 32}$$

$$\frac{\partial \xi}{\partial y} = - \frac{q_y}{q_z} \tag{I. 33}$$

we first note that using Equation I. 17

$$\underline{n} = \frac{q_x \underline{e}_x + q_y \underline{e}_y + q_z \underline{e}_z}{\sqrt{q_x^2 + q_y^2 + q_z^2}} = \frac{\underline{q}}{|\underline{q}|} \tag{I. 34}$$

at the stationary point. Furthermore,

$$\exp\left(j\left(-q_z \frac{\partial \xi}{\partial x} x_\ell - q_z \frac{\partial \xi}{\partial y} y_\ell + q_z \xi(x_\ell, z_\ell)\right)\right)$$

$$= \exp(j q_x x_\ell + j q_y y_\ell + j q_z z_\ell)$$

$$= \exp(j \underline{q} \cdot \underline{r}_\ell) \tag{I. 35}$$

Now define the integral in Equation I. 30 as I_ℓ so that using Equation I. 35 we obtain

$$\underline{E}(\underline{r}_p) = \frac{j}{4\pi k^2} E_0 \frac{\underline{F}_\ell}{\underline{n}_\ell \cdot \underline{e}_z} \frac{\exp\left(-j k |\underline{r}_p| + j \underline{q} \cdot \underline{r}_\ell\right)}{|\underline{r}_p|} I_\ell \tag{I. 36}$$

The integral I_ℓ can be readily evaluated using standard techniques to yield

$$I_\ell = \frac{2\pi j}{q_z D_\ell^{1/2}} \tag{I. 37}$$

where

$$D_\ell = A_\ell C_\ell - B_\ell^2 \tag{I. 38}$$

Now recall that by definition

$$q_z = \underline{q} \cdot \underline{e}_z = |\underline{q}| \underline{n}_\ell \cdot \underline{e}_z \tag{I. 39}$$

since $\underline{n}_\ell$ is the unit normal and at the specular point is in the same direction as $\underline{q}$. Using this in Equation I. 36 we finally obtain

$$\underline{E}(\underline{r}_p) = \frac{E_0}{2k^2} \frac{F_\ell \exp\left(-j\,k\,|\underline{r}_p| + j\,\underline{q} \cdot \underline{r}_\ell\right)}{(\underline{n}_\ell \cdot \underline{e}_z)^2\, |\underline{q}|\, |\underline{r}_p|\, D_\ell^{1/2}} \tag{I. 40}$$

The reflection coefficient for the surface is given by

$$R_\ell(\underline{k}_i\, \underline{k}_s) = \frac{|F_\ell|}{k^3} \tag{I. 41}$$

and has been evaluated by Mitzner. Define the vector $\hat{\underline{q}}$ as

$$\hat{\underline{q}} = \underline{q}/k \tag{I. 42}$$

Using this, the total received field, as a result of all stationary points, is readily obtained by summing over ℓ, i. e., the field at $\underline{r}_p$ coming from direction $\underline{k}_s$ due to a sources incident on S from direction $\underline{k}_i$ is

$$\underline{E}(\underline{r}_p) = \sum_{\ell=1}^{n} \frac{E_0}{2} \frac{F_\ell}{k^3} \frac{\exp\left(-j\,k|\underline{r}_p| + j\,\underline{q} \cdot \underline{r}_\ell\right)}{|\hat{\underline{q}}|\, |\underline{r}_p|\, D_\ell^{1/2}\, (\underline{n}_\ell \cdot \underline{e}_z)^2} \tag{I. 43}$$

Now the scattering cross section for incident direction $\underline{k}_i$ and received direction $\underline{k}_s$ is defined as (see Kerr, p. 33)

$$\sigma(\underline{k}_i, \underline{k}_s) \triangleq 4\pi R^2 \frac{E\left[\left|\underline{E}(\underline{r})\right|^2\right]}{E_0^2} \tag{I.44}$$

where $R = |\underline{r}|$ and $E[\ ]$ represents the expectation operator. Using Equations I.43 and I.41, we readily obtain

$$\sigma(\underline{k}_i, \underline{k}_s) = E\left[\sum_{\ell=1}^{n}\sum_{m=1}^{n} \pi R_\ell(\underline{k}_i, \underline{k}_s) R_m(\underline{k}_i, \underline{k}_s) \frac{\exp(j\,\underline{q}\cdot(\underline{r}_\ell - \underline{r}_m))}{|\hat{\underline{q}}|^2 D_\ell^{1/2} D_m^{1/2} (\underline{n}_\ell \cdot \underline{e}_z)^2 (\underline{n}_m \cdot \underline{e}_z)^2}\right] \tag{I.45}$$

We now assume that the specular points are independent, and distribution such that $\underline{q}\cdot\underline{r}_k$ is uniform on $[0, 2\pi]$. Then

$$\sigma(\underline{k}_i, \underline{k}_s) = E\left[\sum_{\ell=1}^{n} \frac{\pi R_\ell^2(\underline{k}_i, \underline{k}_s)}{|\hat{\underline{q}}|^2 D_\ell (\underline{n}_\ell \cdot \underline{e}_z)^4}\right] \tag{I.46}$$

The term in the denominator, $|\hat{\underline{q}}|^2 D_\ell (\underline{n}_\ell \cdot \underline{e}_z)^4$, can be shown to equal

$$\left[1 + \left(\frac{\partial \xi}{\partial x}\right)^2 + \left(\frac{\partial \xi}{\partial y}\right)^2\right] \cdot \left[\frac{\partial^2 \xi}{\partial x^2}\frac{\partial^2 \xi}{\partial y^2} - \left(\frac{\partial^2 \xi}{\partial x\,\partial y}\right)^2\right] \cdot \left[\frac{1}{\sqrt{1 + \left(\frac{\partial \xi}{\partial x}\right)^2 + \left(\frac{\partial \xi}{\partial y}\right)^2}}\right]^4 \tag{I.47}$$

where we have used Equation I. 34, and all the derivatives are evaluated at x_ℓ, y_ℓ. Following through on the calculations, we observe that

$$\frac{1}{|\hat{q}|^2 D_\ell (\underline{n}_\ell \cdot \underline{e}_z)^4} = \frac{1 + \left(\frac{\partial \xi}{\partial x}\right)^2 + \left(\frac{\partial \xi}{\partial y}\right)^2}{\left[\frac{\partial^2 \xi}{\partial x^2}\frac{\partial^2 \xi}{\partial y^2} - \left(\frac{\partial^2 \xi}{\partial x \partial y}\right)^2\right]}$$

$$\triangleq < R_1 \; R_2 >_\ell \qquad \text{(I. 48)}$$

where $< R_1 \; R_2 >_\ell$ is the product of the principal radii of curvature at point ℓ.

We can now return to Equation I. 46 and, assuming that the specular points have equivalent statistics, we can write Equation I. 46 using Equation I. 48 as

$$\sigma(\underline{k}_i, \underline{k}_s) = \pi \, E[n] \, E[< R_1 \; R_2 >] \; R^2(\underline{k}_i, \underline{k}_s) \qquad \text{(I. 49)}$$

where we have noted that $R(\underline{k}_i, \underline{k}_s)$ does not depend on ℓ. Define the average number of specular reflectors as n_T, and the average of the product of the radii of curvature as $\mathcal{R}$. Then

$$\sigma(\underline{k}_i, \underline{k}_s) = \pi n_T \mathcal{R} R^2(\underline{k}_i, \underline{k}_s) \qquad \text{(I. 50)}$$

which is the fundamental result of this analysis. We can also define the scattering cross section per unit area if, instead of using n_T, the average number of specular points, we use n_A the average number of specular points per unit area, i. e.,

$$\boxed{\sigma(\underline{k}_i, \underline{k}_s) = \pi n_A \mathcal{R} R^2(\underline{k}_i, \underline{k}_s)} \tag{I.51}$$

If we define $\underline{k}_i$ and $\underline{k}_s$ as (see Fig. I-2)

$$\underline{k}_i = k_0 \begin{bmatrix} \cos\theta_i & \sin\phi_i \\ \sin\theta_i & \sin\phi_i \\ -\cos\phi_i & \end{bmatrix} \tag{I.52}$$

$$\underline{k}_s = k_0 \begin{bmatrix} \cos\theta_s & \sin\phi_s \\ \sin\theta_s & \sin\phi_s \\ \cos\phi_s & \end{bmatrix} \tag{I.53}$$

and

$$\delta\theta = \theta_s - \theta_i \tag{I.54}$$

then we obtain for the scattering cross section

$$\boxed{\sigma(\underline{k}_i, \underline{k}_s) = \frac{\sec^4\gamma}{s^2} \exp\left(-\frac{\tan^2\gamma}{s^2}\right) R^2(\underline{k}_i, \underline{k}_s)} \tag{I.55}$$

where

$$R^2(\underline{k}_i, \underline{k}_s) = (\hat{\underline{k}}_i \times \underline{e} \times (\hat{\underline{k}}_i - \hat{\underline{k}}_s))^T \left(\hat{\underline{k}}_s \hat{\underline{k}}_s^T - \underline{I}\right)^T \left(\hat{\underline{k}}_s \hat{\underline{k}}_s^T - \underline{I}\right) (\underline{k}_i \times \underline{e} \times (\hat{\underline{k}}_i - \hat{\underline{k}}_s)) \tag{I.56}$$

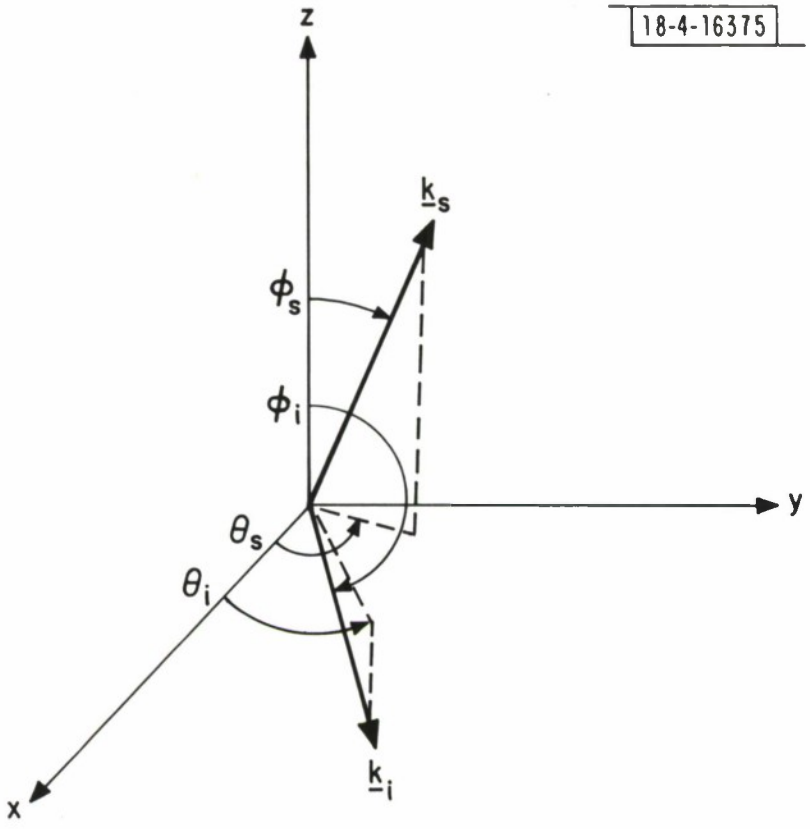

Fig. I. 2. Geometric interpretation of wave vectors.

with

$$\hat{\underline{k}}_s = \frac{\underline{k}_s}{k_0} \tag{I. 57}$$

$$\hat{\underline{k}}_i = \frac{\underline{k}_i}{k_0} \tag{I. 58}$$

APPENDIX II

GEOMETRIC CONSTRAINTS

Consider the scattering geometry shown in Fig.4. Here we define two angles α and β, which correspond to latitude and longitude. Let ϕ be the angle from the horizontal plane of the sensor, and θ be the angle from the normal $\underline{n}_2$ as shown. These correspond to elevation and azimuth, respectively. The scattering surface is at angles α, β. The radius of the earth is given by R_E. We first note that

$$\theta = \frac{\pi}{2} - \beta \tag{II. 1}$$

Also from the geometry, if we project a line normal to the plane of β through the scattering point, then tan ϕ can be shown to equal

$$\tan \phi = \frac{z_1 + R_E(1 - \cos \alpha)}{R_E \sin \alpha} \tag{II. 2}$$

Similarly, we can show by observation that

$$(\pi - \phi_s) + \left(\frac{\pi}{2} - \phi\right) + \alpha = \pi \tag{II. 3}$$

or

$$\phi_s = \frac{\pi}{2} - \phi + \alpha \tag{II. 4}$$

We now want to evaluate the vectors $\underline{s}_1$ and $\underline{s}_2$. Let $\underline{r}_1$ be a vector from the origin O to the receiver. Then

$$\underline{r}_1 = (z_1 + R_E)\, \underline{n}_z \tag{II. 5}$$

where $\underline{n}_z$ is the unit normal in the z directions. Let $\underline{p}$ be the vector from the origin to the scattering surface. Then

$$\underline{p} = R_E(\cos\beta \sin\alpha\, \underline{n}_x + \sin\beta \sin\alpha\, \underline{n}_y + \cos\alpha\, \underline{n}_z) \tag{II. 6}$$

Then $\underline{s}_1$ is

$$\begin{aligned}\underline{s}_1 &= \underline{r}_1 - \underline{p} \\ &= -R_E \cos\beta \sin\alpha\, \underline{n}_x - R_E \sin\beta \sin\alpha\, \underline{n}_y + (z_1 + R_E - R_E\cos\alpha)\, \underline{n}_z\end{aligned} \tag{II. 7}$$

In a similar fashion, we can find $\underline{r}_2$ which is

$$\underline{r}_2 = (z_2 + R_E)[\sin\alpha'\, \underline{n}_y + \cos\alpha'\, \underline{n}_z] \tag{II. 8}$$

where α' is shown in Fig. 4. Thus

$$\begin{aligned}\underline{s}_2 &= \underline{r}_2 - \underline{p} \\ &= -\cos\beta \sin\alpha\, R_E\, \underline{n}_x + [(z_2 + R_E)\sin\alpha' - \sin\beta \sin\alpha\, R_E]\, \underline{n}_y \\ &\quad + [(z_2 + R_E)\cos\alpha' - \cos\alpha\, R_E]\, \underline{n}_z\end{aligned} \tag{II. 9}$$

We now want to find the angle ϕ_i that $\underline{s}_2$ makes with the normal $\underline{n}_s$ on the surface and the angle θ_s, which is the angle between $\underline{s}_1$ and $\underline{s}_2$ projected onto the plane of $\underline{n}_s$. To obtain these values we find it convenient to rotate

the unit vectors $\underline{n}_1$, $\underline{n}_2$ and $\underline{n}_3$ around to the scattering area through angles α, β. Using standard rotation matrices, we find the resulting vectors, $\underline{m}_1$, $\underline{m}_2$, and $\underline{m}_3$ to be

$$\underline{m}_i = \underline{R}\,\underline{n}_i \quad (i = 1,\ 2,\ 3) \tag{II.10}$$

where

$$R = \begin{bmatrix} \cos\beta\cos\alpha & \sin\beta & -\cos\beta\sin\alpha \\ -\sin\beta\cos\alpha & \cos\beta & \sin\beta\sin\alpha \\ \sin\alpha & 0 & \cos\alpha \end{bmatrix} \tag{II.11}$$

This yields

$$\underline{m}_1 = \begin{bmatrix} -\cos\beta\sin\alpha \\ \sin\beta\sin\alpha \\ \cos\alpha \end{bmatrix} \tag{II.12}$$

$$\underline{m}_2 = \begin{bmatrix} \sin\beta \\ \cos\beta \\ 0 \end{bmatrix} \tag{II.13}$$

$$\underline{m}_3 = \begin{bmatrix} \cos\beta\cos\alpha \\ -\sin\beta\cos\alpha \\ \sin\alpha \end{bmatrix} \tag{II.14}$$

In this case, $\underline{m}_1$ is now equivalent to $\underline{n}_s$ so that

$$\underline{m}_1 = \underline{n}_s \tag{II. 15}$$

Now using the dot products, we obtain

$$\phi_i = \cos^{-1}\left(\frac{\underline{m}_1 \cdot \underline{s}_2}{|\underline{s}_1|}\right) \tag{II. 16}$$

and

$$\phi_s = \cos^{-1}\left(\frac{\underline{m}_1 \cdot \underline{s}_1}{|\underline{s}_1|}\right) \tag{II. 17}$$

But

$$|s_1|^2 = R_E^2 \sin^2\alpha + (R_E(1 - \cos\alpha) + z_1)^2 \tag{II. 18}$$

and

$$|s_2|^2 = \cos^2\beta \sin^2\alpha\, R_E^2 + ((z_2 + R_E)\sin\alpha' - \sin\beta \sin\alpha\, R_E)^2$$

$$+ ((z_2 + R_E)\cos\alpha' - \cos\alpha\, R_E)^2 \tag{II. 19}$$

Yet, we already have ϕ_s so that all we require is ϕ_i. Thus

$$\underline{m}_1 \cdot \underline{s}_2 = R_E \cos^2\beta \sin^2\beta$$

$$+ \sin\beta \sin\alpha[(z_2 + R_E) \sin\alpha' - \sin\beta \sin\alpha R_E]$$

$$+ \cos\alpha[(z_2 + R_E) \cos\alpha' - \cos\alpha R_E] \qquad \text{(II.20)}$$

We also have

$$\frac{\underline{m}_2 \cdot \underline{s}_1}{|\underline{s}_1|} = \sin\phi_s \cos\theta_1 \qquad \text{(II.21)}$$

$$\frac{\underline{m}_2 \cdot \underline{s}_2}{|\underline{s}_2|} = \sin\phi_i \cos\theta_2 \qquad \text{(II.22)}$$

$$\frac{\underline{m}_3 \cdot \underline{s}_1}{|\underline{s}_1|} = \sin\phi_s \sin\theta_1 \qquad \text{(II.23)}$$

$$\frac{\underline{m}_3 \cdot \underline{s}_2}{|\underline{s}_2|} = \sin\phi_i \sin\theta_2 \qquad \text{(II.24)}$$

Thus combining these we obtain

$$\theta_1 = \tan^{-1}\left(\frac{\underline{m}_3 \cdot \underline{s}_1}{\underline{m}_2 \cdot \underline{s}_1}\right) \tag{II. 25}$$

$$\theta_2 = \tan^{-1}\left(\frac{\underline{m}_3 \cdot \underline{s}_2}{\underline{m}_2 \cdot \underline{s}_2}\right) \tag{II. 26}$$

where

$$\underline{m}_3 \cdot \underline{s}_1 = -\cos^2\beta \sin\alpha \cos\alpha R_E + \sin^2\beta \sin\alpha \cos\alpha R_E + \sin\alpha (r_1 + R_E(1 - \cos\alpha)) \tag{II. 27}$$

$$\underline{m}_3 \cdot \underline{s}_2 = -\cos^2\beta \cos\alpha \sin\alpha R_E - \sin\beta \cos\alpha \cdot [(r_2 + R_E) \sin\alpha' - \sin\beta \sin\alpha R_E] + \sin\alpha \cdot [(r_2 + R_E) \cos\alpha' - \cos\alpha R_E] \tag{II. 28}$$

$$\underline{m}_2 \cdot \underline{s}_1 = -\sin\beta \cos\beta \sin\alpha R_E - \sin\beta \cos\beta \sin\alpha R_E \tag{II. 29}$$

$$\underline{m}_2 \cdot \underline{s}_2 = -\sin\beta \cos\beta \sin\alpha R_E + \cos\beta [(r_2 + R_E) \sin\alpha' - \sin\beta \sin\alpha R_E] \tag{II. 30}$$

The angle between $\underline{k}_i$ and $\underline{k}_s$ then in the plane of $\underline{n}_s$ is θ_s

$$\theta_s = \pi + \theta_2 - \theta_1 \quad . \tag{II. 31}$$

Thus ϕ_i, ϕ_s and θ_s are the values that correspond to ϕ_i, ϕ_s and $\delta\theta$ in the last section.

Having ϕ_i, ϕ_s and θ_s, we have enough information to describe $\sigma(\underline{k}_i, \underline{k}_s)$, which we know depends on only these three parameters. Thus we make the equality

$$\sigma(\underline{k}_i, \underline{k}_s) = \sigma(\theta_s, \phi_s; \phi_i) \tag{II. 32}$$

Also, both $|\underline{s}_1|^2$ and $|\underline{s}_2|^2$ have been evaluated in Equations II. 18 and II. 19, respectively. The only remaining term is dA. From the geometry we know that

$$dA = R_E^2 \sin\alpha \, d\alpha \, d\beta \quad . \tag{II. 33}$$

From Section 3, we know that

$$d\beta = d\theta \quad . \tag{II. 34}$$

We now want to find $d\alpha$ in terms of $d\phi$. Recall that Equation II-2 gives ϕ in terms of α so that

$$d \tan \phi = \sec^2 \phi \, d\phi$$

$$= \left(\csc^2 \alpha - \csc \alpha \cot \alpha \left(\frac{z_1}{R_E} + 1 \right) \right) d\alpha \quad . \tag{II. 35}$$

But;

$$\sec^2 \phi = \tan^2 \phi + 1$$

$$= \left[\frac{z_1 + R_E(1 - \cos \alpha)}{R_E \sin \alpha} \right]^2 + 1$$

$$= \frac{z_1^2 + R_E^2 (1 - \cos \alpha)^2 + z_1 R_E (1 - \cos \alpha) + R_E^2 \sin^2 \alpha}{R_E^2 \sin^2 \alpha} \tag{II. 36}$$

Yet from Equation II. 18, we see that the denominator is nothing more than $|\underline{s}_1|^2$. Therefore, using Equation II. 35 in Equation II. 34, we obtain

$$d\alpha = \frac{|\underline{s}_1|^2}{R_E^2 \sin^2 \alpha} \frac{d\phi}{\left[\csc^2 \alpha - \csc \alpha \cot \alpha \left(\frac{z_1}{R_E} + 1 \right) \right]} \tag{II. 37}$$

Combining with Equation II. 33, we obtain for dA

$$dA = \frac{|\underline{s}_1|^2}{\left[\csc^2 \alpha - \csc \alpha \cot \alpha \left(\frac{z_1}{R_E} + 1 \right) \right]} \frac{d\theta \, d\phi}{\sin \alpha} \tag{II. 38}$$

which is the desired result.

APPENDIX III

SHADOWING EFFECTS

Consider the geometry shown in Fig. III. 1. Here we have depicted a ray coming from infinity, incident at x, y equal to zero. The height of the surface is given by $\xi(x)$, and it is sufficient to consider only one dimension variation. Let the curve

$$z = \xi_0 + (\tan \psi)\, x \tag{III. 1}$$

represent the incident ray where ψ is the angle between the x, y plane and the normal (x axis). Note that $\psi = \pi/2 - \phi_i$. Furthermore,

$$\xi_0 = \xi(0) \quad . \tag{III. 2}$$

Now define $S(\psi \,|\, \xi_0, \xi_0')$ as the conditional probability that the point ξ_0 is illuminated given ξ_0 and ξ_0' (the slope at x_0, y_0) with the incident ray defined as in Equation III. 1. Then by definition

$$S(\psi \,|\, \xi_0, \xi_0') = P[\xi_p \text{ illuminated} \,|\, \xi_0, \xi_0'] \tag{III. 3}$$

$$= P[\xi \text{ will not cross } \xi_0 + \tan \psi\, x$$

$$\text{for any } x > 0 \;|\, \xi_0, \xi_0']$$

$$\triangleq \lim_{\tau \to \infty} S(\psi \,|\, \xi_0, \xi_0'; \tau)$$

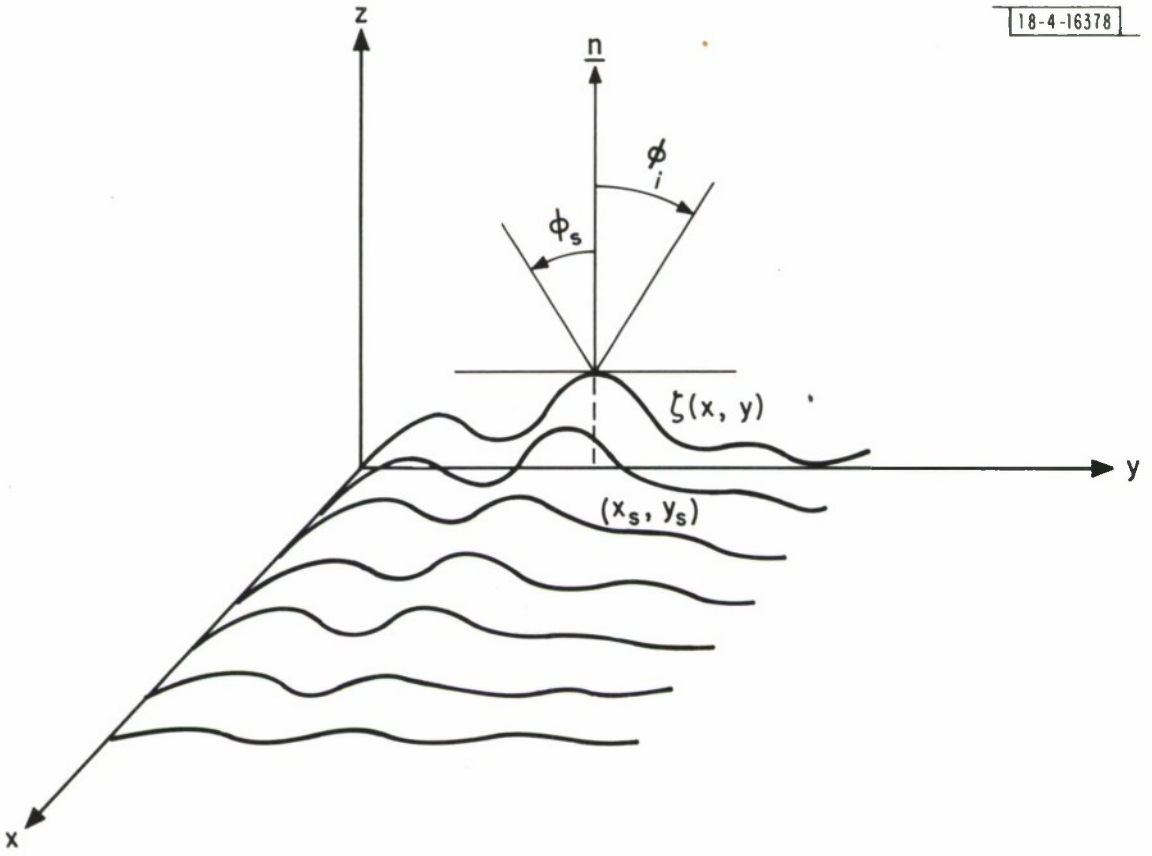

Fig. III. 1. Geometry of shadowing effects.

where

$$S(\psi \mid \xi_0, \xi_0'; \tau) = P[\xi \text{ will not cross } \xi_0 + \tan \psi \, x$$

$$\text{for } x \in (0, \tau) \mid \xi_0 \; \xi_0'] \quad . \qquad \text{(III. 4)}$$

Now define

$$q(\tau)\, d\tau = P[\xi \text{ crosses the ray in } x \in (\tau, \; \tau + d\tau)$$

$$\mid \xi \text{ does not cross in } x \in (0, \tau); \; \xi_0, \; \xi_0'] \quad . \qquad \text{(III. 5)}$$

Then

$$S\left(\psi \mid \xi_0; \; \xi_0'; \; \tau + d\tau\right)$$

$$= S\left(\psi \mid \xi_0, \xi_0'; \; \tau\right) [1 - q(\tau)\, d\tau] \qquad \text{(III. 6)}$$

or

$$\frac{dS}{d\tau}\left(\psi \mid \xi_0, \xi_0' ; \; \tau\right) = - \, q(\tau) \, S\left(\psi \mid \xi_0, \xi_0'; \; \tau\right) \quad . \qquad \text{(III. 7)}$$

This then implies that

$$S\left(\psi \,|\, \xi_0, \xi_0'; \tau\right) = C \exp\left[-\int_0^{\tau} q(u)\, du\right] \quad . \tag{III. 8}$$

Now as $\tau \to 0$ we have

$$\lim_{\tau \to 0} S\left(\psi \,|\, \xi_0, \xi_0'; \tau\right) = 0 \qquad \text{if } \xi_0' > \tan \psi \tag{III. 9}$$

or

$$\lim_{\tau \to 0} S\left(\psi \,|\, \xi_0, \xi_0'; \tau\right) = 1 \qquad \text{if } \xi_0' < \tan \psi \ . \tag{III. 10}$$

That is, if the slope at the origin is greater than that of the incoming ray, then the point will be shadowed. Therefore,

$$C = u_{-1}(\tan \psi - \xi_0') \tag{III. 11}$$

where $u_{-1}(\ )$ is the unit step function. We really want $S(\psi)$, the probability that any point will be irradiated by a ray with angle ψ. This is the unconditional probability of Equation III. 8. But we assume that we know the joint probability densities of $\xi(x)$ and $\xi'(x)$. Let this be $p_{\xi, \xi'}(u, v)$. Then

$$S(\psi) = \int\int S\left(\psi \,|\, u, v\right) p_{\xi, \xi'}(u, v)\, du\, dv \quad . \tag{III. 12}$$

Now Equation III. 12 can be solved if we had $q(\tau)$. This is difficult to obtain in general, so we approximate it by

$$q(\tau)\, d\tau \approx P[\xi \text{ crosses } \xi_0 + \tan\psi \; x \text{ in } x \epsilon (\tau, \; \tau + d\tau)$$

$$\text{with slope} > \tan\psi \,|\, \xi_0, \; \xi_0'] \qquad \text{(III. 13)}$$

This probability has been evaluated by Wagner and is

$$q(\tau) = \frac{1}{2\pi \sigma_0^2 \sigma_1^2} \int_{\tan\psi \, = \, \eta_0}^{\infty} (\mu - \mu_0)$$

$$\exp\left[-\left(\frac{(\xi_0 + \mu_0 \tau)^2}{2\sigma_0^2} \right) - \frac{\mu^2}{2\sigma_1^2} \right] d\mu \qquad \text{(III. 14)}$$

where

$$\sigma_0^2 = E[\xi^2(x)] \qquad \text{(III. 15)}$$

$$\sigma_1^2 = E\left[\frac{d\xi(x)}{dx} \; \frac{d\xi(x)}{dx} \right] \qquad \text{(III. 16)}$$

From our discussion in Section 3, we know that

$$E[\xi(x)\,\xi(x')] = \sigma_h^2 \exp\left(-r^2/\sigma_\ell^2\right) \tag{III. 17}$$

where here $r^2 = (x - x')^2$. Thus

$$\sigma_0^2 = \sigma_h^2 \tag{III. 18}$$

and

$$\sigma_1^2 = \frac{2\sigma_h^2}{\sigma_\ell^2} = s^2 \quad . \tag{III. 19}$$

Furthermore, we know that

$$E\left[\xi(x)\,\frac{d}{dx}\,\xi(x)\right] = 0 \tag{III. 20}$$

for this given correlation function which implies that ξ and ξ' are independent. Now Equation III. 18 can be used in Equation III. 8 and then in Equation III. 12 to obtain $S(\psi)$. However, this is for the monostatic problem. For the bistatic problem as shown in Fig. 6, we have a ψ_i and ψ_s or equivalently ϕ_i and ϕ_s. Then the probability that we see a wave scattered to ϕ_s from ϕ_i given ξ_0, and ξ_0' becomes

$$S\left(\phi_i, \phi_s \,|\, \xi_0, \xi_0'\right) = S\left(\phi_i \,|\, \phi_s;\, \xi_0, \xi_0'\right)\, S\left(\phi_s \,|\, \xi_0, \xi_0'\right) \quad . \tag{III. 21}$$

However, for the cases of interest, ϕ_i and ϕ_s represent scattering into two different and independent directions. Thus

$$S\left(\phi_i \middle| \phi_s;\ \xi_0, \xi_0'\right) = S\left(\phi_i \middle| \xi_0, \xi_0'\right) \quad . \tag{III. 22}$$

Therefore, following the procedure outlined before, we have

$$S(\phi_i, \phi_s) = \int\int S\left(\phi_i \middle| \xi_0, \xi_0'\right) S\left(\phi_s \middle| \xi_0, \xi_0'\right)$$

$$p_{\xi_0}(u)\, p_{\xi_0'}(v)\, du\, dv \quad . \tag{III. 23}$$

This integral has been evaluated by Wagner to yield the result of Section 3.

APPENDIX IV

PERFORMANCE BOUND CALCULATIONS

In general, the integrals appearing in Section 4 are difficult to evaluate. However, if we assume that $K(\mu)$ is such that

$$K(\mu) \to 0, \quad \mu = \pm 1 \tag{IV.1}$$

then considerable simplification arises. This is, in general, the case as discussed in the last section. We now evaluate the integrals

$$\int_{-\infty}^{\infty} K(\mu') \frac{\partial^2}{\partial \mu'^2} B(\mu')\, d\mu' \tag{IV.2}$$

$$\int_{-\infty}^{\infty} K(\mu')\, B(\mu')\, d\mu' \tag{IV.3}$$

and the integrals appearing in the evaluation of the performance of the monopulse processor.

These integrals can be related to the integrals of their Fourier transforms via Parseval's theorem. Namely, let

$$\mathcal{B}(f) = \int_{-\infty}^{\infty} \exp(-j2\pi f\mu)\, B(\mu)\, d\mu \qquad \text{(IV.4)}$$

$$\mathcal{K}(f) = \int_{-\infty}^{\infty} \exp(-j2\pi f\mu)\, K(\mu)\, d\mu \qquad \text{(IV.5)}$$

Then we can write for Equations IV. 2 and IV. 3

$$\int_{-\infty}^{\infty} K(\mu)\, \frac{\partial^2}{\partial \mu^2} B(\mu)\, d\mu = -\int_{-\infty}^{\infty} (2\pi f)^2 \mathcal{K}(f)\, \mathcal{B}(f)\, df \qquad \text{(IV.6)}$$

$$\int_{-\infty}^{\infty} K(\mu)\, B(\mu)\, d\mu = \int_{-\infty}^{\infty} \mathcal{K}(f)\, \mathcal{B}(f)\, df \qquad \text{(IV.7)}$$

Now note that

$$\underline{\tilde{m}}(\mu')\, \underline{\tilde{m}}^{\dagger}(\mu' + \mu) = \sum_{i=1}^{N} \exp(-j2\pi\mu d_i/\lambda)$$

(IV.8)

so that

$$B(\mu) = \sum_{i=1}^{N} \sum_{k=1}^{N} \exp(j\, 2\pi\, \mu(d_i - d_k)/\lambda) \qquad \text{(IV. 9)}$$

The Fourier transform of this is obtained quite readily as

$$\mathcal{B}(f) = \sum_{i=1}^{N} \sum_{k=1}^{N} \delta(f - (d_i - d_k)/\lambda) \qquad \text{(IV. 10)}$$

Using this in Equations IV. 6 and IV. 7 we obtain

$$\int_{-\infty}^{\infty} K(\mu) \frac{\partial^2}{\partial \mu^2} B(\mu)\, d\mu$$

$$= -\sum_{i=1}^{N} \sum_{k=1}^{N} (2\pi)^2 \left(\frac{d_i - d_k}{\lambda}\right)^2 \mathcal{K}\left(\frac{d_i - d_k}{\lambda}\right) \qquad \text{(IV. 11)}$$

and

$$\int_{-\infty}^{\infty} K(\mu)\, B(\mu)\, d\mu = \sum_{i=1}^{N} \sum_{k=1}^{N} \mathcal{K}\left(\frac{d_i - d_k}{\lambda}\right) \qquad \text{(IV. 12)}$$

Thus, knowing the Fourier transform of the channel spread function at the specified number of points, the integrals in Equations IV. 6 and IV. 7 are directly evaluated.

A special case of interest is that of a uniformly spaced array. Namely,

$$d_{k+1} - d_k = d \quad ; \quad k = 1, 2, \cdots N \; . \tag{IV. 13}$$

For this case, the double sum in Equation IV. 10 can be shown to be equivalent to

$$\mathcal{B}(f) = \sum_{k=-N}^{N} (N - |k|)\, \delta(f + k\, d/\lambda) \quad . \tag{IV. 14}$$

The corresponding integrals for a uniformly spaced array are

$$\int_{-\infty}^{\infty} K(\mu)\, \frac{\partial^2}{\partial \mu}\, B(\mu)\, d\mu = -\sum_{k=-N}^{N} \left(\frac{2\pi\, k\, d}{\lambda}\right)^2 (N - |k|)\, \chi\left(\frac{kd}{\lambda}\right) \tag{IV. 15}$$

$$\int_{-\infty}^{\infty} K(\mu)\, B(\mu)\, d\mu = \sum_{k=-N}^{N} (N - |k|)\, \chi\left(\frac{kd}{\lambda}\right) \quad . \tag{IV. 16}$$

Thus for symmetric $\mathcal{K}(f)$, we must evaluate the transform at only N + 1 locations. This is a considerable savings over direct evaluation of the integral. One can also note that the evaluation of the second partial derivative of $B(\mu)$ at $\mu = 0$ is equavalent to using a $K(\mu)$ equal to $\delta(\mu)$. Thus

$$\left.\frac{\partial^2 B(\mu)}{\partial \mu^2}\right|_{\mu = 0} = \int_{-1}^{1} \delta(\mu') \frac{\partial^2}{\partial \mu'^2} B(\mu')\, d\mu'$$

$$= -(2\pi)^2 \sum_{i=1}^{N} \sum_{k=1}^{N} \left(\frac{d_i - d_k}{\lambda}\right)^2 . \qquad \text{(IV.17)}$$

For the case of a uniformly spaced array we have

$$\left.\frac{\partial^2}{\partial \mu^2} B(\mu)\right|_{\mu = 0} = -(2\pi)^2 \sum_{k=-N}^{N} \left(\frac{kd}{\lambda}\right)^2 (N - |k|)$$

$$= -\frac{2}{3} N^2 \left(\frac{2\pi d}{\lambda}\right)^2 \left[\left(\frac{N}{2}\right)^2 - \left(\frac{1}{2}\right)^2\right]. \qquad \text{(IV.18)}$$

Now Equations IV. 15, IV. 16, and IV. 17 can be used to evaluate σ_μ^2.

For the case of monopulse performance with a linear uniformly spaced array we have

$$G_{\Delta}(\mu - \mu') = -\sum_{k=1}^{N/2} \exp\left(j\, k\, \frac{d_0}{\lambda}\, 2\pi\, (\mu - \mu')\right)$$

$$+ \sum_{k=N/2+1}^{N} \exp\left(j\, k\, \frac{d_0}{\lambda}\, 2\pi(\mu - \mu')\right) \quad . \tag{IV.19}$$

Using standard substitutions, we can show that

$$G_{\Delta}(\mu - \mu') = 4\, \frac{\sin^4\left(\frac{N}{4}\, \frac{d_0}{\lambda}\, 2\pi(\mu - \mu')\right)}{\sin^2\left(\frac{d_0}{2\lambda}\, 2\pi(\mu - \mu')\right)} \tag{IV.20}$$

Following the use of transform techniques as discussed previously, we can now directly evaluate the integral appearing in the monopulse bound. Namely

$$\int_{-1}^{1} K(\mu)\, |G_{\Delta}(\mu)|^2\, d\mu$$

$$= \int_{-\infty}^{\infty} \mathcal{K}(f)\, (\mathcal{G}_{\Delta}(f) * \mathcal{G}_{\Delta}(f))\, df \tag{IV.21}$$

where $\mathcal{G}_{\Delta}(f)$ is the transform of $G_{\Delta}(\mu)$. Using the previous techniques, it is readily shown that

$$\int_{-1}^{1} K(\mu) \left| G_{\Delta}(\mu) \right|^2 d\mu$$

$$= N \mathcal{K}(0) + 2 \sum_{k=1}^{N/2} (N - 3k) \mathcal{K}\left(\frac{kd_0}{\lambda}\right)$$

$$+ 2 \sum_{k=N/2+1}^{N} (-N + k) \mathcal{K}\left(\frac{kd_0}{\lambda}\right) \quad . \qquad \text{(IV.22)}$$

These expressions can now be used directly to evaluate performance. Note that in all cases the transform need only be evaluated at N + 1 points.

ACKNOWLEDGMENT

The author would like to thank Dr. D. Kocher for his assistance in gathering the data that appears in this report and for his continued insight into the general area of multipath. Stanley Miller has also provided continued support and encouragement, and the assistance of Larry Guisti in experimental data gathering is also gratefully acknowledged. Discussions with David Burton at Raytheon led to the presentations on monopulse performance. The programming assistance of Louise Balboni and Kathleen Knox has been invaluable.

GLOSSARY OF TERMS

A	-	antenna area
$\tilde{b}(\theta, \phi)$	-	complex envelope of time invariant portion of diffuse field
$\tilde{b}(\theta, \phi, t)$	-	complex envelope of diffuse field
c	-	velocity of propagation
d_i	-	distance to ith dipole
d_o	-	interdipole spacing
$E[\ ]$	-	expectation
erf ( )	-	error function
E	-	energy of transmitted signal
$\underline{E}_{sc}$	-	scattered field
$\tilde{f}(t)$	-	complex envelope of transmitted signal
$G(\theta, \psi)$	-	antenna gain
$G_\Delta(\theta, \phi)$	-	difference antenna gain
$G_\Sigma(\theta, \phi)$	-	sum antenna gain
$I_n(\ )$	-	Bessel function
$\underline{J}(\_)$	-	current density
k	-	monopulse slope
$\underline{k}$	-	plane wave vector
k_x, k_y, k_z	-	components of propagation vector
$K(\theta)$	-	channel spread function; azimuth only
$K(\theta, \phi)$	-	channel spread function

$K_s(\underline{r}, \underline{r}')$ - covariance of diffuse signal

$\underline{\tilde{m}}(\mu)$ - array delay vector

N - number of array elements

$\underline{n}$ - normal vector

$\tilde{n}(t)$ - complex envelope of receiver noise

n_A - average number of scatterers

$\frac{N_o}{2}$ - noise spectral density

P_o - power of transmitter

R - ground range

$R(\xi)$ - reflection coefficient

R_E - radius of earth

R_h - range to horizon

R_T - range from aircraft to antenna

r - range

$\underline{r}$ - point in space

$\tilde{r}(t)$ - complex envelope of received signal

$\underline{r}_0$ - scattering plane displacement

$\underline{r}_1$ - location of receiver

$\underline{r}_2$ - location of transmitter

S - scattering surface

$S(\phi_1, \phi_2)$ - shadowing functions

$s(t)$ - transmitted signal

$\tilde{s}(t)$ - complex envelope of transmitted signal

$\tilde{s}(\underline{r})$ - complex envelope of time invariant diffuse signal

$\tilde{s}(r, t)$	-	complex envelope of time variance diffuse signal
SNR	-	signal-to-noise ratio
t	-	time
t_0	-	signal emission time of source
t_1	-	transmission time from transmitter to receiver
t_s	-	transit time of scattered path
var ( )	-	variance
x_1, y_1	-	antenna phase center location
z_1	-	antenna height
x_2, y_2, z_2	-	location of aircraft
$z(X, Y)$	-	random surface
$\underline{\Gamma}(\underline{r}, \underline{r}')$	-	Greens function
γ	-	noise-to-signal ratio
$\tilde{\Delta}$	-	difference signal
∇	-	del operator (gradient or divergence)
$\delta(\underline{k} - \underline{k}')$	-	delta function
ϵ_i	-	dielectric constant of ith scattering plane
η	-	diffuse multipath to free space signal ratio
$\hat{\theta}$	-	azimuth estimate
θ_B	-	beamwidth
λ	-	free space wavelength
μ	-	direction cosine
μ_B	-	beamwidth

$\xi(x, y)$	-	random surface height
ξ	-	interference-to-signal ratio
ρ_D	-	diffuse reflection coefficient
Σ	-	sum signal
σ_b	-	channel attenuation coefficient
σ_h	-	standard deviation of surface height
σ_I^2	-	diffuse signal energy
σ_i^2	-	power in diffuse field
σ_i	-	scattering cross section
σ_i	-	conductivity of ith scattering plane
σ_ℓ	-	correlation length of surface
σ_n^2	-	noise covariance
σ_s^2	-	signal energy
$\sigma(\theta_s, \phi_s; \phi_i)$	-	scattering cross sections
σ_θ^2	-	variance of azimuth estimate
σ_μ^2	-	variance of μ
ϕ_i	-	elevation (incident or ith signal)
ϕ_s	-	elevation of scattered signal
ψ_i	-	phase difference
$\tilde{\psi}_k$	-	multipath phase
ψ_{R_i}	-	phase due to range
ω_c	-	carrier frequency
$\mathcal{B}(\mu)$	-	array ambiguity function

REFERENCES

Ament, W. S.

[1] "Toward a Theory of Reflection by a Rough Surface," Proc. IRE, 41 (1953) pp. 142-146.

[2] "Forward and Back Scattering From Certain Rough Surfaces," IRE, AP-4 (1965) pp. 369-373.

Barrick, D. E.

[1] "Rough Surface Scattering Based on the Specular Point Theory," IEEE, AP-16, No. 4, (July 1968) pp. 449-454.

[2] "Unacceptable Weight Correlation Coefficients and the Quasi-Specular Component in Rough Surface Scattering," Radio Science, Vol. 5, No. 4, (April 1970) pp. 647-654.

[3] "Theory of HF and UHF Propagation Across the Rough Sea," Radio Science, Vol. 6, No. 5, (May 1971).

[4] "First-Order Theory and Analysis of MF/HF/VHF Scatter from the Sea," IEEE AP-20, 1972, pp. 2-10.

Barrick, D. E., and Peake, W. H.

[1] "A Review of Scattering From Surfaces With Different Roughness Scales," Radio Science Vol. 3, No. 8, (August 1968) pp. 865-868.

Barton, D. K.

[1] "Low Angle Radar Tracking," Proc. IEEE, Vol. 81, 1974, pp. 687-704.

[2] Personal Correspondence.

Barton, D. K., and Ward, H. R.

[1] Handbook of Radar Measurement, (Prentice-Hall, Englewood Cliffs, N. J., 1969).

Bass, F. G., et al.

[1] "Very High Frequency Radio Wave Scattering by a Distributed Sea Surface Pt. I," IEEE, Vol. AP-16, No. 5, (Sept. 1968) pp. 554-559.

[2] "Very High Frequency Radio Wave Scattering by a Distributed Sea Surface Pt. II," IEEE, Vol. AP-16, No. 5, pp. 560-588.

Beard, C. I.

[1] "Coherent and Incoherent Scattering of Microwaves From the Ocean," IEEE, Vol. AP-9, No. 5, (Sept. 1961) pp. 470-483.

[2] "Behavior of Non-Rayleigh Statistics of Microwave Forward Scatter From a Random Water Surface," IEEE, Vol. AP-15, No. 5 (Sept. 1967) pp. 649-657.

Beard, C. I., et al.

[1] "Phenomenological Vector Model of Microwave Reflection From the Ocean," IRE, Vol. AP-4, (1956) pp. 162-167.

Beckmann, P.

[1] "Scattering by Composite Rough Surfaces," Proc. IEEE, (Aug. 1965) pp. 1, 012-1, 015.

[2] "Scattering of Light by Rough Surface," Progress in Optics, IV, (E Wolf, Ed., J. Wiley, N. Y., 1967) pp. 55-70.

[3] "Shadowing of Random Rough Surfaces," IEEE, AP-14, (1965) pp. 384-388.

Beckmann, P., and Spizzichino, A.

[1] The Scattering of Electromagnetic Waves From Rough Surfaces, (Pergamon, N. Y., 1963).

Born, M., and Wolf, E.

[1] Principles of Optics (Pergamon, N. Y. 1970).

Boyd, M. L., and Deavenport, R. L.

[1] "Forward and Specular Scattering From a Rough Surface," JASA Vol. 53, 1973, pp. 791-800.

Brennan, L. E.

[1] "Angular Accuracy of Phased Array Radar," IRE, Vol. AP-9, 1961, pp. 268-275.

Brokelmann, R. A., and Hagfors, J.

[1] "Note on the Effect of Shadowing on the Backscattering of Waves From a Random Rough Surface," IEEE, Vol. AP-14, No. 5, (Sept. 1966), pp. 621-629.

Capon, J.

[1] "High Resolution Frequency-Wavenumber Spectrum Analysis," Proc. IEEE, Vol. 57, No. 8, August 1968, pp. 1408-1418.

Clarke, R. H., and Hendry, G. O.

[1] "Prediction and Measurement of Coherent and Incoherent Power Reflected From a Rough Surface, IEEE, Vol. AP-13, No. 3, (1964), 353-363.

Davies, H.

[1] "The Reflection Electromagnetic Waves From a Rough Surface," Proc. IEEE, Vol. 101, pp. 209 (1954).

DeLorenzo, J. K., and Cassedy, E. S.

[1] "A Study of the Mechanism of Sea Surface Scattering," IEEE, Vol. AP-14, No. 15, (Sept. 1966), pp. 611-620.

Eckart, C.

[1] "The Scattering of Sound from the Sea Surface," J. A. S. A., Vol. 25, No. 3 (May 1953) pp. 566-570.

Fante, R. L.

[1] "Discussion of a Model for Rough Surface Scattering," IEEE, Vol. AP-13, pp. 652-659 (July 1965).

Felsen, L. B., and Marcuvitz, N.

[1] Radiation and Scattering of Waves (Prentice-Hall, Englewood Cliffs, N. J., 1973).

Friis, H. T., and Lewis, W. D.

[1] "Radar Antennas," B. S. T. J., Vol. 26, No. 2, (April 1947) pp. 219-280.

Fung, A. K., and Moore, R. K.

[1] "The Correlation Function in Kirchoff's Method of Solution of Scattering of Waves From Statistically Rough Surfaces," J. Geo. Res., Vol. 71, No. 12, (June 1966) pp. 2939-2943.

Furutsu, K.

[1] "A Statistical Theory of Ridge Diffraction," Radio Science, Vol. 1, No. 1, (Jan. 1966) pp. 79-98.

Goldfischer, I.

[1] "Autocorrelation Function and Power Spectral Density Laser Produces Speckle Patterns," J. O. S. A., Vol. 55, No. 5, pp. 247-251, 1965.

Greenwood, D. P., and Powers, E. J.

[1] "The Scattering From Curved Rough Surfaces of an EM Wave Transmitted Through a Turbulent Medium," IEEE, Vol. AP-20, 1972, pp. 19-30.

Hagfors, T.

[1] "Backspacing From an Undulating Surface With Applications to Radar Return From the Moon," J. Geo. Res., Vol. 69. No. 18, (Sept. 1964), pp. 3779-3784.

Hayre, H. S., and Moore, R. K.

[1] "Theoretical Scattering Coefficient for Near Vertical Incidence From Contour Maps," Jour. Res. Nat. Bur. Sts., Series D, Vol. 65D, No. 5 (Sept.-Oct. 1961) pp. 427-432.

Hinich, M., and Shaman, P.

[1] "Parameter Estimation for an R-Dimensional Plane Wave Observed With Additive Independent Gaussian Errors," Ann. Math Stat., Vol. 93, (1972), pp. 153-169.

Hoffman, W. C.

[1] "Scattering of Electromagnetic Waves From a Random Surface," Quant. Appl. Math., 13, (1955) pp. 291-304.

Hofstetter, E. M., and DeLong, D. F.

[1] "Detection and Parameter Estimation in an Amplitude Comparison Monopulse Radar," IEEE, Vol. IT-15, No. 1, 1969, pp. 22-30.

Jackson, J. D.

[1] Classical Electrodynamics, Wiley, New York, 1962.

Jordan, E. C., and Balmain, K. G.

[1] Electromagnetic Waves and Radiating Systems, (Prentice-Hall, Englewood Cliffs, N. J., 1968).

Kerr, D. E.

[1] Propagation of Short Radio Waves, (Dover, N. Y., 1965).

Kodis, R. D.

[1] "A Note on the Theory of Scattering From an Irregular Surface," IEEE, Vol. AP-14, No. 1, (Jan. 1966) pp. 77-82.

Lonquet-Higgins, M. S.

[1] "Reflection and Refraction at a Random Moving Surface," Pt. I, J. O. S. A., Vol. 50., No. 9, (Sept. 1960) pp. 838-844.

[2] "Reflection and Refraction at a Random Moving Surface," Pt. II, J. O. S. A., Vol. 5, No. 9 (Sept. 1960) pp. 845-850.

Lynch, P. J., and Wagner, R. J.

[1] "Rough Surface Scattering: Shadowing, Multiple Scattering and Energy Conservation," J. Math. Phys., Vol. 11, No. 10, Oct. 1970, pp. 3032-3042.

Maltz, F. H., and Meecham, W. C.

[1] "The Effect of Curvature Variations on the Scattering From Rough Surfaces," J. Stat. Phys., Vol. 3, No. 4, (1971), pp. 385-394.

McAulay, R. J.

[1] "The Effects of Interference on Monopulse Performance," Lincoln Laboratory, M. I. T., Technical Note, TN-1973-30, (1 Aug. 1973), ESD-TA-73-176.

McAulay, R. J., and McGarty, T. P.

[1] "An Optimum Interference Detector for DABS Monopulse Data Editing," Lincoln Laboratory, M. I. T., Technical Note, TN-1973-48, (26 Sept. 1973) ESD-TR-73-253.

McDonald, J. F., and Spindel, R. C.

[1] "Implications of Fresnel Corrections in a Non-Gaussian Surface Scatter Channel," JASA, Vol. 50, No. 3, 1971, pp. 746-757.

McGarty, T. P.

[1] "Azimuth-Elevation Estimation Performance of a Spatially Dispersive Channel," IEEE Vol. AES-10, No. 1 (January 1974), pp. 58-69.

[2] "Models of Multipath Propagation Effects in a Ground-to-Air Surveillance System," M. I. T., Lincoln Laboratory, Technical Note, TN-1974-7, ESD-TR-74-40, (25 February 1974).

[3] "On the Structure of Random Fields Generated by Multiple Scatter Media," Ph. D. Thesis, M. I. T., 1971.

[4] "The Effect of Interfering Signals on the Performance of Angle of Arrival Estimates, IEEE Vol. AES-10, No. 1, January 1974, pp. 60-77.

[5] "The Effects of Diffuse Multipath on Antenna Performance," Proc. IEEE International Radar Conference, 1975.

Mitzner, K. M.

[1] "Change in Polarization on Reflection from a Tilted Plane," Rad. Science., Vol. 1, No. 1, (January 1966) pp. 27-29.

Rice, S. O.

[1] "Reflection of Electromagnetic Waves from Slightly Rough Surfaces," Comm. Pure and Appl. Math, 4, (1951) pp. 351-378.

Sancer, M. M.

[1] "Shadow Corrected Electromagnetic Waves from a Slightly Rough Surface," IEEE, Vol. AP-17, No. 5, Sept. 1969, pp. 577-585.

Seidman, L. P.

[1] "Bearing Estimation Error with a Linear Array," IEEE Vol. AU-19, No. 2, 1971, pp. 147-157.

Sharenson, S.

[1] "Angle Estimation Accuracy with a Monopulse Radar in the Search Mode," IRE, Vol. ANE-9, 1962, pp. 175-179.

Silver, S.

[1] Microwave Antenna Theory and Design, (Dover, N. Y. 1965).

Smith, B. G.

[1] "Geometrical Shadowing of a Random Rough Surface," IEEE, Vol. AP-15, No. 3, (Sept. 1967), pp. 668-671.

Spingler, G. F.

[1] "Analysis of Sidelobe Suppression Capabilities at Joint Use Radar Beacon Sites," FAA Report No. RD-67-59.

Stratton, J. A.

[1] Electromagnetic Theory, (McGraw-Hill, N. Y., 1941).

Twersky, V.

[1] "Reflection Coefficients for Certain Rough Surfaces," J. App. Phy., 24, (1953) pp. 659-660.

[2] "Certain Transmission and Reflection Theorems," J. App. Phys., Vol. 25, No. 7, (July 1954) pp. 859-862.

[3] "On the Scattering and Reflection of Sound by Rough Surfaces," J. A. S. A. Vol. 29, No. 2, (Feb. 1957) pp. 209-225.

[4] "On the Scattering and Reflection of Electromagnetic Waves From Rough Surfaces," IRE, AP-5, (1957) pp. 81-90.

Van Trees, H. L.

[1] Detection Estimation and Modulation Theory, Pt. I, (J. Wiley, N. Y. 1968).

[2] Detection Estimation and Modulation Theory, Pt. III (J. Wiley, N. Y. 1971).

Venetsanopoulos, A. N., and Tuteur, F. B.

[1] "Stochastic-Filter Modeling for the Sea-Surface Scattering Channel," J. A. S. A., 49, (1971) pp. 1100-1107.

Wagner, R. J.

[1] "Shadowing of Randomly Rough Surfaces," J. A. S. A, Vol. 41, No. 1, (1967) pp. 138-147.

Waterman, P. C.

[1] "New Formulation of Acoustic Scattering," J. A. S. A., Vol, 45, No. 6, pp. 1417-1969.

Yaglom, A. M.

[1] "Second-Order Homogenous Random Fields," Proc. 4th Berkeley Symp. Math. Stat. and Prob. 2, pp. 593-620.